

# American Earthquake Joint System for Resistance to Earthquake-Induced Ground Deformation

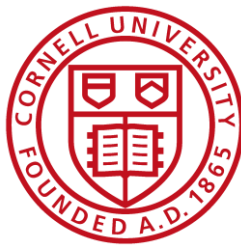
Final Report

Submitted to:

Mr. David Drake  
American Cast Iron Pipe Company  
P.O. Box 2727  
Birmingham, AL 35202 USA

By

C. Pariya-Ekkasut  
H. E. Stewart  
B. P. Wham  
T.D. O'Rourke  
T.K. Bond  
C. Argyrou



Cornell University  
School of Civil and Environmental Engineering  
Hollister Hall  
Ithaca, NY 14853

January, 2017

## **EXECUTIVE SUMMARY**

American Cast Iron Pipe Company has developed a hazard resistant ductile iron (DI) pipe joint, called the AMERICAN Earthquake Joint System (EJS). Sections of 6-in. (150-mm) ductile iron pipes with the AMERICAN Earthquake Joint Systems were tested at Cornell University to 1) evaluate the stress-strain-strength characteristics of the DI, 2) determine the capacity of the joint in direct tension and compression, 3) evaluate the bending resistance and moment vs. rotation relationship of an AMERICAN Flex-Ring (FR-FRE) joint and the AMERICAN Earthquake Joint System (EJS), and 4) evaluate the capacity of a 6-in. (150-mm) DI pipeline with AMERICAN Earthquake Joint Systems to accommodate fault rupture using the Cornell full-scale split-basin testing facility.

Test results are summarized for tensile stress-strain-strength characteristics, direct joint tension and compression, bending test results, pipeline response to fault rupture. Numerical simulations of the large-scale testing are presented, and compared with the results of the physical test. The significance of test results are given under the headings that follow.

### **Tensile Stress-Strain-Strength Characteristics**

The uniaxial tension testing of ductile iron (DI) from AMERICAN specimens was completed in accordance with ASTM – E8 2013 standards (ASTM, 2013). The ductile iron had a modulus, yield stress, and ultimate stress of 24,200 ksi, 50.6 ksi, and 65.3 ksi (167 GPa, 348 MPa, and 450 MPa), respectively. The specimens exceeded ANSI/AWWA C151/A21.51-09 60-42-10 specifications (AWWA, 2009). The yield and ultimate stresses are 20.5% and 8.8% greater than the specifications, respectively.

### **Direct Joint Tension and Compression**

Two tension tests and one compression test were performed on the 6-in. (150-mm)-diameter AMERICAN earthquake joint system (EJS) ductile iron pipes. Tension Test 1 reached a maximum force of 155 kips (689 kN) at 0.45 in. (11 mm) of FR joint opening and 5.1 in. (130 mm) of SE joint displacement. The maximum axial load for Tension Test 2 was 144 kips (641 kN) at 0.41 in. (10 mm) of FR joint opening and 5.1 in. (130 mm) of SE joint displacement. In both tests, the FR bell cracked circumferentially at the peak tensile forces resulting in loss of pressure. The average maximum tensile force of the two tension tests was 149.5 kips (665 kN). This force exceeds Class

A of ISO16134-2006 (ISO, 2006) tensile capacity of  $17D$ , where  $D$  is the nominal diameter in inches, and the force is expressed in kips. For the nominal 6-in. (150-mm)-diameter pipe this ISO capacity is 102 kips (450 kN).

The compressive testing showed that the AMERICAN EJS was able to accommodate axial loads to a compressive level at about the DI proportional limit. When the test pipe reached a compressive load of 256 kips (1,140 kN), which exceeded the proportional limit of 212 kips (943 kN), localized plastic deformation within the joint occurred, resulting in leakage.

### **Bending Test Results**

Four-point bending tests were performed on sections of 6 in. (150 mm) ductile iron (DI) with an AMERICAN Flex-Ring (FR-FRE) joint and on a nominal 6-in. (150-mm) section with the AMERICAN Earthquake Joint System (EJS). The purpose of these tests was to develop moment vs. rotation relationships for these types of joints.

The first leak of 3.5 ml/min in the FR-FRE joint occurred at a deflection of  $7.8^\circ$  and an applied moment of 155 kip-in. (17.5 kN-m). In the EJS bending test, first leakage of 25 ml/min was observed at the FR joint at an FR joint rotation of  $10^\circ$  and an EJS deflection of  $\theta_{EJS} = 12.7^\circ$  with an associated moment of 323 kip-in. (36.5 kN-m). Both of the AMERICAN Flex-Ring joint pipe and the AMERICAN EJS tested at Cornell exceeded the performance criteria for allowable deflection of  $5^\circ$  and  $8^\circ$ , respectively, without any leaks or pipe damage.

### **Pipeline Response to Fault Rupture**

A 36-ft (11-m)-long, five-piece section of a ductile pipeline was tested at the Cornell Large-Scale Lifelines Facility. The pipe had a total of four AMERICAN Earthquake Joint Systems. Two EJS castings were located 5 and 15 ft (1.5 and 3.6 m) north of the fault and two EJS castings at the same distances south of the fault. The pipe was pressurized to approximately 80 psi (550 kPa). The pipe was placed on a bed of compacted partially saturated sand, aligned, instruments checked, and then backfilled with compacted sand to a depth of cover of 31 in. (787 mm) above the pipe crown. The north section of the test basin was displaced along a  $50^\circ$  fault at a rate of 12 in. (300 mm) per minute. At a fault displacement of roughly 36.0 in. (914 mm), the pipe lost pressure. Additional 2.5 in. (63.5 mm) of test basin movement was applied to ensure a complete pressure loss in the system, and the test was then stopped. The 36.0 in. (914 mm) fault displacement

corresponds to 23.1 in. (587 mm) of axial extension of the test basin. Following excavation, a fracture was observed near the west springline of the FR Bell of the S15 EJS.

The test measurements confirm that the pipeline was able to accommodate fault rupture through axial displacements and deflections at all four Earthquake Joint Systems. They also provide a comprehensive and detailed understanding of how the movement was accommodated at each joint, the sequence of movements, and combined axial pullout and rotation at each joint. The combined axial movement of the four joints was 21.5 in. (561 mm), which exceeds the performance criteria of  $4 \times 4.8$  in. (122 mm) = 19.2 in. (488 mm) joint displacement for all four earthquake joint systems. On average, each EJS displaced on the order of 5.4 in. (137 mm). This displacement was close to movement during previous direct tension testing of the AMERICAN EJS. The maximum deflection measured at the EJS closest to the fault was about 9.4 degrees, thus demonstrating the ability of the joints to sustain significant levels of combined axial pullout and deflection. The maximum stresses sustained by the pipeline, corresponding to the largest pipeline deformation, were well within the elastic range of pipeline behavior.

The ductile iron pipeline equipped with AMERICAN Earthquake Joint System (EJS) was able to accommodate significant fault movement through axial pullout and rotation of the joints. Fault rupture simulated in the large-scale test is also representative of the most severe ground deformation that occurs along the margins of liquefaction-induced lateral spreads and landslides.

### **Finite Element Simulations**

Two-dimensional (2D) finite element (FE) analyses were performed for a 6- in. (150-mm)-diameter pipeline with AMERICAN EJS joints. The geometry and material characteristics used for the soil, pipe, and test dimensions were consistent with the large-scale split basin test performed at Cornell University. All pipeline dimensions used in the FE simulations are consistent with those for thickness Pressure Class 350 ductile iron available from AMERICAN.

The FE simulation results for joint opening vs. fault displacement and joint rotation vs. fault displacement, respectively, are in close agreement with the experimental measurements from the 6 in. (150 mm) pipeline used in the large-scale split basin test. The FE simulations show that the maximum axial force in the pipe were approximately 87 kips, and those measured approximately 81 kips (385 and 360 kN, respectively.) The maximum bending moments from the analytical

simulations were approximately 250 kip-in. and those measured were 200 kip-in. (28 and 23 kN-m, respectively.) The maximum axial strain predicted for the 6-in. (150-mm)-diameter pipelines was approximately 580  $\mu\epsilon$  (vs. 540 measured), and the maximum predicted bending strains were 1050  $\mu\epsilon$  (vs. 840 measured). The FE simulations for 6-in. (150-mm)-diameter pipe compare well with the measurements of maximum axial and bending responses measured in the large-scale split basin test at Cornell, thus providing confidence in the FE results.

### **Significance of Test Results**

The amount of tensile strain that can be accommodated with the ductile iron pipeline will depend on the spacing of the AMERICAN Earthquake Joint Systems and the positioning of the spigot within the bell at the pipeline joints. The four-joint pipeline used in the large-scale split-basin test was able to accommodate at least 21.5 in. (461 mm) of axial extension, corresponding to an average tensile strain of 4.4% along the pipeline. Such extension is large enough to accommodate the great majority (over 99%) of liquefaction-induced lateral ground strains measured by high resolution LiDAR after each of four major earthquakes during the recent Canterbury Earthquake Sequence (CES) in Christchurch, NZ. These high resolution LiDAR measurements for the first time provide a comprehensive basis for quantifying the ground strains caused by liquefaction on a regional basis. To put the CES ground strains in perspective, the levels of liquefaction-induced ground deformation measured in Christchurch exceed those documented in San Francisco during the 1989 Loma Prieta earthquake and in the San Fernando Valley during the 1994 Northridge earthquake. They are comparable to the levels of most severe liquefaction-induced ground deformation documented for the 1906 San Francisco earthquake, which caused extensive damage to the San Francisco water distribution system. The fault rupture test confirms that the ductile iron pipes equipped with the AMERICAN Earthquake Joint Systems are able to sustain without leakage large levels of ground deformation through axial displacement and deflection under full-scale conditions of abrupt ground rupture.

## TABLE OF CONTENTS

Executive Summary .....	i
Table of Contents .....	v
List of Figures .....	vii
List of Tables .....	ix

<b><u>Section</u></b>	<b><u>Page</u></b>
1 Introduction and Organization	1
2 Tensile Coupon Tests	2
2.1 Introduction	2
2.2 Testing and Procedure	2
2.3 Testing Results	3
2.3.1 Stress vs. Strain Curves	3
2.3.2 Young's Modulus, Yield Strength, and Proportional Limit	5
2.3.3 Ultimate Tensile Strength and Strain	5
2.3.4 Poisson's Ratio	6
2.4 Comparison of Test Results to ANSI/AWWA C151/A21.51-09	7
3 Earthquake Joint System (EJS) Joint Tension and Compression Tests	9
3.1 Introduction	9
3.2 Tension Test 1	9
3.2.1 Instrumentation	9
3.2.2 Force vs. Displacement	10
3.2.3 FR Bell Axial Strains	13
3.2.4 SE Spigot Axial Strains	13
3.2.5 SE Spigot Hoop Strains	18
3.3 Tension Test 2 and Comparisons	18
3.4 Compression Test	20
3.4.1 Instrumentation and Test Procedures	20
3.4.2 Force vs. Displacement	21
3.2.3 SE Spigot Axial Strains	25
3.2.4 FR Bell Axial Strains	25
3.5 Summary of Joint Tension and Compression Tests	28
4 Four-Point Bending of Flex-Ring and EJS Pipe	29
4.1 Introduction	29
4.2 Four-Point Bending of Flex-Ring Joint Pipe	29
4.2.1 Joint Description	29
4.2.2 Instrumentation and Testing Procedures	29
4.2.3 Calculation Approach	32

## TABLE OF CONTENTS (continued)

<b><u>Section</u></b>	<b><u>Page</u></b>
4.2.4 Test Procedures	33
4.2.5 Pressure	34
4.2.6 String Pot Measurements	34
4.2.7 Moment vs. Rotations	36
4.3 Four-Point Bending of Earthquake Joint System	38
4.3.1 Joint Description	38
4.3.2 Instrumentation and Testing Procedures	38
4.3.3 Calculation Approach	40
4.3.4 Test Procedures	41
4.3.5 Pressure	41
4.3.6 String Pot Measurements	41
4.3.7 Moment vs. Rotations	43
4.4 Summary of Four-Point Bending Tests	45
5 Large Scale Testing of Fault Rupture Effects	47
5.1 Introduction	47
5.2 Experimental Setup	47
5.2.1 Test Procedure	49
5.2.2 Instrumentation	49
5.2.3 Soil Preparation	54
5.3 Experimental Results of Split Basin Test	54
5.3.1 Test Basin Movements	54
5.3.2 Internal Water Pressure	55
5.3.3 Joint Pullout	56
5.3.4 Joint Rotations (Deflections)	59
5.3.5 End Loads and Pipe Axial Forces	63
5.3.6 Bending Moments	65
5.3.7 Deformed Shape and Pipe Failure	68
5.4 Summary of Large-Scale Testing	70
6 Finite Element Simulations	73
6.1 Large-Scale Split Basin Test	73
6.2 Finite Element Simulations	75
6.3 Finite Element Model Characteristics	75
6.4 Finite Element Simulation Results	77
6.5 Summary of Finite Element Simulations	80
7 Summary	81
References	85

## TABLE OF CONTENTS (continued)

### LIST OF FIGURES

<b><u>Figure</u></b>	<b><u>Page</u></b>
2.1 Schematic of Tensile Coupon Specimen	3
2.2 Baldwin Testing Apparatus	3
2.3 Stress vs. Strain Curve for Specimen 1	4
2.4 Stress vs. Strain Curve for Specimen 2	4
2.5 Stress vs. Strain Curve for Specimen 3	4
2.6 Average Young's Modulus and Yield Stress	4
2.7 Stress vs. Strain Curve to Failure Using Clip-on Extensometer Data	6
2.8 Specimen 1 Tensile Crack Locations	6
2.9 Transverse vs. Axial Strain in Used to Determine Poisson's Ratio in Elastic Range	7
3.1 AMERICAN Earthquake Joint System (EJS)	10
3.2 Tension Test Layout	10
3.3 Pressure vs. Average Joint Opening	12
3.4 Tensile Force vs. Average FR Joint Opening	12
3.5 Tensile Force vs. Average SE Joint Opening	13
3.6 Circumferential Crack on Bell Section in Test 1	14
3.7 Tensile Force vs. FR Spigot Axial Strains	15
3.8 FR Spigot Axial Strains vs. Average FR Joint Opening	15
3.9 FR Spigot Axial Strains vs. Average SE Joint Opening	15
3.10 Tensile Force vs. SE Spigot Axial Strains	16
3.11 SE Spigot Axial Strains vs. Average FR Joint Opening	16
3.12 Spigot Axial Strains vs. Average SE Joint Opening	16
3.13 Tensile Force vs. SE Spigot Hoop Strains	17
3.14 SE Spigot Hoop Strains vs. Average FR Joint Opening	17
3.15 SE Spigot Hoop Strains vs. Average SE Joint Displacement	17
3.16 Tensile Force vs. Average FR Joint Opening for Tests 1 and 2	19
3.17 Tensile Force vs. Average SE Joint Opening for Tests 1 and 2	19
3.18 Tensile Force vs. Average Total Joint Opening for Tests 1 and 2	20
3.19 Compression Test Layout	22
3.20 Test Specimen in Compression Frame	23
3.21 Internal Pressure vs. Time	23
3.22 Actuator Compressive Displacement vs. Time	23
3.23 Compressive Force vs. FR Joint Displacement	24
3.24 Compressive Force vs. SE Joint Displacement	24
3.25 Compressive Force vs. Total Joint Displacement	25

## TABLE OF CONTENTS (continued)

<b><u>Figure</u></b>	<b><u>Page</u></b>
3.26 Compressive Force vs. SE Spigot Axial Strains	26
3.27 SE Spigot Axial Strains vs. Average FR Joint Closure	26
3.28 SE Spigot Axial Strains vs. Average SE Joint Closure	26
3.29 Compressive Force vs. FR Bell Axial Strains	27
3.30 FR Bell Axial Strains vs. Average FR Joint Closure	27
3.31 FR Bell Axial Strains vs. Average SE Joint Closure	27
4.1 Cutaway View of AMERICAN Flex-Ring Joint prior to Snap Ring Assembly	30
4.2 Schematic of Instrumentation for FR-FRE Bending Test	30
4.3 Photo of FR-FRE Bending Specimen before Testing	31
4.4 Pressure vs Time for FR-FRE Bending Test	35
4.5 VSP Measurements for FR-FRE Bending Test	35
4.6 HSP Measurements vs. VSP Rotation for FR-FRE Bending Test	35
4.7 Moment vs. Rotation for FR-FRE Bending Test	36
4.8 FR-FRE First Leakage of 3.5 ml/min	37
4.9 FR-FRE Leakage of 100 ml/min at End of Test	37
4.10 AMERICAN Earthquake Joint System (EJS)	38
4.11 Schematic of Instrumentation for EJS Bending Test	39
4.12 Photo of AMERICAN EJS Bending Specimen before Testing	39
4.13 Pressure vs. Time for EJS Bending Test	42
4.14 VSP Measurements for EJS Bending Test	42
4.15 HSP Measurements vs. VSP Rotation for EJS Bending Test	42
4.16 Moment vs. Rotation for EJS Bending Test	43
4.17 First Leak (25 ml/min) at FR Joint in EJS	44
4.18 Leak (1,430 ml/min) at FR Joint in EJS	44
4.19 Pipe Failure at FR Bell in EJS	45
4.20 Moment-Rotation Results from Four-Point Bending Tests on American DI Pipe Joints	46
5.1 Plan View of Pipe Centered EJS Specimen in Test Basin	48
5.2 Setup of String Pots	52
5.3 Pipe Joints with Protective Shielding	52
5.4 Particle Size Distribution of RMS Graded Sand	55
5.5 Fault Displacement vs. Time	56
5.6 Internal Water Pressure vs. Fault Displacement	56
5.7 Average FR Joint Openings vs. Fault Displacement	57
5.8 Average SE Joint Openings vs. Fault Displacement	57
5.9 Total EJS Openings for All Joints vs. Fault Displacement	57

## TABLE OF CONTENTS (continued)

<b><u>Figure</u></b>	<b><u>Page</u></b>
5.10 FR Rotations vs. Fault Displacement	60
5.11 FR Rotations vs. Fault Displacement	60
5.12 Total EJS Deflections vs. Fault Displacement	60
5.13 Joint Deflections from Leica Survey Data	62
5.14 Comparison of Average End Force from Load Cells and Strain Gages	64
5.15 Axial Forces in Pipe vs. Distance from Fault	66
5.16 Bending Moments in Pipe vs. Distance from Fault	67
5.17 Fault Rupture at Pipe Failure	68
5.18 Images of Pipeline (a) before burial and (b) after excavation	69
5.19 Ruptured Pipe at S15 FR Bell Following Test without Protective Shield	70
6.1 Plan View of Large-Scale Split Basin Test for AMERICAN Test	74
6.2 2D FE Model Setup for a Pipeline under Fault Rupture	74
6.3 Nonlinear Axial Force-Displacement and Moment-Deflection Relationships for EJS Analytical Modeling	76
6.4 Total EJS Joint Opening vs. Fault Displacement for 6 in. (150 mm) Pipes	78
6.5 Total EJS Joint Deflections vs. Fault Displacement for 6 in. (150 mm) Pipes	78
6.6 Axial Pipe Forces vs. Fault Displacement	79
6.7 Axial Pipe Forces at Fault Crossing vs. Fault Displacement	79
6.8 Bending Moment vs. Fault Displacement for 6 in. (150 mm) Pipes	79

## LIST OF TABLES

<b><u>Table</u></b>	<b><u>Page</u></b>
2.1 Young's Modulus, Yield Stress, and Proportional Limit	5
2.2 Summary of Ultimate Tensile Stress and Strain	6
2.3 Poisson's Ration in Elastic Range	7
2.4 Comparison of Material Strengths to ANSI/AWWA C151/A21.51-09	8
3.1 Instrumentation for AMERICAN EJS Tension Test	11
3.2 Instrumentation for AMERICAN EJS Compression Test	22
4.1 Instrumentation for AMERICAN FR-FRE Bending Test	31
4.2 Instrumentation for AMERICAN EJS Bending Test	40
4.3 Results of Four-Point Bending Tests	46
5.1 Strain Gage Locations and Coding System for EJS Split-basin Test	50
5.2 String Pot Locations and Labeling for EJS Split-basin Test	53
5.3 Load Cell Locations and Labeling for EJS Split-basin Test	53

## TABLE OF CONTENTS (completed)

<b><u>Table</u></b>	<b><u>Page</u></b>
5.4 Joint Openings at 36 in. (914 mm) Fault Movement	58
5.5 Joint Deflections	63
6.1 FEA and Measured Maximum Axial Forces, Moments, and Strains for 6 in. (150 mm) AMERICAN Pipe with EJS	80

## **Section 1**

### **Introduction and Organization**

This report is submitted to the American Cast Iron Pipe Company (herein referred to as AMERICAN), and presents the results of physical testing on the standard 6-in. (216-mm)-diameter ductile iron pipe and pipe with an AMERICAN Earthquake Joint System (EJS). The purpose of the testing is to demonstrate the ability of the EJS to accommodate axial pullout and deflection and characterize the pipe mode of failure. The work was undertaken in the Cornell Large Scale Lifelines Testing Facility, which is part of the Bovay Laboratory Complex at Cornell University.

The report is organized into seven sections, the first of which provides introductory remarks and describes the report organization. Section 2 presents the results of tensile coupon tests to characterize the basic stress-strain-strength characteristics of the ductile iron. Section 3 presents test results from two direct tension and one compression test on DI pipe section with the Earthquake Joint System (EJS). The tension and compression capacities of the joints are evaluated, and limit conditions of pipe leakage are provided. Section 4 describes and reports on the results of four-point bending tests in standard Flex-Ring pipe with an FR-FRE joint and also a bending test with the EJS. A large-scale split basin test with four AMERICAN EJSs is described in Section 5. Joint extensions, deflections, and pipe strains and forces from the full-scale test are given. Section 6 presents the results of the 2-D finite element simulation of the experimental pipeline. The modeling procedures are discussed, and results compared with key experimental measurements. Section 7 provides a summary of the testing and concluding remarks.

## **Section 2**

### **Tensile Coupon Tests**

#### **2.1 Introduction**

This section of the report describes the uniaxial tension testing of ductile iron (DI) specimens provided by the American Cast Iron Pipe Company (AMERICAN). The test results are used to determine the strength and ductility of the material. Tensile coupons were machined from a DI pipe specimen and tested in tension to determine the yield strength, ultimate strength, and ultimate strain of the material. All testing was completed in accordance with ASTM – E8 2013 standards (ASTM, 2013) to ANSI/AWWA C151/A21.51-09 60-42-10 [60 ksi (414 MPa) ultimate tensile strength, 42 ksi (290 MPa) yield, and 10% elongation] specifications (AWWA, 2009.)

#### **2.2 Testing and Procedure**

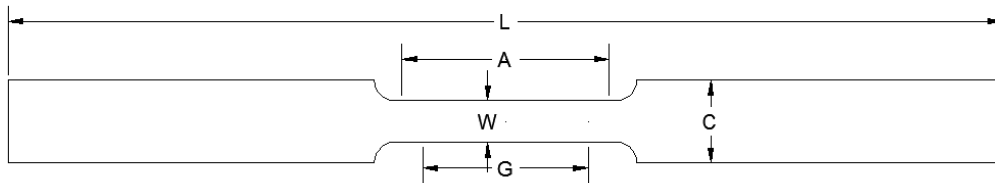
The tensile coupons were machined from the pipe to obtain the nominal dimensions shown in Figure 2.1. These dimensions comply with ASTM - E8 2013 (ASTM, 2013) for large diameter tubes. A Baldwin Hamilton 60 BTE Universal Testing Machine was used to apply tensile loads. This load frame was fitted with a pressure sensor to measure force in the system. The machine was calibrated in April of 2015. A photo of the test setup is provided in Figure 2.2.

Three tensile coupon specimens were tested. All three specimens were instrumented with axial and transverse strain gages. Bondable axial and transverse strain gages were used in testing to measure small strains. These gages were mounted in the center of the reduced area of the specimen. Strain gages were used to evaluate the stress vs. strain relationship at lower strains because they are considerably more accurate at these levels. These gages debond typically at strains of 2 to 4%, rendering them ineffective at larger strain levels. A clip-on extensometer was used to measure axial strain to failure. This device is not as accurate as the strain gages at smaller strains, but provides for a reliable assessment of strain at larger values, specifically those past the failure of the bonded strain gages.

## 2.3 Testing Results

### 2.3.1 Stress vs. Strain Curves

The engineering uniaxial stresses vs. axial strains for all three Specimens are shown in Figures 2.3 to 2.5. These figures show both the bondable strain gage and extensometer data.



Sheet-Type, .5 in Wide	
<i>Dimensions</i>	<i>Length (in.)</i>
G - Gauge Length	2.00
W - Width	0.50
T - Thickness	
R - Radius	0.50
L - Overall Length	8.00
A - Length of Reduced Section	2.25
C - Width of Grip Section	1.00

Figure 2.1. Schematic of Tensile Coupon Specimen



Figure 2.2. Baldwin Testing Apparatus

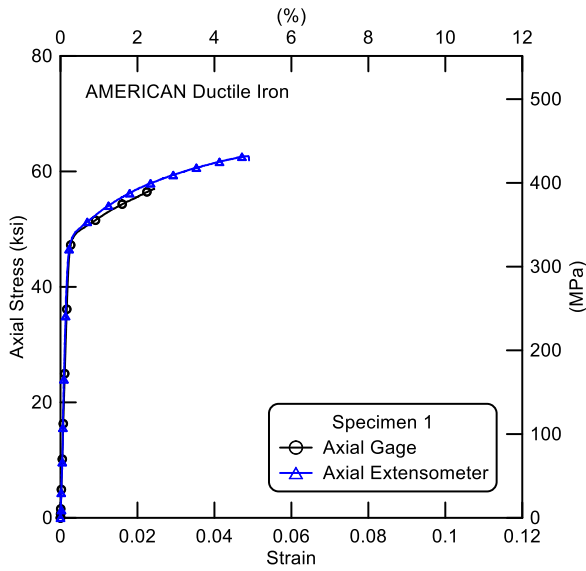


Figure 2.3. Stress vs. Strain Curve for Specimen 1

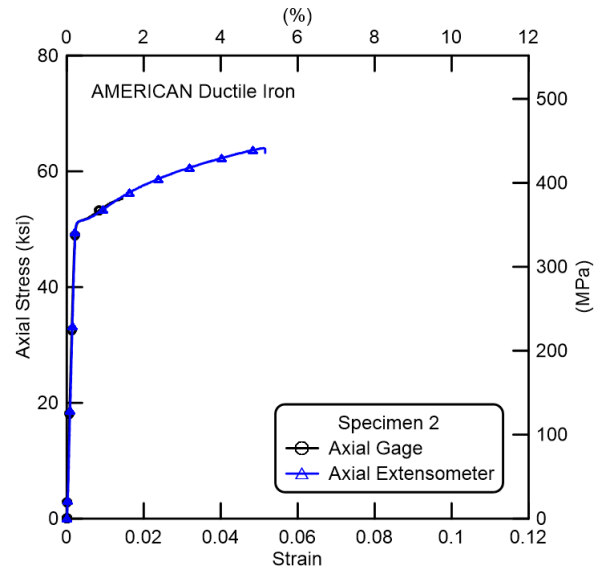


Figure 2.4. Stress vs. Strain Curve for Specimen 2

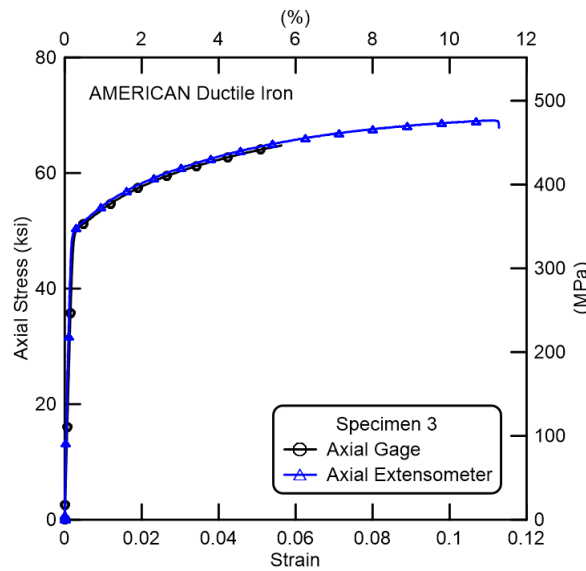


Figure 2.5. Stress vs. Strain Curve for Specimen 3

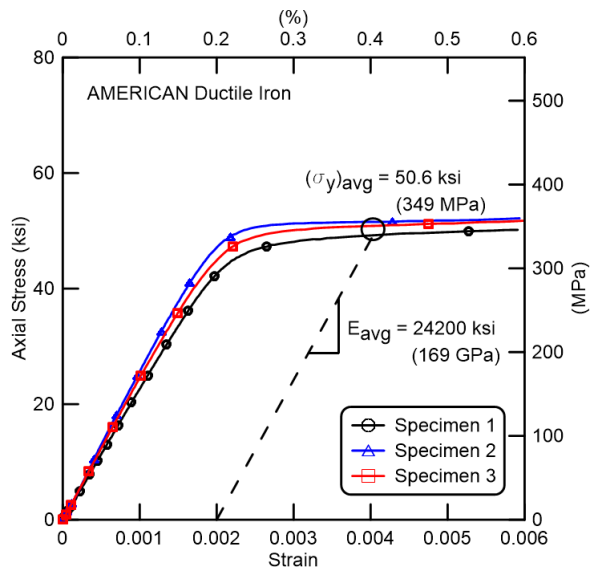


Figure 2.6. Average Young's Modulus and Yield Stress

Table 2.1. Young's Modulus, Yield Stress, and Proportional Limit

Specimen	Young's Modulus E (ksi)	Offset Yield $\sigma_y$ (ksi)	Proportional Limit $\sigma_{prop}$ (ksi)
1	22,500	49.4	35.9
2	25,600	51.5	35.6
3	24,500	50.9	30.8
Average	24,200	50.6	34.1
Std. Dev.	1,280	0.9	2.3

1 ksi = 6.89 MPa

### 2.3.2 Young's Modulus, Yield Strength, and Proportional Limit

Young's modulus was computed using the elastic region of the stress vs. strain curve and the bonded axial strain gage data. These data are shown to a strain of 0.006 in Figure 2.6. Young's modulus was determined by performing a linear regression for stress vs. strain from 2 ksi to 30 ksi (14 to 207 MPa). The yield strength,  $\sigma_y$ , was computed using the offset method, in which a line parallel to the linear part of the stress vs. strain plot is projected from 0.2% strain. The intersection of this line and the stress vs. strain curve provides an estimate of the yield stress for each specimen. The yield strains derived from the 0.2% offset are about 0.41%, which is almost double the 0.2% strain. The 0.14% strain is taken as a proportional limit, beyond which the relationship between stresses and the strains is no longer linear. The Young's modulus, yield stress, and proportional limit for the specimens are presented in Table 2.1. The average Young's modulus is 24,200 ksi (169 GPa) with a standard deviation of 1,280 ksi (8.8 GPa). The average yield stress is 50.6 ksi (349 MPa) with a standard deviation of 0.9 ksi (6.2 MPa). The average proportional stress is 34.1 ksi (235 MPa) with a standard deviation of 2.3 ksi (16 MPa).

### 2.3.3 Ultimate Tensile Strength and Strain

Axial stress vs. strain data from the clip-on extensometers were used to determine the ultimate strength and strain, as shown in Figure 2.7. Table 2.2 gives the failure tensile stress and failure strain for these three specimens. The average ultimate tensile stress was 65.3 ksi (450 MPa) with a standard deviation of 2.8 ksi (19 MPa). However, the ultimate strain could not be accurately measured because all three specimens broke outside of the clip-on lengths of the extensometers. Figure 2.8 shows the tensile crack location for specimen 1, which is outside the extensometer measurement range.

Table 2.2. Summary of Ultimate Tensile Stress and Strain

Specimen	Ultimate Tensile	
	Strength (ksi)	Strain (%)
1	62.7	5.3
2	64.0	5.3
3	69.1	11.7
Average	65.3	N/A
Std. Dev.	2.8	N/A

1 ksi = 6.89 MPa

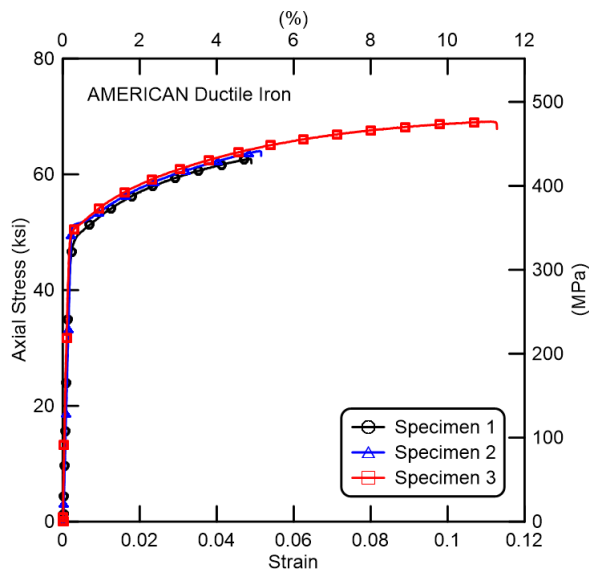


Figure 2.7. Stress vs. Strain Curve to Failure Using Clip-on Extensometer Data



Figure 2.8. Specimen 1 Tensile Crack Locations

### 2.3.4 Poisson's Ratio

Poisson's ratio,  $\nu$ , is the negative ratio of transverse strain to axial strain for uniaxial loading. Poisson's ratio was derived from the transverse and axial strain gage data while the stresses were in the elastic range, as shown in Figure 2.9. Poisson's ratio data are presented in Table 2.3. Poisson's ratio for all specimens was approximately 0.28 with a very small standard deviation of 0.004.

Table 2.3. Poisson’s Ratio in Elastic Range

Specimen	Poisson’s Ratio, $\nu$
1	0.27
2	0.28
3	0.28
Average	0.28
Std. Dev	0.004

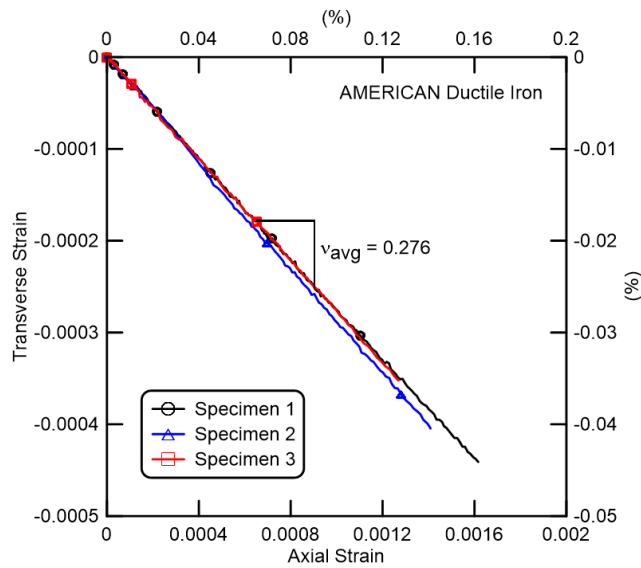


Figure 2.9. Transverse vs. Axial Strain in Used to Determine Poisson’s Ratio in Elastic Range

## 2.4 Comparison of Test Results to ANSI/AWWA C151/A21.51-09

The uniaxial tension testing of ductile iron (DI) from AMERICAN specimens was completed in accordance with ASTM – E8 2013 standards (ASTM, 2013). The yield stress, ultimate stress, and strain at failure are tabulated in Table 2.4 to compare the material properties with ANSI/AWWA C151/A21.51-09 60-42-10 specifications (AWWA, 2009). The yield and ultimate stresses are 20.5% and 8.8% greater than the specifications, respectively. However, the strain at failure could not be measured reliably because the specimens broke outside of the extensometer range.

Table 2.4. Comparison of Material Strengths to ANSI/AWWA C151/A21.51-09

Parameter	AMERICAN	ANSI/AWWA specifications	Difference (%)
Yield Stress (ksi)	50.6	42	20.5
Ultimate Stress (ksi)	65.3	60	8.8
Strain at Failure (%)	N/A	10	N/A

1 ksi = 6.89 MPa

## **Section 3**

### **Earthquake Joint System (EJS) Joint Tension and Compression Tests**

#### **3.1 Introduction**

This section summarizes the results of two tension tests and one compression test on the AMERICAN earthquake joint system (EJS) ductile iron pipes. The deep socket and FR bells have rubber gaskets to prevent leakage. The SE and FRE spigots are equipped with weld rings and iron locking rings. In each joint the weld ring bears against the locking ring preventing joint pullout. A schematic of the EJS is shown in Figure 3.1.

#### **3.2 Tension Test 1**

The tension test specimens were 15.5 ft. (4.72 m) long with an outside diameter of 6.9 in. (175 mm) and a wall thickness of 0.3 in. (7.6 mm.). The spigot was fully inserted inside the bell at the beginning of the test. Full insertion refers to the position when the ends of the SE and FRE spigots are in contact with the base of the deep socket and FR bell sockets, respectively. Figure 3.2 provides a schematic of the tension test.

##### **3.2.1 Instrumentation**

Four strain gages were mounted 40 in. (1016 mm) north of the FR bell face on the FR bell side of the pipe at the positions of 12, 3, 6, and 9 o'clock (crown, east springline, invert, and west springline, respectively). Four strain gages were also mounted 51 in. (1295 mm) south of the FR bell face on the FRE spigot side at the same positions. Four string pots were installed at quarter points around the pipe circumference to measure axial pullout of the SE spigot from the deep socket. Four additional string pots were also mounted to measure the FR joint opening. An actuator and load cell were installed on the load frame to apply and measure tensile force at the end of the pipe. An electronic pressure transducer, located at the north end cap, measured internal water pressure during the test sequence. The instrument locations and gage names are listed in Table 3.1.



a) Complete Joint System



b) Cutaway Views of AMERICAN EJS

Figure 3.1. AMERICAN Earthquake Joint System (EJS)

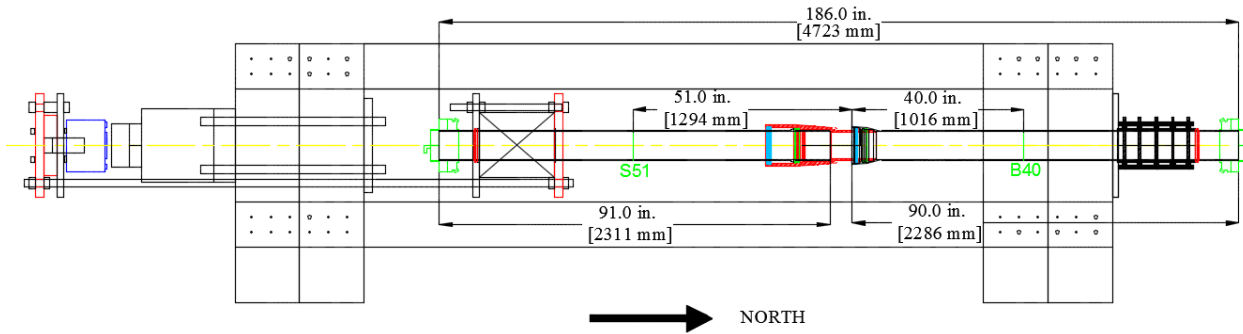


Figure 3.2. Tension Test Layout

### 3.2.2 Force vs. Displacement

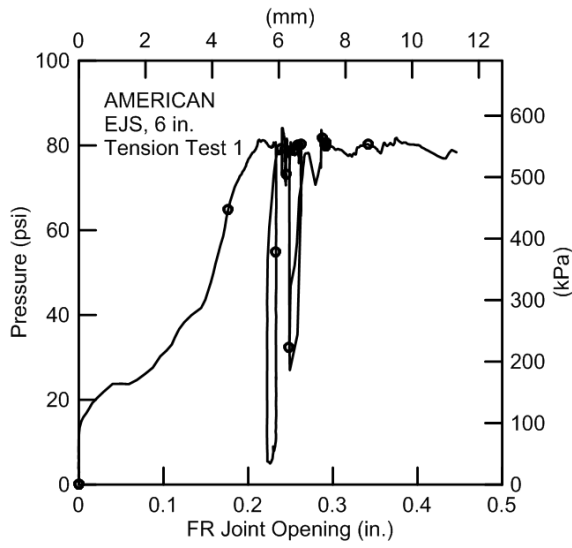
The specimen was filled with water and pressurized. As the pipe was filled with water, air inside the pipe was released. This procedure was repeated several times to make sure that no air remained in the pipe. The pressurizing sequence is shown in Figure 3.3. As the pressure was increased to approximately 12 psi (62 kPa), there were small pullout movements at both joints. Both joints opened slowly during the pressurization. When the SE joint reached 2.3 in. (58.4 mm), the joint suddenly opened to 4.5 in. (114 mm). The FR and SE joints continued to open slowly to 5.0 and 0.29 in. (127 and 7.4 mm), respectively. At an internal pressure of 80 psi (550 kPa), the axial loads on the pipe end caps were 2.4 kips (13 kN). Axial loading by the actuator was subsequently applied while the pipe was under the initial thrust load.

Table 3.1. Instrumentation for AMERICAN EJS Tension Test

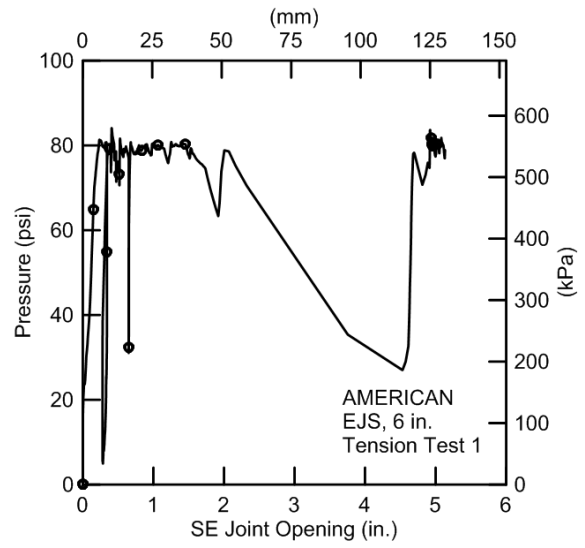
Location	Instrument	Instrument Name
40 in. North of FR Bell Face	Crown, Axial Strain	B40C
40 in. North of FR Bell Face	Invert, Axial Strain	B40I
40 in. North of FR Bell Face	East Springline, Axial Strain	B40E
40 in. North of FR Bell Face	West Springline, Axial Strain	B40W
51 in. South of FR Bell Face	Crown, Axial Strain	S51C
51 in. South of FR Bell Face	Invert, Axial Strain	S51I
51 in. South of FR Bell Face	East Springline, Axial Strain	S51E
51 in. South of FR Bell Face	West Springline, Axial Strain	S51W
51 in. South of FR Bell Face	Crown, Circumferential Strain	S51CC
51 in. South of FR Bell Face	Invert, Circumferential Strain	S51IC
51 in. South of FR Bell Face	East Springline, Circumferential Strain	S51EC
51 in. South of FR Bell Face	West Springline, Circumferential Strain	S51WC
SE Bell Face	SE Joint Crown String Pot	SE Crown
SE Bell Face	SE Joint Invert String Pot	SE Invert
SE Bell Face	SE Joint East Springline String Pot	SE East
SE Bell Face	SE Joint West Springline String Pot	SE West
FR Bell Face	FR Joint Crown String Pot	FR Crown
FR Bell Face	FR Joint Invert String Pot	FR Invert
FR Bell Face	FR Joint East Springline String Pot	FR East
FR Bell Face	FR Joint West Springline String Pot	FR West
Actuator	Load Cell	Interface Load
Actuator	Displacement	Act. Disp.
Internal Pressure	Pressure Transducer	Pressure

1 in. = 25.4 mm

Loading began at a rate of 1 in. (25.4 mm) per minute. Figures 3.4 and 3.5 show the tensile force plotted against FR and SE average joint opening, respectively. Prior to failure the pipe reached a peak load of 155 kips (689 kN) at 0.45 and 5.1 in. (11 and 130 mm) of axial displacement at the FR and SE joints, respectively. The pipe had a large circumferential crack around the FR bell section. Figure 3.6 shows the Test 1 specimen after the test. Figure 3.6 a) is a view looking into the bell. Figure 3.6 b) shows a view of the fracture from inside the bell. Figures 3.6c) to f) show the bell crack starting at the crown (Figure 3.6 c) and rotating to the west springline (Figure 3.6f.)



a) FR Joint



b) SE Joint

Figure 3.3. Pressure vs. Average Joint Opening

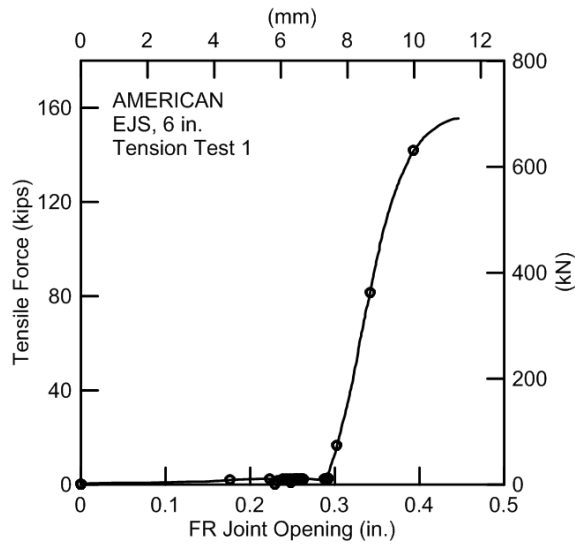
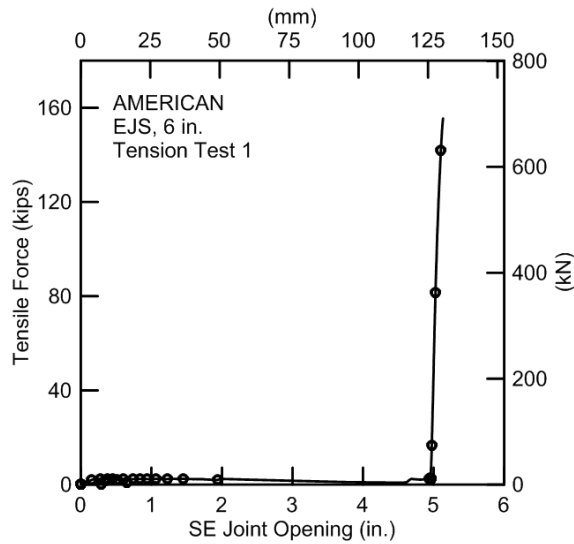
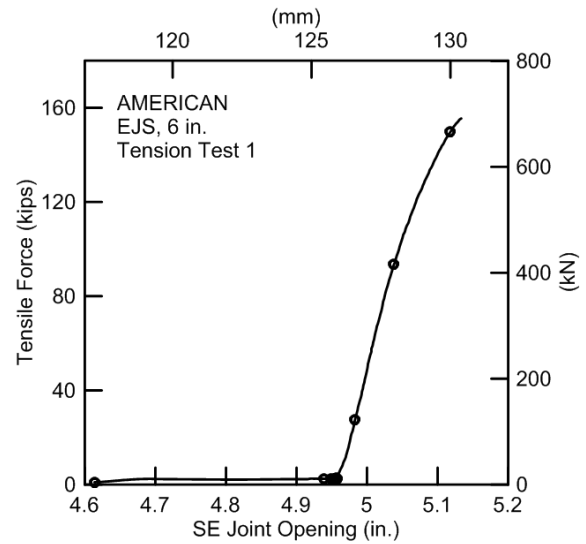


Figure 3.4. Tensile Force vs. Average FR Joint Opening



a) Full Displacement Range



b) Between 4.6 and 5.2 in. (119 to 132 mm) of Joint Opening

Figure 3.5. Tensile Force vs. Average SE Joint Opening

### 3.2.3 FR Bell Axial Strains

The maximum axial tensile strain on the FR bell side was  $1,450 \mu\epsilon$  (0.145%) and developed at the invert when the maximum load of 155 kips (689 kN) was attained at 0.45 and 5.1 in. (11 and 130 mm) of the FR and SE joint opening, respectively. The relationships between FR bell axial strains and the tensile force, FR joint opening, and SE joint opening are shown in Figures 3.7, 3.8, and 3.9, respectively. Recall that there were rapid SE and FR joint displacements of 5.0 and 0.29 in. (127 and 7.4 mm), respectively, as internal pressure was applied.

### 3.2.4 SE Spigot Axial Strains

The relationships between SE spigot axial strains and the tensile force, FR joint opening, and SE joint opening are shown in Figures 3.10, 3.11, and 3.12, respectively. A maximum axial tensile strain of  $1,710 \mu\epsilon$  (0.171%) was measured at the invert of the SE spigot when the maximum load reached 155 kips (689 kN).



a) Bell Face



b) Inside East Springline



c) Crown



d) East Springline



e) Invert



f) West Springline

Figure 3.6. Circumferential Crack on Bell Section in Test 1

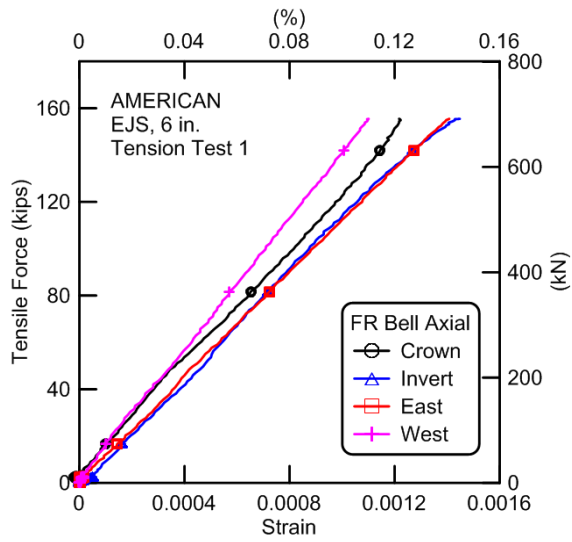


Figure 3.7. Tensile Force vs. FR Bell Axial Strains

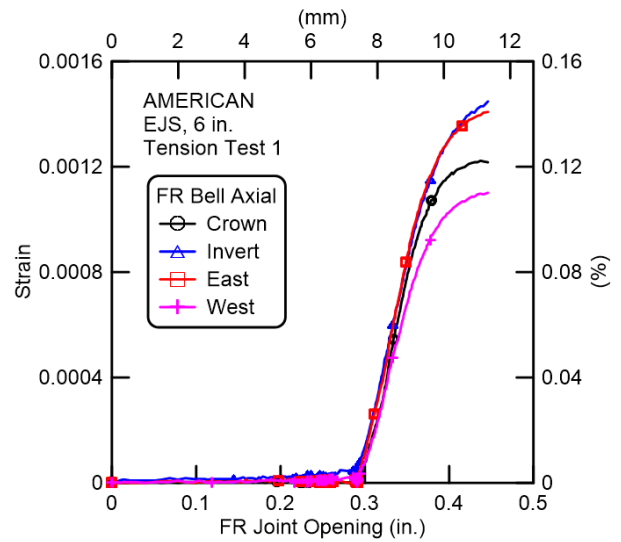
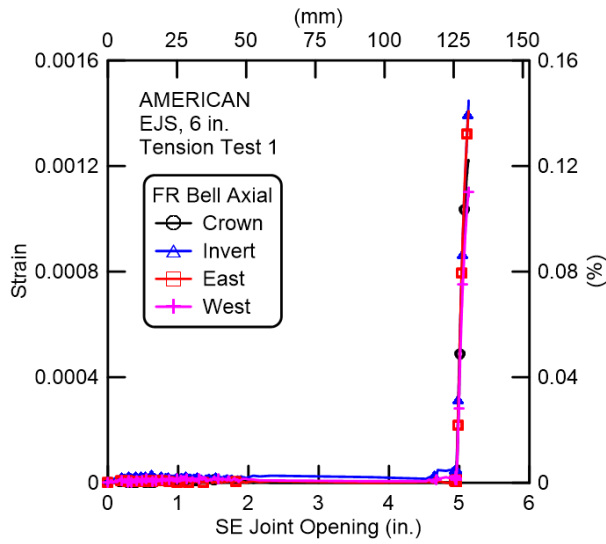
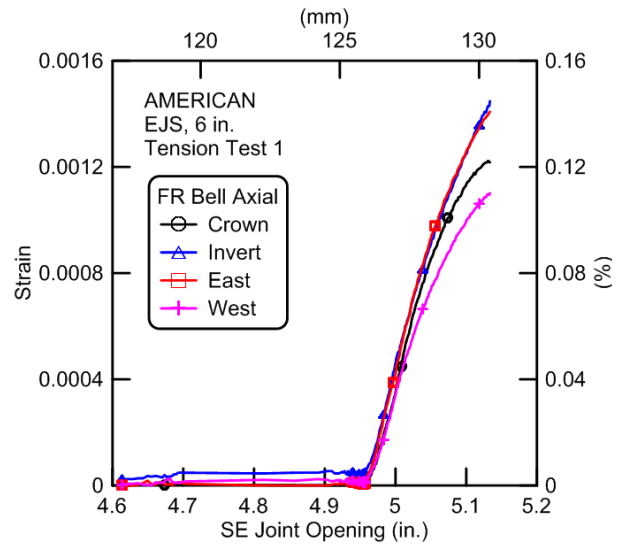


Figure 3.8. FR Bell Axial Strains vs. Average FR Joint Opening



a) Full Displacement Range



b) Between 4.6 to 5.2 in. (119 to 132 mm) of SE Joint Opening

Figure 3.9. FR Bell Axial Strains vs. Average SE Joint Opening

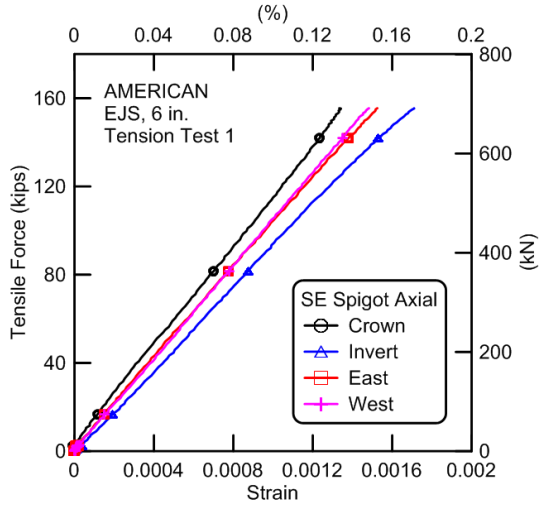


Figure 3.10. Tensile Force vs. SE Spigot Axial Strains

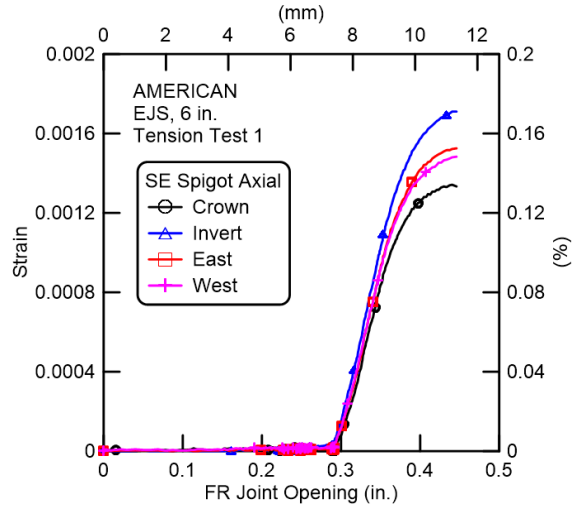
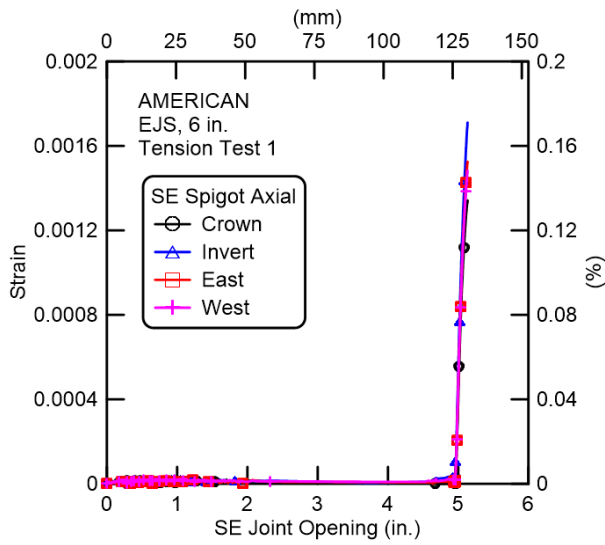
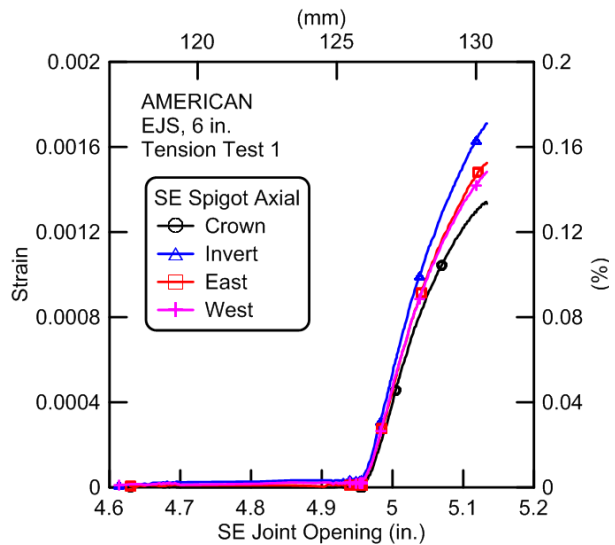


Figure 3.11. SE Spigot Axial Strains vs. Average FR Joint Opening



a) Full Displacement Range



b) Between 4.6 to 5.2 in. (119 to 132 mm) of SE Joint Opening

Figure 3.12. SE Spigot Axial Strains vs. Average SE Joint Opening

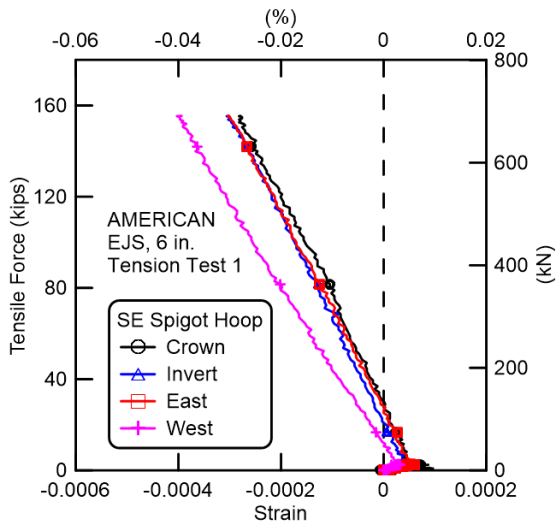


Figure 3.13. Tensile Force vs. SE Spigot Hoop Strains

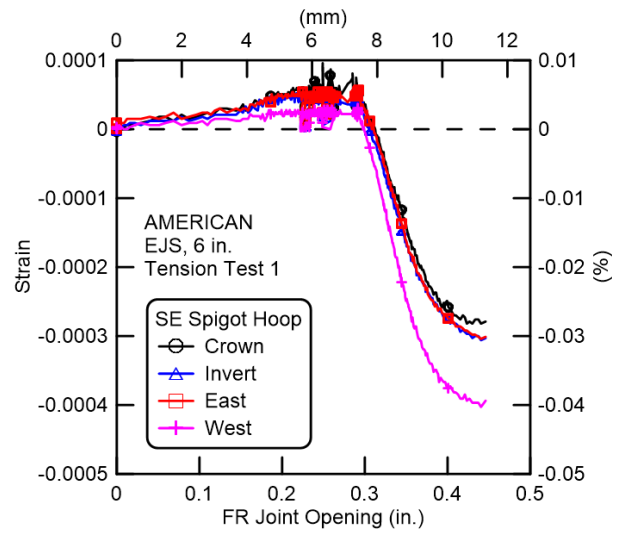
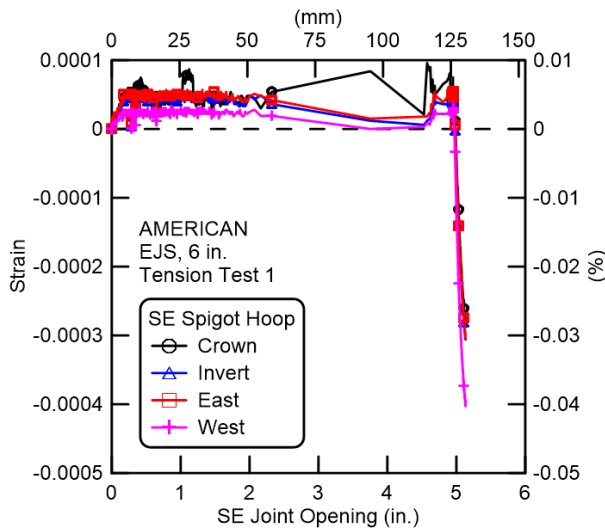
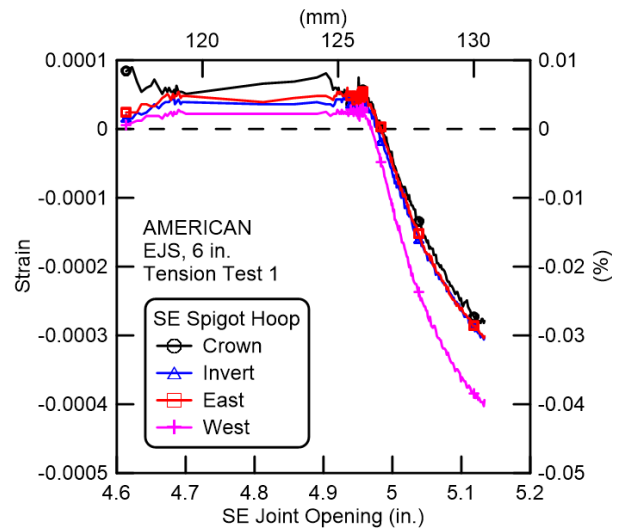


Figure 3.14. SE Spigot Hoop Strains vs. Average FR Joint Opening



a) Full Displacement Range



b) Between 4.6 to 5.2 in. (119 to 132 mm) of SE Joint Opening

Figure 3.15. SE Spigot Hoop Strains vs. Average SE Joint Displacement

### 3.2.5 SE Spigot Hoop Strains

Figures 3.13, 3.14, and 3.15 show the tensile force vs. the SE spigot hoop strain, the spigot hoop strain vs. the average FR joint opening, and the spigot hoop strain vs. the average SE joint opening, respectively. Spigot hoop strains at four positions (crown, invert, east, and west) were all initially positive (tensile), caused by internal pressure. The actuator then began applying axial displacement to the spigot. When the spigot weld ring made contact with the locking ring, tensile stresses were developed in the longitudinal direction of the pipe with attendant compressive stresses in the hoop direction. As a result, the spigot hoop strain become negative (compressive). The maximum compressive hoop strain of  $400 \mu\epsilon$  (0.04%) was measured at the west springline.

### 3.3 Tension Test 2 and Comparisons

A second tension test was performed on the AMERICAN EJS. Its purpose was to provide a replicate test to confirm tensile capacity and axial pullout displacement. The pipe was initially fully inserted. The pipe dimensions and instrumentation were identical to that of Tension Test 1.

This section presents a comparison of the two test results. Figures 3.16, 3.17, and 3.18 show nearly identical plots of tensile force vs. average FR, SE, and total joint openings for the two tests, respectively. The FR and SE joints of both tests opened approximately 0.3 and 5 in. (7.6 and 127 mm) upon pressurization, respectively. Test 1 reached a maximum force of 155 kips (689 kN) at 0.45 in. (11 mm) of FR joint opening and 5.1 in. (130 mm) of SE joint displacement. The maximum axial load for Test 2 was 144 kips (641 kN) at 0.41 in. (10 mm) of FR joint opening and 5.1 in. (130 mm) of SE joint displacement. When the maximum tensile load was achieved, the FR bell cracked circumferentially in both tests. The average maximum tensile force of the two tests was 149.5 kips (665 kN). This force exceeds Class A of ISO 16134-2006 (ISO, 2006) tensile capacity of  $17D$ , where  $D$  is the nominal diameter in inches, and the force is expressed in kips, which is equivalent to 102 kips (450 kN). The average total joint opening, which is an average of the summation of the FR and SE joint displacements for both tests, was 5.53 in. (140 mm).

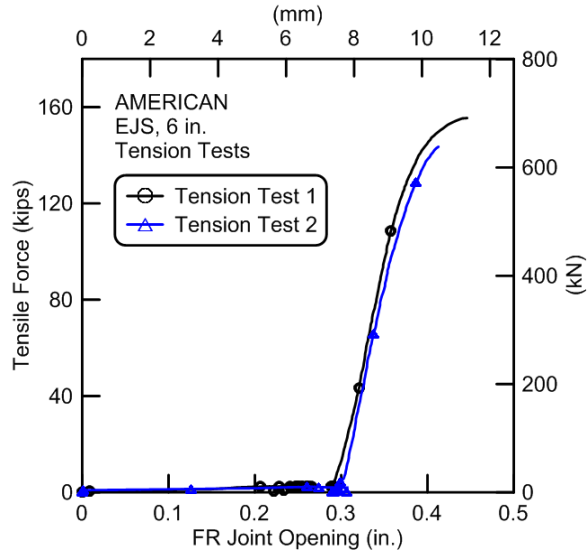
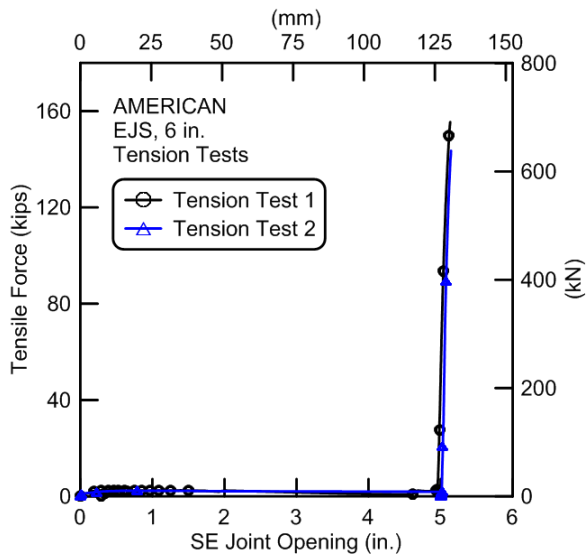
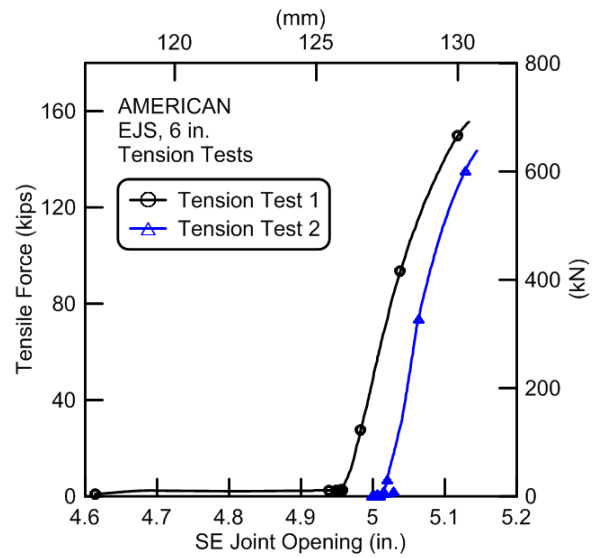


Figure 3.16. Tensile Force vs. Average FR Joint Opening for Tests 1 and 2

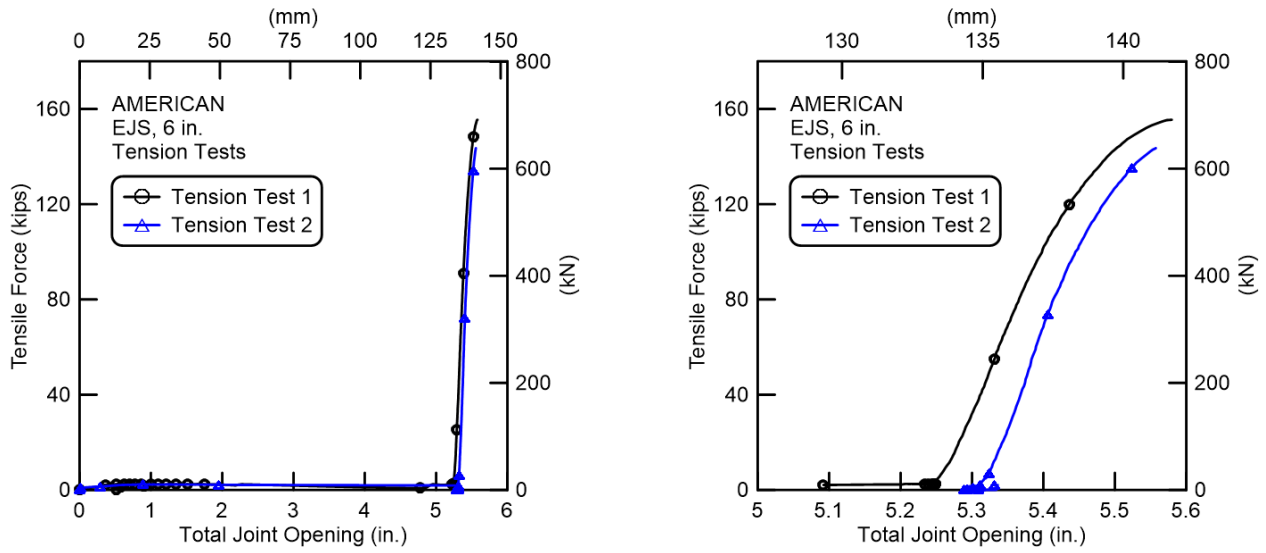


a) Full Displacement Range



b) Between 4.6 to 5.2 in. (119 to 132 mm) of SE Joint Opening

Figure 3.17. Tensile Force vs. Average SE Joint Opening for Tests 1 and 2



a) Full Displacement Range

b) Between 4.6 to 5.2 in. (119 to 132 mm) of SE Joint Opening

Figure 3.18. Tensile Force vs. Average Total Joint Opening for Tests 1 and 2

### 3.4 Compression Test

The compression test specimen was 13.1 ft. (4.0 m) long with an outside diameter of 6.9 in. (175 mm) and a wall thickness of 0.3 in. (7.6 mm.). The joint was fully extended at the beginning of the test. Full extension refers to the position when the weld rings of the SE and FRE spigots are in contact with the lips of the deep socket and FR bell sockets, respectively. Figure 3.19 provides a schematic of the compression test.

#### 3.4.1 Instrumentation and Test Procedures

Four strain gages were mounted 23 in. (584 mm) north of the FR bell face on the FR bell side of the pipe (B23 in Figure 3.19) at the positions of 12, 3, 6, and 9 o'clock (crown, east springline, invert, and west springline, respectively). Four other strain gages were also mounted 38 in. (965 mm) south of the FR bell face on the FRE spigot side (S38 in Figure 3.19) at the same positions. Four string pots were installed at quarter points around the pipe circumference to measure axial movement of the SE spigot into the deep socket. Four additional string pots were also mounted to measure the FR joint axial compressive displacement. An actuator and load cell were installed on the load frame to apply and measure compressive force at the end of the FRE spigot. An electronic

pressure transducer, located at the north end cap, measured internal water pressure during the test sequence. The instrument locations and gage names are listed in Table 3.2.

After the specimen was instrumented and centered in the test frame, the test was initiated by starting the data acquisition system and laboratory hydraulic systems. Figures 3.20 a) and b) show the test specimen mounted in the compression test frame. The specimen was filled with water and pressurized to approximately 80 psi (552 kPa). As the actuator was pushing on the FRE spigot end and closing the joints, the internal pressure was manually readjusted to be within  $\pm 5$  psi (34 kPa) of 80 psi (550 kPa). The test was performed under displacement control using the servo-hydraulic actuator at a rate of 1 in. (25.4 mm) per minute. Compression was applied by the actuator in two discrete steps. The actuator had a range of 3.9 in. (99 mm.) for this test. After the full range of the actuator was reached, the pipe was depressurized, the actuator was retracted, and additional compression displacements were applied to the specimen. Figures 3.21 and 3.22 show the internal pressure and actuator displacement vs. time, respectively.

### 3.4.2 Force vs. Displacement

Compressive force and joint displacements were measured by the load cell and string potentiometers. Figures 3.23 and 3.24 show the compressive force plotted against the FR and SE average joint displacements, respectively. When the joint was fully engaged at 0.38 and 4.9 in. (9.7 and 124 mm) of FR and SE displacements there was a significant increase of compressive load. The pipe reached a compressive load of 256 kips (1,140 kN) at 0.58 in. (15 mm) of FR joint displacement and 5.3 in. (134 mm) of SE joint displacement before a leak was observed at the SE joint. The relationship of the compressive force vs. total joint displacement is presented in Figure 3.25. Forces at the proportional limit,  $P_{prop}$ , and yield limit,  $P_y$ , are shown in Figures 3.23, 3.24, and 3.25. The axial force,  $P$ , is given as:

$$P = \sigma A \tag{3.1}$$

where  $\sigma$  is the proportional stress of 34.1 ksi (235 MPa) or yield stress of 50.6 (349 MPa) based on the tensile coupon test data, and  $A$  is the cross-sectional area of the specimen of 6.22 in<sup>2</sup> (4010 mm<sup>2</sup>). Equation 3.1 gives forces at the proportional limit,  $P_{prop}$ , and yield limit,  $P_y$ , of 212 kips (943 kN) and 315 kips (1,400 kN), respectively. When the compressive force in the specimen exceeded the proportional limit, localized plastic deformation within the joint occurred, resulting in leakage when the load was about halfway between the proportional and plastic limits.

Table 3.2. Instrumentation for AMERICAN EJS Compression Test

Location	Instrument	Instrument Name
23 in. North of FR Bell Face	Crown, Axial Strain	B23C
23 in. North of FR Bell Face	Invert, Axial Strain	B23I
23 in. North of FR Bell Face	East Springline, Axial Strain	B23E
23 in. North of FR Bell Face	West Springline, Axial Strain	B23W
38 in. South of FR Bell Face	Crown, Axial Strain	S38C
38 in. South of FR Bell Face	Invert, Axial Strain	S38I
38 in. South of FR Bell Face	East Springline, Axial Strain	S38E
38 in. South of FR Bell Face	West Springline, Axial Strain	S38W
SE Bell Face	SE Joint Crown String Pot	SE Crown
SE Bell Face	SE Joint Invert String Pot	SE Invert
SE Bell Face	SE Joint East Springline String Pot	SE East
SE Bell Face	SE Joint West Springline String Pot	SE West
FR Bell Face	FR Joint Crown String Pot	FR Crown
FR Bell Face	FR Joint Invert String Pot	FR Invert
FR Bell Face	FR Joint East Springline String Pot	FR East
FR Bell Face	FR Joint West Springline String Pot	FR West
Actuator	Load Cell	Interface Load
Actuator	Displacement	Act. Disp.
Internal Pressure	Pressure Transducer	Pressure

1 in. = 25.4 mm

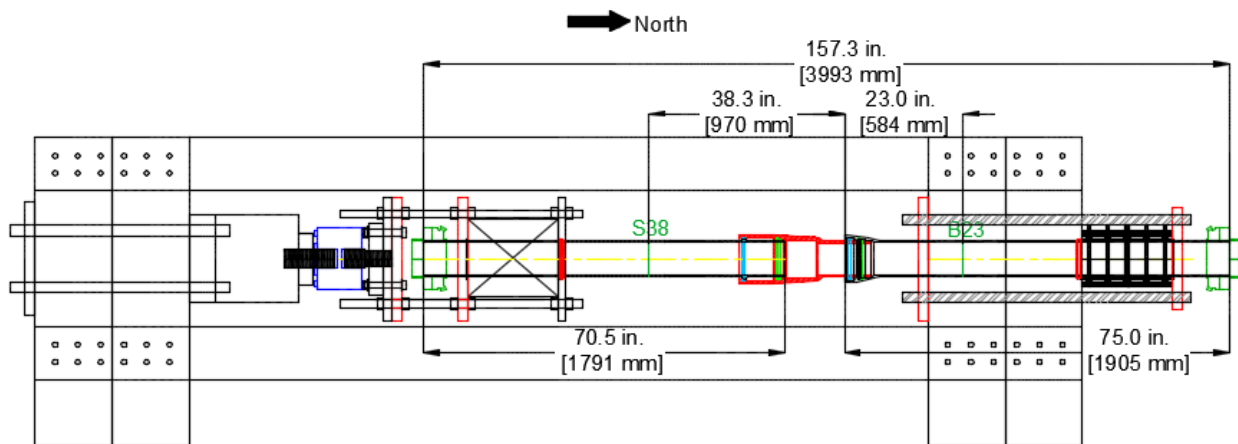


Figure 3.19. Compression Test Layout



a) Looking North



b) Looking South

Figure 3.20. Test Specimen in Compression Frame

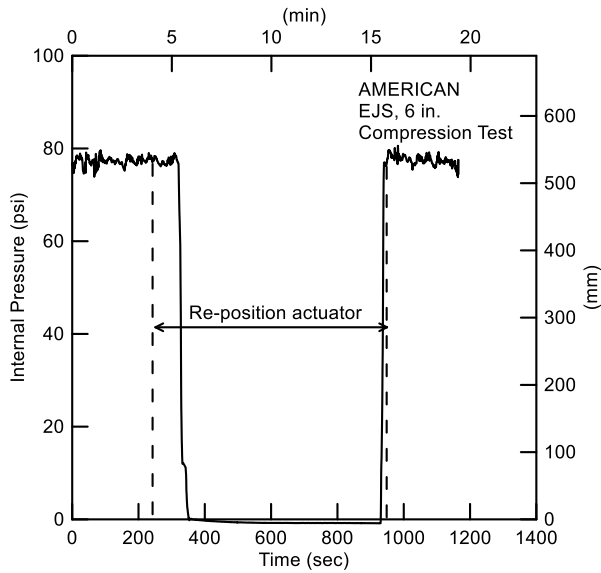


Figure 3.21. Internal Pressure vs. Time

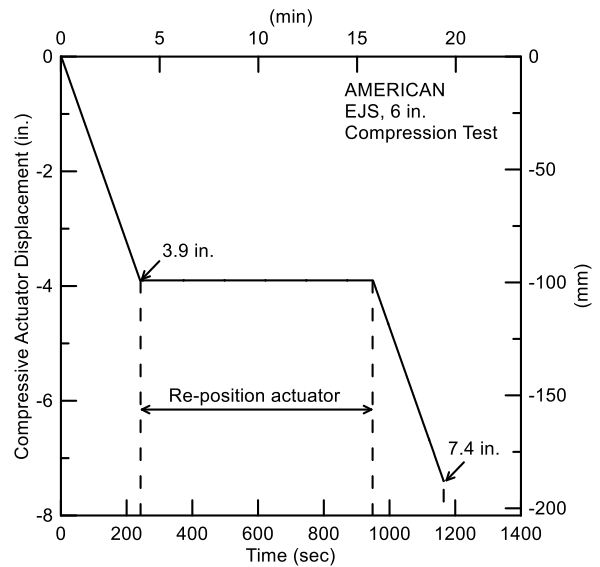


Figure 3.22. Actuator Compressive Displacement vs. Time

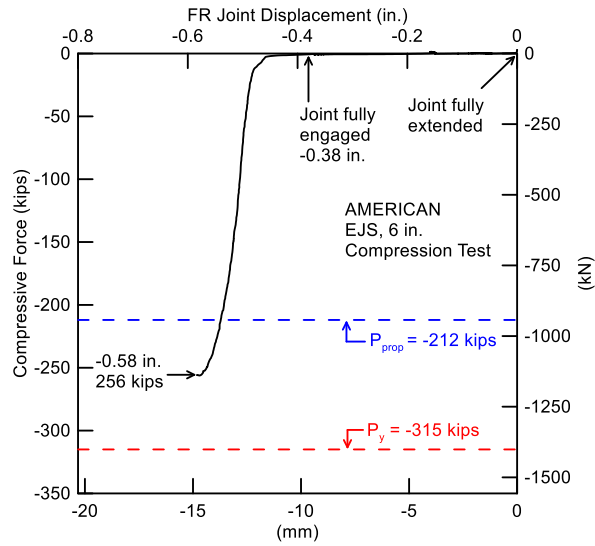
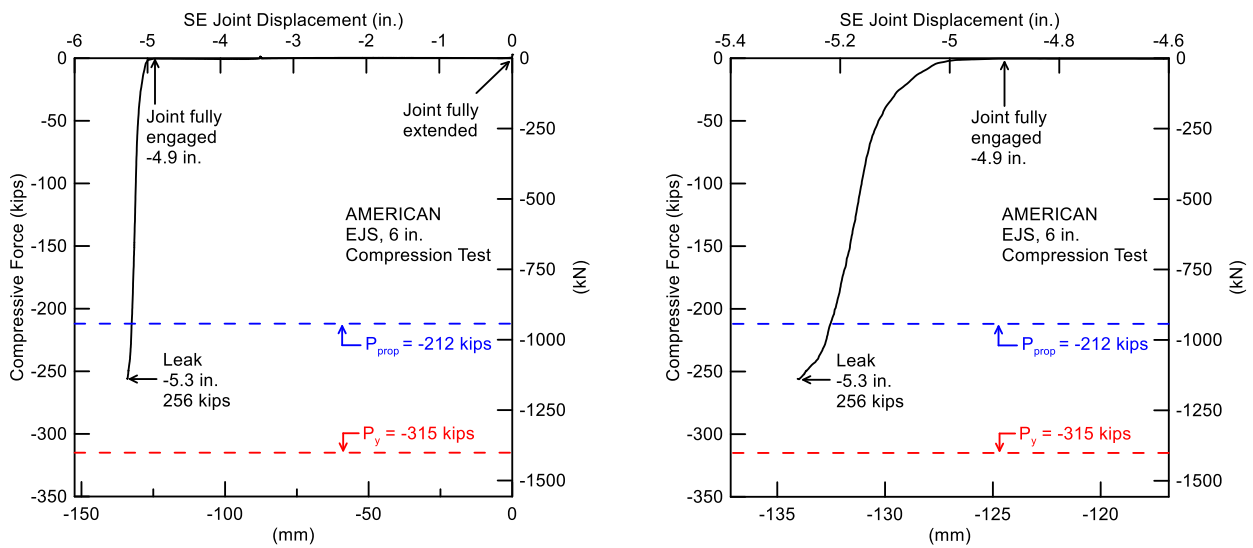


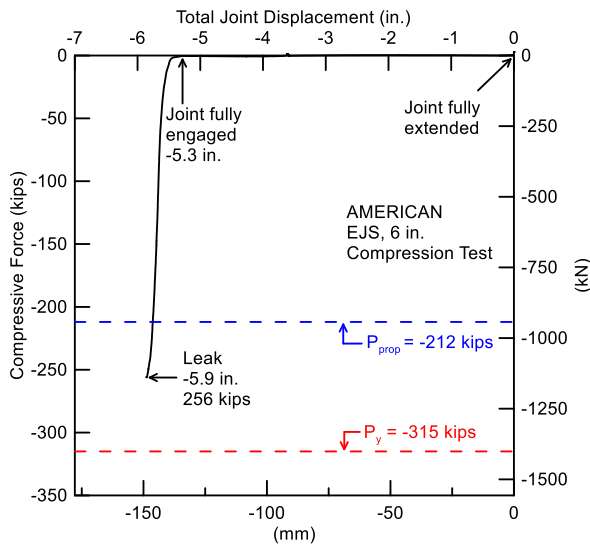
Figure 3.23. Compressive Force vs. FR Joint Displacement



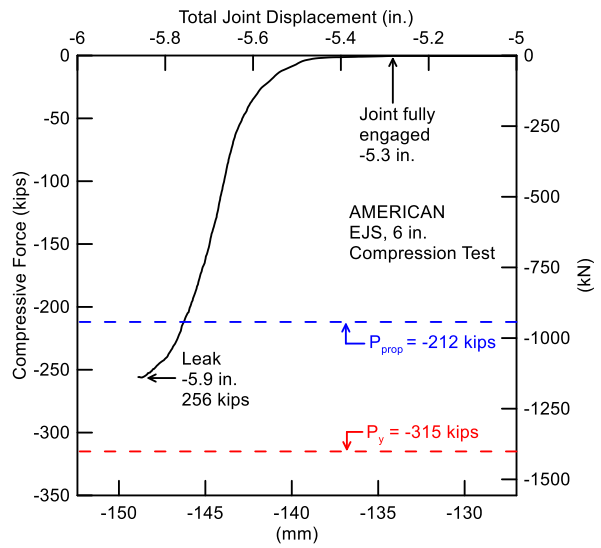
a) Full Displacement Range

b) Between 4.6 to 5.4 in. (119 to 137 mm) of SE Joint Closure

Figure 3.24. Compressive Force vs. SE Joint Displacement



a) Full Displacement Range



b) Between 5 to 6 in. (127 to 152 mm) of Total Joint Closure

Figure 3.25. Compressive Force vs. Total Joint Displacement

### 3.4.3 SE Spigot Axial Strains

The relationships between SE spigot axial strains and the tensile force, FR joint closure, and SE joint closure are shown in Figures 3.26, 3.27, and 3.28, respectively. A maximum axial compressive strain of  $5,400 \mu\epsilon$  (0.54%) was measured at the west springline of the SE spigot. This level of strain exceeds the proportional strain of  $1,400 \mu\epsilon$  (0.14%), which was determined from tensile coupon tests, and indicated the localized plastic deformation.

### 3.4.4 FR Bell Axial Strains

The maximum axial tensile strain on the FR bell side was  $2,300 \mu\epsilon$  (0.23%) and developed at the east springline. The relationships between FR bell axial strains and the tensile force, FR joint opening, and SE joint opening are shown in Figures 3.29, 3.30, and 3.31, respectively.

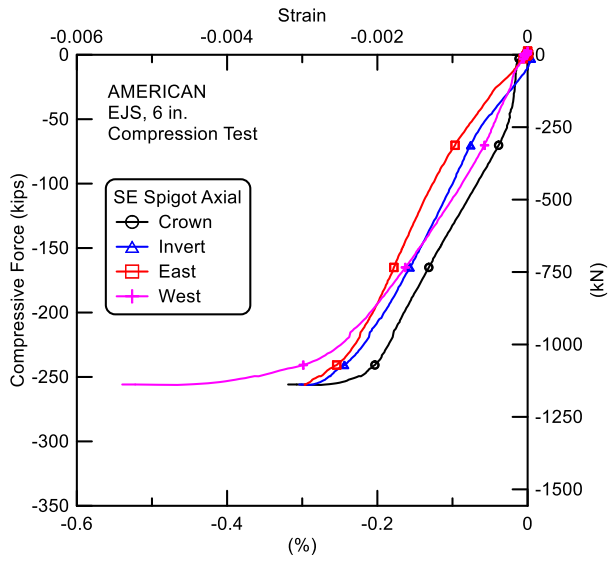


Figure 3.26. Compressive Force vs. SE Spigot Axial Strains

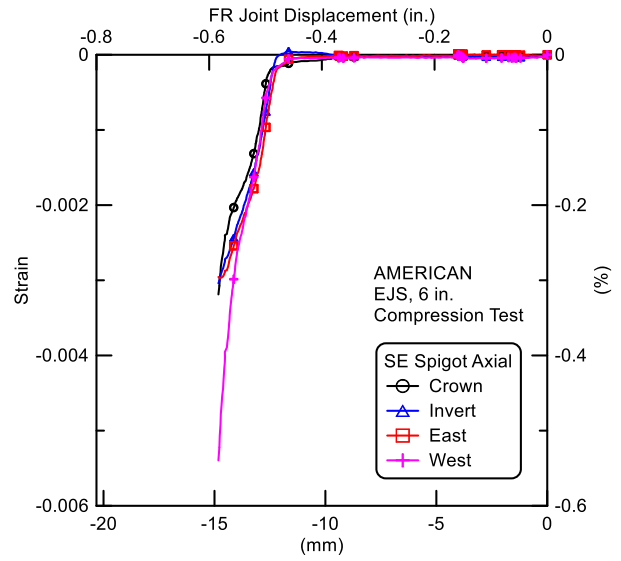
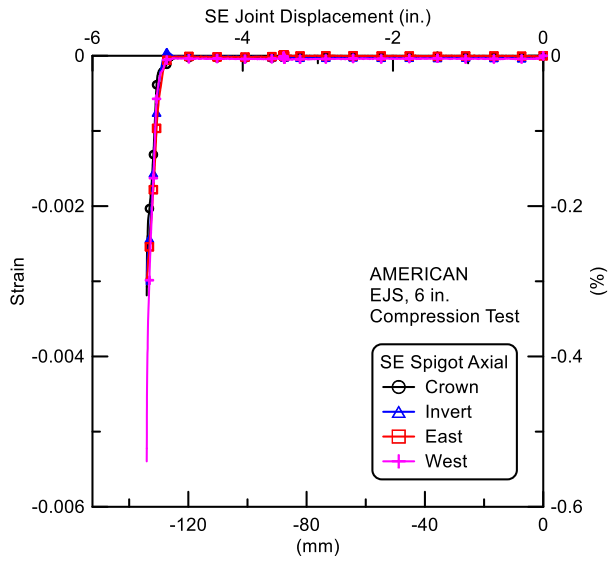
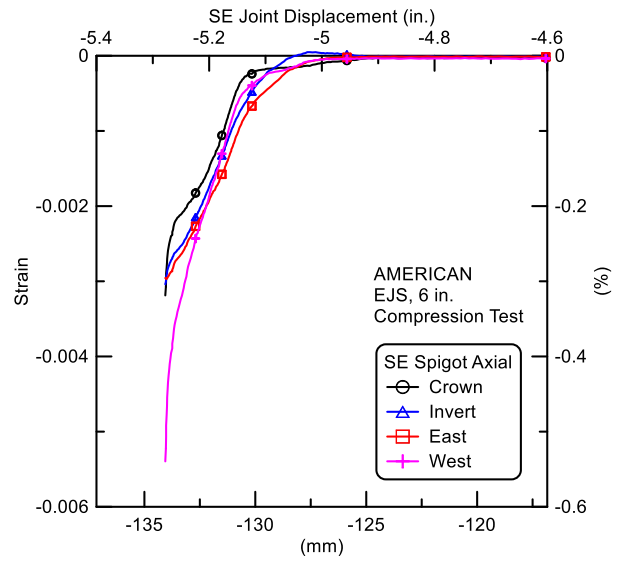


Figure 3.27. SE Spigot Axial Strains vs. Average FR Joint Closure



a) Full Displacement Range



b) Between 4.6 to 5.4 in. (119 to 137 mm) of SE Joint Opening

Figure 3.28. SE Spigot Axial Strains vs. Average SE Joint Closure

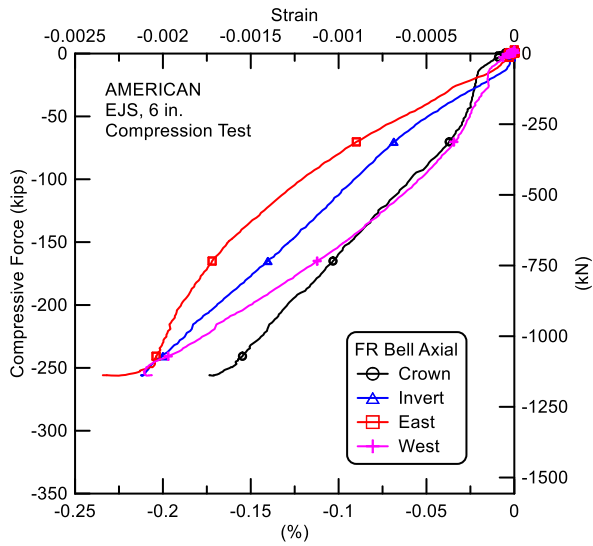


Figure 3.29. Compressive Force vs. FR Bell Axial Strains

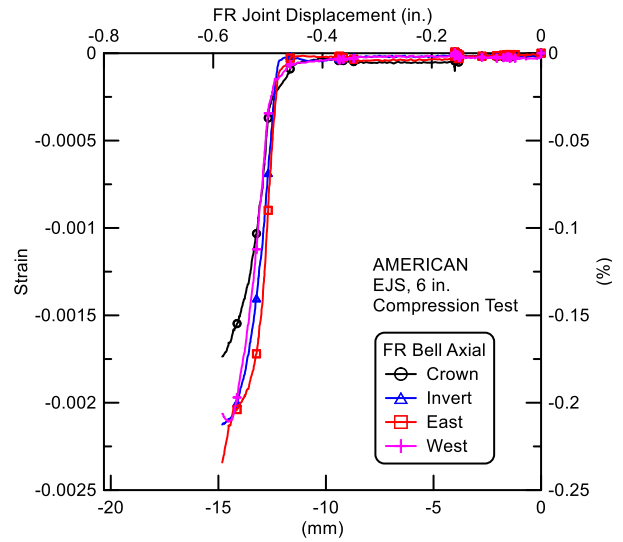
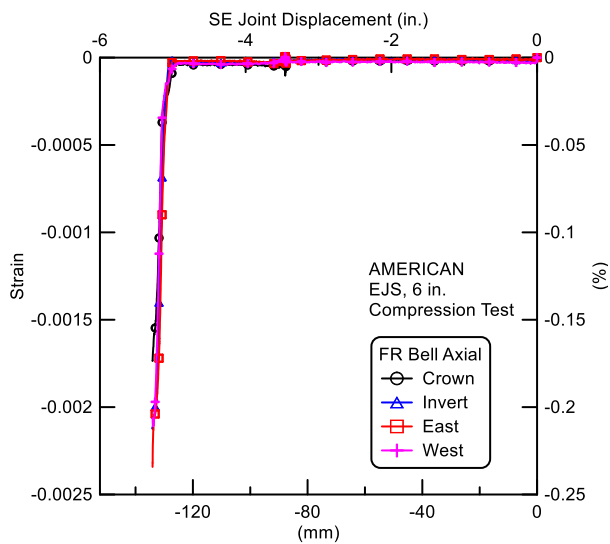
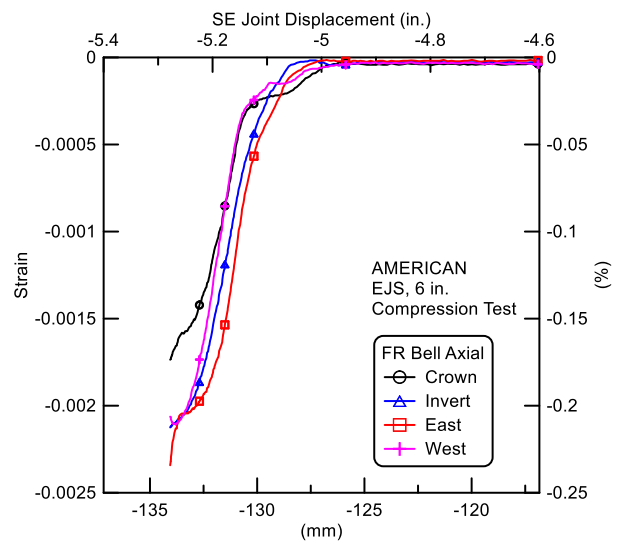


Figure 3.30. FR Bell Axial Strains vs. Average FR Joint Closure



a) Full Displacement Range



b) Between 4.6 to 5.4 in. (119 to 137 mm) of SE Joint Opening

Figure 3.31. FR Bell Axial Strains vs. Average SE Joint Closure

### 3.5. Summary from Joint Tension and Compression Tests

Two tension tests and one compression test were performed on the 6-in. (150-mm)-diameter AMERICAN earthquake joint system (EJS) ductile iron pipes. Both tension tests began with the SE and FRE spigots fully inserted in the deep socket and FR bell sockets, respectively. The compression test began with the SE and FRE spigots fully extended.

As the pipe was pressurized in the tension tests, the spigots were displaced from the bell seat at approximately 12 psi (62 kPa) internal pressure. The slip was 0.3 in. (7.6 mm) for the FR joint and 5 in. (127 mm) for the SE joint before the weld rings became engaged with the locking rings. Tension Test 1 reached a maximum force of 155 kips (689 kN) at 0.45 in. (11 mm) of FR joint opening and 5.1 in. (130 mm) of SE joint displacement. The maximum axial load for Tension Test 2 was 144 kips (641 kN) at 0.41 in. (10 mm) of FR joint opening and 5.1 in. (130 mm) of SE joint displacement. In both tests, the FR bells cracked circumferentially at the peak tensile forces resulting in loss of pressure. The average maximum tensile force of the two tension tests was 149.5 kips (665 kN). This force exceeds Class A of ISO 16134-2006 (ISO, 2006) tensile capacity of  $17D$ , where  $D$  is the nominal diameter in inches, and the force is expressed in kips, which is equivalent to 102 kips (450 kN). In these tests, the average tensile capacity divided by the nominal pipe diameter of  $D = 6.9$  in. (175 mm) is 21.3 which is substantially greater the ISO specification. The average total joint opening, which is the average sum of the FR and SE joint displacements for both tests, was 5.53 in. (140 mm).

The compressive testing showed that the AMERICAN EJS was able to accommodate axial loads to a compressive level at about the DI proportional limit. When pipe reached a compressive load of 256 kips (1,140 kN), which exceeded the proportional limit of 212 kips (943 kN), localized plastic deformation within the joint occurred, resulting in leakage.

## Section 4

### Four-Point Bending of Flex-Ring and EJS Pipe

#### 4.1. Introduction

This section presents the results of four-point bending tests for 1) sections of nominal 6-in. (150-mm) ductile iron (DI) pipe with an AMERICAN Flex-Ring (FR-FRE) joint and 2) a nominal 6-in. (150-mm) section with the AMERICAN Earthquake Joint System (EJS). The purpose of the tests was to develop moment vs. rotation relationships for these types of joints. The tests, with the experiments described previously to characterize the direct compression and tension capacity of these joints, are used with the results a large-scale split-basin test to evaluate the performance of the EJS under severe earthquake-induced ground deformation. The work was undertaken in the Cornell Large Scale Lifelines Testing Facility, which is part of the Bovay Laboratory Complex at Cornell University.

#### 4.2. Four-Point Bending of Flex-Ring Joint Pipe

##### 4.2.1. Joint Description

This section summarizes the results of the four-point bending test of a conventional AMERICAN Flex-Ring DI pipe. Figure 4.1 presents a cutaway view of the AMERICAN Flex-Ring joint assembly, showing both the bell (FR) and spigot (FRE) ends. Sections of DI pipe were shipped to Cornell by AMERICAN and were used in a support assembly with a 400 kip (1.78 MN) hydraulic loading capacity. The pipe was a nominal 6-in- (150-mm)-diameter pipe with the FR-FRE bell-spigot ends. The test specimen was assembled using a gasket and lubricant provided by AMERICAN, after which a DI split snap ring was installed to complete the boltless joint. Mechanical joint end caps with Megalug restraints were used on the ends to allow for water pressurization. A nominal internal pressure of 80 psi (550 kPa) was used throughout the bending test.

##### 4.2.2. Instrumentation and Testing Procedures

Figure 4.2 shows a schematic cross-section of the FR-FRE bending test. There were two temporary supports beneath the central loading points. The supports are used to level the test specimen and to support the self-weight of the pipe (including water for pressurized pipe) before vertical loading. Figure 4.3 is a photograph of the test before the central supports were removed.

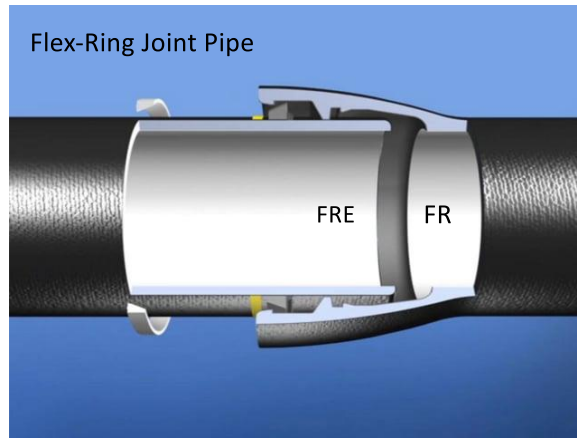


Figure 4.1. Cutaway View of AMERICAN Flex-Ring Joint prior to Snap Ring Assembly

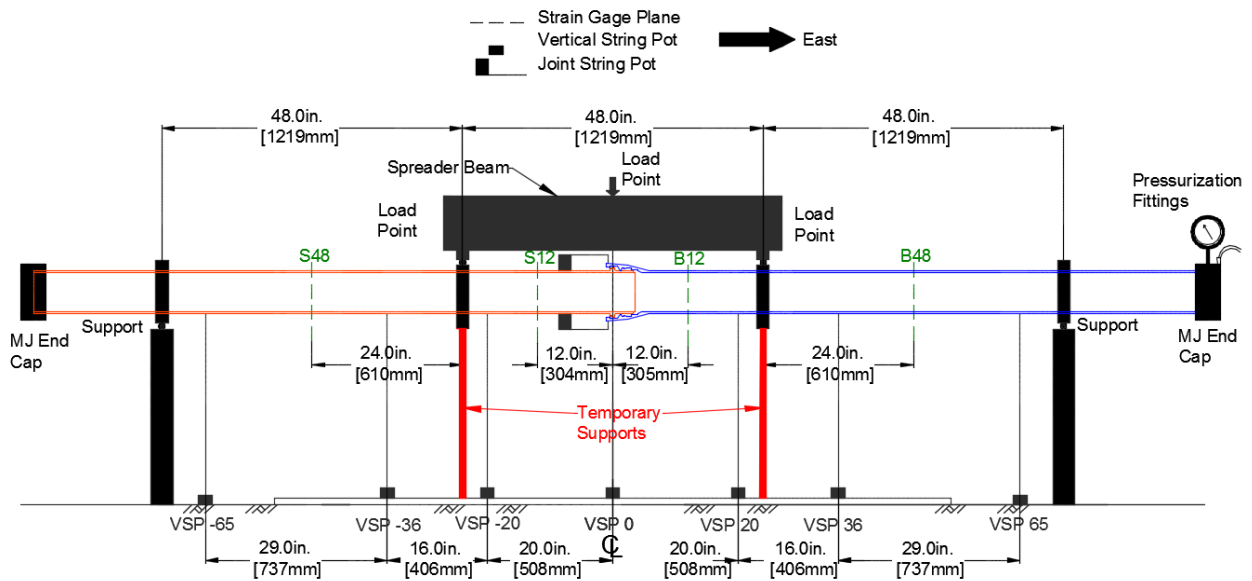


Figure 4.2. Schematic of Instrumentation for FR-FRE Bending Test

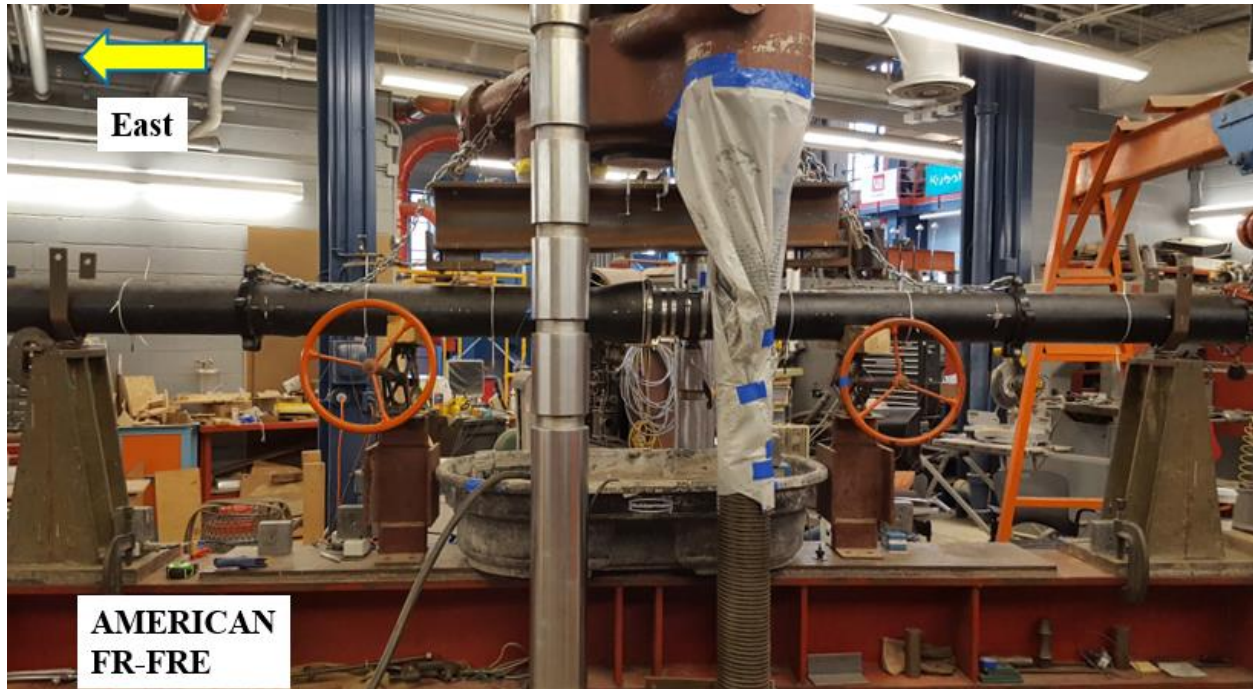


Figure 4.3. Photo of FR-FRE Bending Specimen before Testing

Table 4.1. Instrumentation for AMERICAN FR-FRE Bending Test

Location	Instrument Description	Instrument Name
-65 in. from Joint	Vertical String Pot on Bell End	VSP-65
-36 in. from Joint	Vertical String Pot on Bell End	VSP-36
-20 in. from Joint	Vertical String Pot on Bell End	VSP-20
0 in. from Joint	Vertical String Pot on Spigot End	VSP 0
20 in. from Joint	Vertical String Pot on Spigot End	VSP 20
36 in. from Joint	Vertical String Pot on Spigot End	VSP 36
65 in. from Joint	Vertical String Pot on Spigot End	VSP 65
0 in. from Joint	Horizontal String Pot at Crown	HSP_C
0 in. from Joint	Horizontal String Pot at Invert	HSP_I
-48 in. from Joint	Axial Gage at Invert on Spigot End	S48I
-48 in. from Joint	Axial Gage at Crown on Spigot End	S48C
-12 in. from Joint	Axial Gage at Invert on Spigot End	S12I
-12 in. from Joint	Axial Gage at Crown on Spigot End	S12C
-12 in. from Joint	Axial Gage at S Springline on Spigot End	S12S
-12 in. from Joint	Axial Gage at N Springline on Spigot End	S12N

Table 4.1. Instrumentation for AMERICAN FR-FRE Bending Test (completed)

Location	Instrument Description	Instrument Name
12 in. from Joint	Axial Gage at Invert on Bell End	B12I
12 in. from Joint	Axial Gage at Crown on Bell End	B12C
12 in. from Joint	Axial Gage at S Springline on Bell End	B12S
12 in. from Joint	Axial Gage at N Springline on Bell End	B12N
48 in. from Joint	Axial Gage at Invert on Bell End	B48I
48 in. from Joint	Axial Gage at Crown on Bell End	B48C
Top Center	Load Cell	Load
East End Cap	Pressure Gage	Pressure

1 in. = 25.4 mm

Table 4.1 lists the location, instrument type, and number for the FR-FRE joint test. The instrumentation consisted of string potentiometers (string pots) to measure horizontal displacements at the crown and invert of the pipe FR bell, which were used to measure the bell rotation, and are referred to as HSPs. Vertical displacements along the length of the specimen were measured using seven vertical string pots (VSPs). The VSPs were used to determine the vertical deformation of the test specimen and to calculate the rotation at various locations along the pipe. Strain gages were installed to measure axial and bending strains in the DI pipe.

#### 4.2.3. Calculation Approach

The length of the test specimens between the outer supports was  $l_t = 12$  ft (3.66 m). The pipe weight was 15 lb/ft (2.63 kN/m) and the water weight was 16.2 lb/ft (2.84 kN/m.) The combined distributed weight of the pipe and water inside the pipe was  $w = 31.2$  lb/ft (5.46 kN/m.)

Using a simply-supported beam approach, the maximum moment at the pipe centerline was:

$$M_{\text{distrib}} = \frac{w l_t^2}{8} \quad (4.1)$$

where:

$w$  = uniform load due to pipe and water, and

$l_t$  = the total pipe length between the outer supports.

The three equal distances between the load and support points each were 48 in. (1.22 m). The additional moment applied to the central portion of the specimen,  $M_{\text{central}}$ , was calculated as

$$M_{\text{central}} = \frac{P l_t}{6} \quad (4.2)$$

where:

$P$  = the applied load due to the weight of the spreader beam [ $W = 216$  lb (0.96 kN)] plus the load applied by the hydraulic actuator,  $P$ , in the load frame, and

$l_t$  = the total pipe length between the outer supports.

The moment due to the pipe, water, and spreader beam weights are included in the moment vs. rotation calculations.

Two methods were used to calculate joint rotations. One method uses the horizontal string pots (HSPs) at the top and bottom of the bell and the vertical separation distance to calculate the joint rotation. Equation 2.3 provides the method used for this approach, as follows

$$\theta \text{ (degrees)} = \tan^{-1} \left[ \frac{(\text{invert disp.} - \text{crown disp.})}{\text{distance between centers of HSPs} = 8.9 \text{ in.}} \frac{180^\circ}{\pi} \right] \quad (4.3)$$

An alternate approach is to assume the pipe sections act as rigid bodies in rotation, take the difference between the vertical string pot measurement (VSPs) at the specimen center and another point along the pipe, and divide by the pot separation distance. The arctangent of this result is the rotation of each side. The overall joint rotation is the sum of the two side angles, as follows

$$\begin{aligned} \theta \text{ (degrees) FRE side} &= \tan^{-1} \left[ \frac{(\text{VSP } 0) \text{ in.} - (\text{VSP } -20) \text{ in.}}{20 \text{ in.}} \frac{180^\circ}{\pi} \right] + \\ \theta \text{ (degrees) FR side} &= \tan^{-1} \left[ \frac{(\text{VSP } 0) \text{ in.} - (\text{VSP } 20) \text{ in.}}{20 \text{ in.}} \frac{180^\circ}{\pi} \right] \end{aligned} \quad (4.4)$$

where (VSP 0) in. is at the specimen center, (VSP-20) in. is -20 in. on the FRE side of the joint, and (VSP 20) in. is +20 in. on the FR side.

#### 4.2.4. Test Procedures

The pipe for the bending test was installed in the loading frame, leveled, and all instrumentation and data acquisitions systems were checked. The test was then performed as follows:

- 1) Fill the pipe with water, pressurize, and bleed the system to extend fully the bell/spigot connection. An internal pressure of 80 psi (550 kPa) generated approximately 2000 lb (8.8 kN) of axial force, which was sufficient to expand the joint.
- 2) Remove the temporary supports.
- 3) Lower the spreader beam onto the pipe.
- 4) Apply hydraulic force to develop moment and rotation at the joint.

Leakage was first observed in the joint at rotation of about 8 degrees. The test was stopped when 100-ml/min leak occurred at a rotation of approximately 10 degrees.

#### **4.2.5. Pressure**

The specimen was pressurized with water to approximately 80 psi (552 kPa), and the joint was fully extended. Internal pressure was adjusted during the test to maintain a nearly constant pressure. Figure 4.4 shows the pressure vs. time from the bending test. The test was stopped when a leak of 100 ml/min in the joint developed, and the pipe was depressurized.

#### **4.2.6. String Pot Measurements**

The spigot and bell side VSP measurements shown in Figure 4.5 indicate that there is good agreement between vertical movement measurements at equal distances from the center point of the test. The continuous progression of these displacements is a further indication that the assumption of rigid body motion can be used in Equation 4.4 to determine rotations.

The horizontal string pots (HSPs) at the crown and invert of the pipe joint provide quantitative data for the evaluation of rotation. Figure 4.6 shows the HSP measurements vs. the VSP rotation for the FR-FRE specimen. The HSP rotations beyond a few degrees are considered less reliable than the VSP rotations. There is an early zero offset of roughly 0.08 in. (2 mm) in the displacements corresponding to the release of the central supports, which allowed the specimen to deflect at the joint under the pipe weight plus water. This force was not measured in the hydraulic load system. The weight of the pipe plus water caused a joint rotation of 1.2 degrees. When the weight of the spreader beam was added, the joint rotated about 5.5°. The additional weight of the spreader beam caused substantial rotations at small force. After the full weight of the spreader beam was added, additional forces were applied by the Baldwin system.

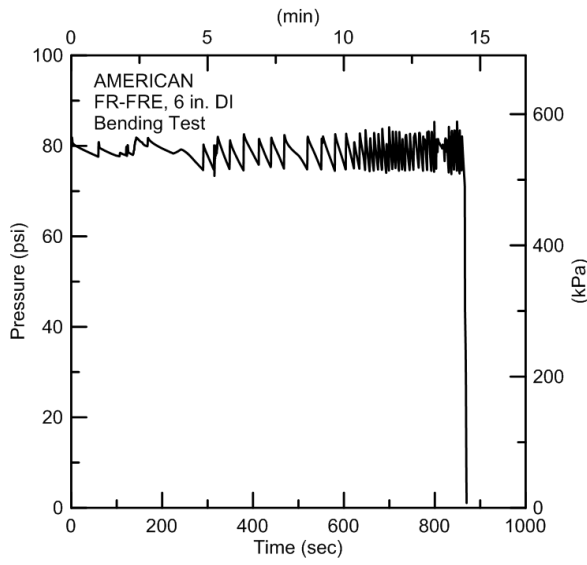


Figure 4.4. Pressure vs. Time for FR-FRE Bending Test

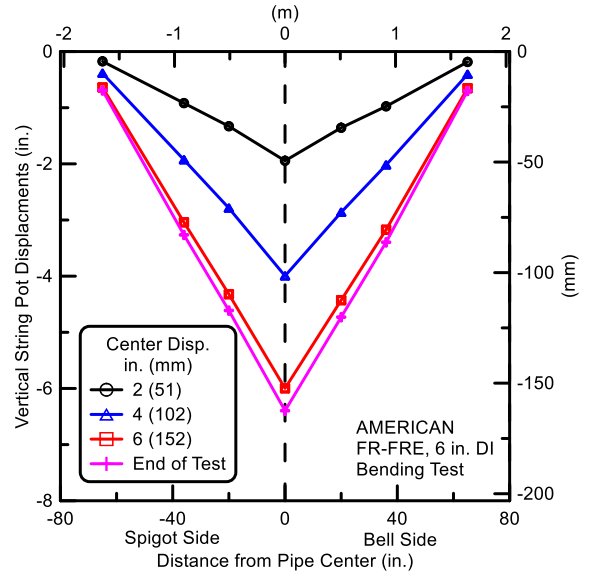


Figure 4.5. VSP Measurements for FR-FRE Bending Test

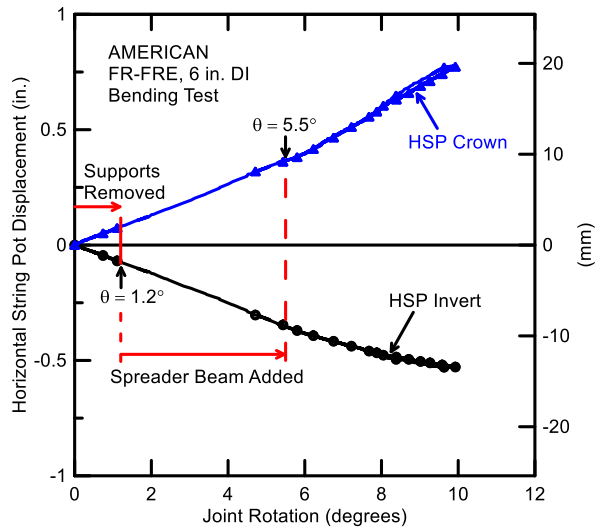


Figure 4.6. HSP Measurements vs. VSP Rotation for FR-FRE Bending Test

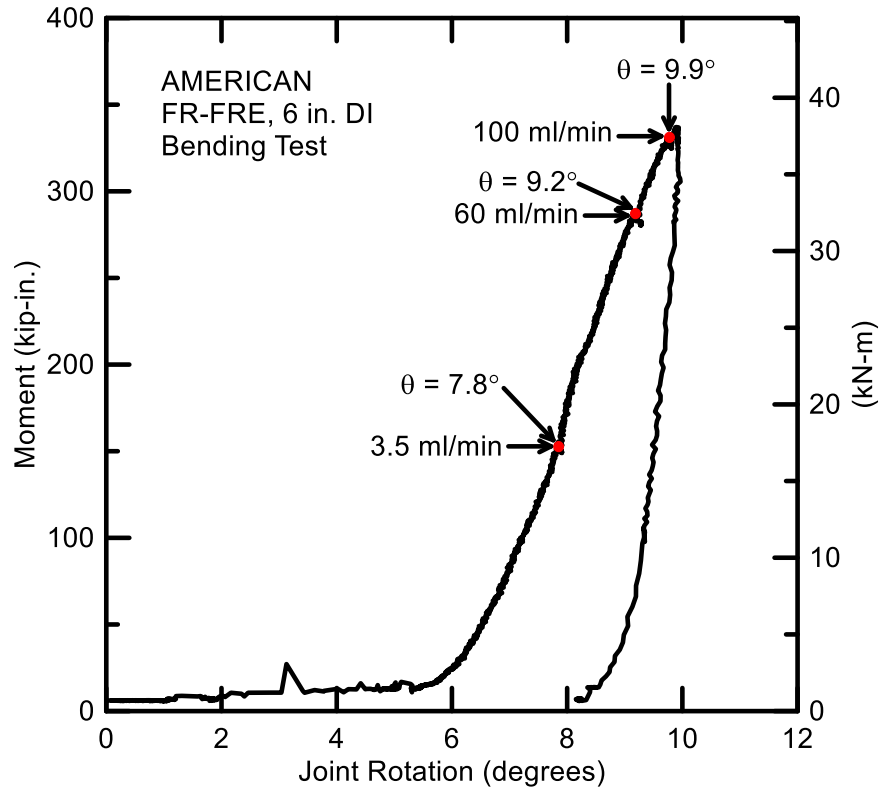
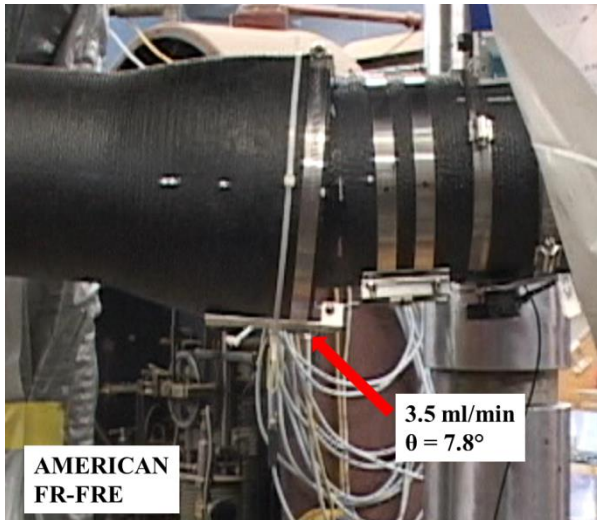


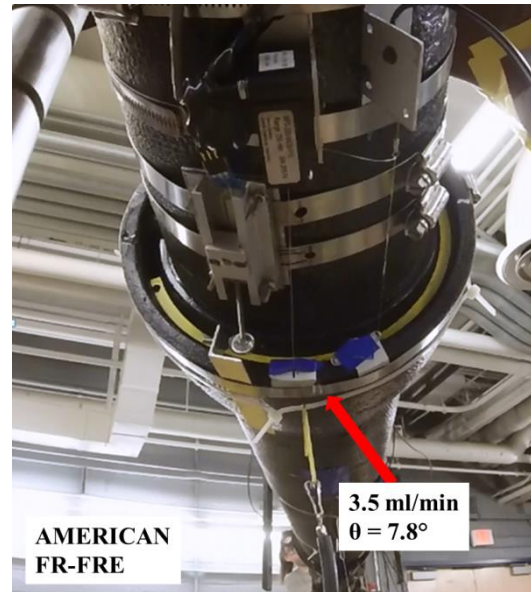
Figure 4.7. Moment-Rotation for FR-FRE Bending Test

#### 4.2.7. Moment vs. Rotations

Joint rotations determined using the VSPs for the FR-FRE specimen are shown in Figure 4.7. Leakage was measured three times during this test as indicated in the figure. The first leak in the FR-FRE joint developed at a rotation of  $\theta = 7.8^\circ$  and an applied moment of 155 kip-in. (17.5 kN-m). The leak rate was 3.5 ml/min (Figure 4.8). When the test was continued, the leakage rate was higher. The leakage of 60 ml/min was measured at a joint rotation of  $\theta = 9.2^\circ$  and a moment of 289 kip-in. (32.7 kN-m). The test was continued until continuous flow of 100 ml/min developed at a rotation of  $\theta = 9.9^\circ$  and a moment of 337 kip-in. (38.1 kN-m). The test was then stopped. Figure 4.9 presents a photo of the joint with leakage at the end of test. No visible damage was observed.

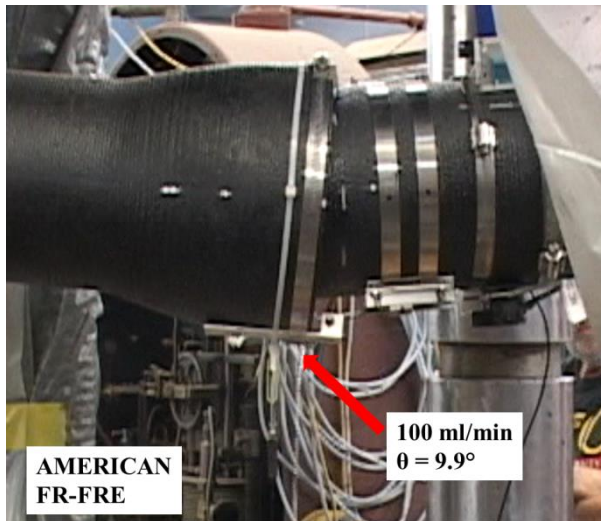


a) Side View

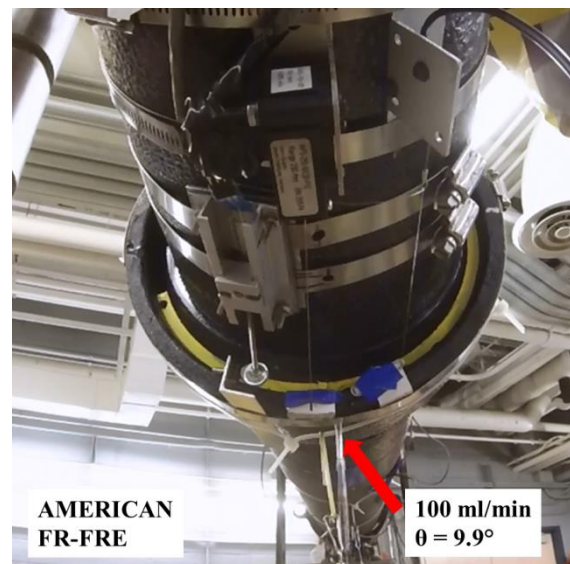


b) Underside View

Figure 4.8. FR-FRE First Leakage of 3.5 ml/min



a) Side View



b) Underside View

Figure 4.9. FR-FRE Leakage of 100 ml/min at End of Test

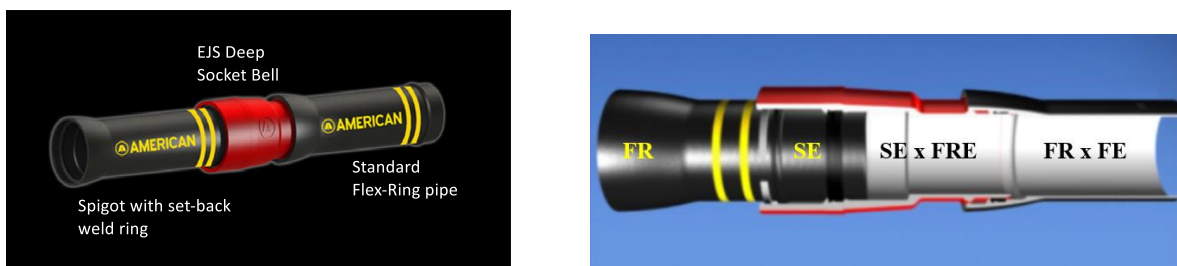
### 4.3. Four-Point Bending of Earthquake Joint System

#### 4.3.1. Joint Description

This section summarizes the results of the four-point bending test of the AMERICAN Earthquake Joint System (EJS). Figures 4.10 a) and b) show a representative exterior and cutaway view, respectively, of the joint. Sections of DI pipe were shipped to Cornell by AMERICAN and were used in a support assembly with a 400 kip (1.78 MN) hydraulic loading capacity. The pipe was a nominal 6-in.-(150-mm)-diameter pipe with a FE-SE spigot, EJS Deep Socket, and FR-FE bell section. The joint system was assembled with gaskets, lubricant, and DI split snap ring supplied by AMERICAN. Mechanical joint end caps with Megalug restraints were used on the ends to allow for water pressurization. A nominal internal pressure of 80 psi (550 kPa) was used throughout the bending testing.

#### 4.3.2. Instrumentation and Testing Procedures

Figure 4.11 shows a schematic cross-section of the EJS bending test. There were two temporary supports beneath the central loading points similar to those used in the previous test. Figure 4.12 shows the test set-up before the central supports were removed. The test sequence was the same as for the FR-FRE joint. Table 4.2 lists location, instrument type, and number for the EJS instrumentation.



a) Complete Joint System

b) Cutaway Views of AMERICAN EJS

Figure 4.10. AMERICAN Earthquake Joint System (EJS)

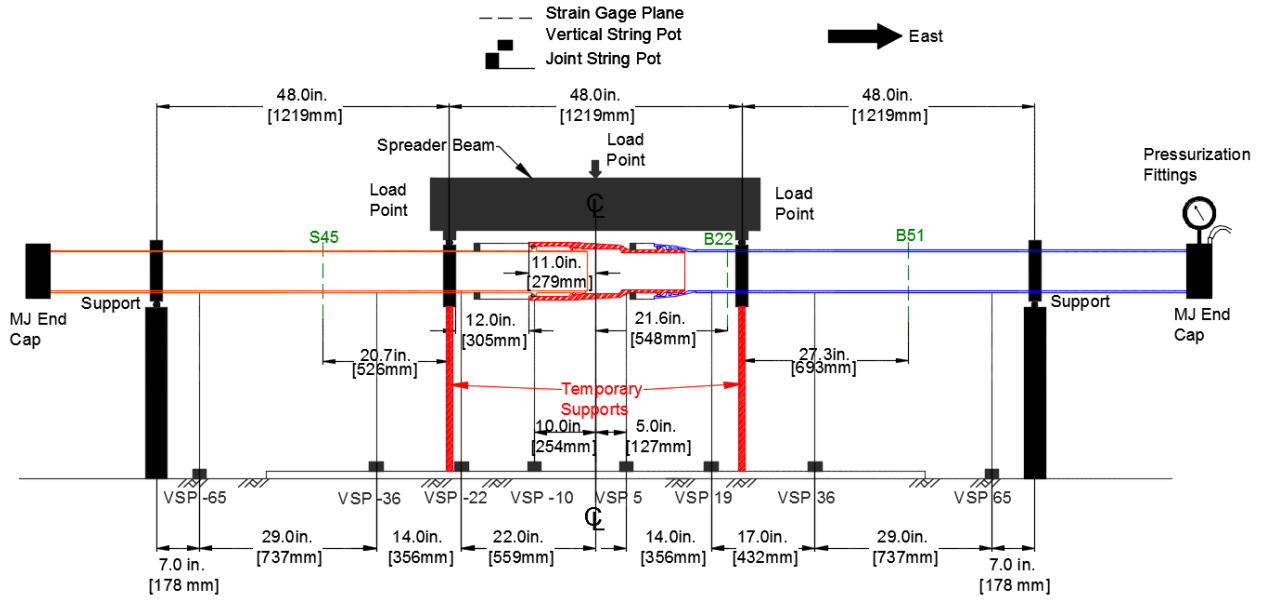


Figure 4.11. Schematic of Instrumentation for EJS Bending Test



Figure 4.12. Photo of AMERICAN EJS Bending Specimen before Testing

Table 4.2. Instrumentation for AMERICAN EJS Bending Test

Location	Instrument Description	Instrument Name
-65 in. from Centerline	Vertical String Pot on Bell End	VSP-65
-36 in. from Centerline	Vertical String Pot on Bell End	VSP-36
-22 in. from Centerline	Vertical String Pot on Bell End	VSP-22
-10 in. from Centerline	Vertical String Pot on Bell End	VSP-10
5 in. from Centerline	Vertical String Pot on Spigot End	VSP 5
19 in. from Centerline	Vertical String Pot on Spigot End	VSP 19
36 in. from Centerline	Vertical String Pot on Spigot End	VSP 36
65 in. from Centerline	Vertical String Pot on Spigot End	VSP 65
-11 in. from Joint	Horizontal String Pot at Crown at SE Joint	HSP_C
-11 in. from Joint	Horizontal String Pot at Invert at SE Joint	HSP_I
9.6 in. from Joint	Horizontal String Pot at Crown at FR Joint	B_HSP_C
9.6 in. from Joint	Horizontal String Pot at Invert at FR Joint	B_HSP_I
-45 in. from Centerline	Axial Gage at Invert on Spigot End	S45I
-45 in. from Centerline	Axial Gage at Crown on Spigot End	S45C
22 in. from Centerline	Axial Gage at Invert on Bell End	B22I
22 in. from Centerline	Axial Gage at Crown on Bell End	B22C
22 in. from Centerline	Axial Gage at S Springline on Bell End	B22S
22 in. from Centerline	Axial Gage at N Springline on Bell End	B22N
51 in. from Centerline	Axial Gage at Invert on Bell End	B51I
51 in. from Centerline	Axial Gage at Crown on Bell End	B51C
Top Center	Load Cell	Load
East End Cap	Pressure Gage	Pressure

1 in. = 25.4 mm

### 4.3.3. Calculation Approach

The calculation methods used for determining the joint rotations for the EJS rotation test are similar to those for the FR-FRE joint test, with small differences in instrument locations and specific dimensions. Assuming rigid body rotation of the pipe sections, VSP rotations are calculated by taking the string pot measurement on the FR bell or SE spigot sections divided by its distance from the closest support. The arctangent of this result is the rotation of each side. The deep socket rotation is calculated by taking the difference between the two string pot measurements on the deep socket and dividing by the pot separation distance. Its arctangent gives the deep socket rotation. The FR joint rotation is the sum of the FR bell and deep socket angles, as follows

$$\theta_{FR} \text{ (degrees)} = \tan^{-1} \left[ \frac{(\text{VSP } 19) \text{ in.}}{(72-19) \text{ in.}} \right] + \tan^{-1} \left[ \frac{(\text{VSP } 5) \text{ in.} - (\text{VSP } -10) \text{ in.}}{15 \text{ in.}} \right] \quad (4.5)$$

The SE joint rotation is the SE spigot angle subtracted by the deep socket angle as

$$\theta_{SE} \text{ (degrees)} = \tan^{-1} \left[ \frac{(\text{VSP } -22) \text{ in.}}{(72-22) \text{ in.}} \right] - \tan^{-1} \left[ \frac{(\text{VSP } 5) \text{ in.} - (\text{VSP } -10) \text{ in.}}{15 \text{ in.}} \right] \quad (4.6)$$

The sum of the FR bell and SE spigot gives the total EJS deflection as

$$\theta_{EJS} \text{ (degrees)} = \tan^{-1} \left[ \frac{(\text{VSP } -22) \text{ in.}}{(72-22) \text{ in.}} \right] + \tan^{-1} \left[ \frac{(\text{VSP } 19) \text{ in.}}{(72-19) \text{ in.}} \right] \quad (4.7)$$

where VSPs are the measurements (in inches) of the vertical string posts listed in Table 4.2.

#### 4.3.4. Test Procedures

The test procedures for loading the EJS specimen were similar the FR-FRE joint test. The equipment used and general instrumentation were similar.

#### 4.3.5. Pressure

The specimen was pressurized with water to approximately 85 psi (587 kPa). The line transmitting water pressure was open for the duration of the test to be representative of conditions in the field for the EJS as well as conditions associated with the large-scale split-basin test. Figure 4.13 presents the pressure vs. time from the EJS bending test. The test was stopped when the pipe failed at the FR bell.

#### 4.3.6. String Pot Measurements

The VSP measurements on the pipe sections with EJS are shown in Figure 4.14. The measurements show the continuous progression of each pipe segment. Figure 4.15 shows the HSP vs. the VSP rotation for the FR and SE joints. The internal pressure caused the SE joint to open an additional 0.07 in. (1.78 mm) and rotate  $\theta_{SE} = -0.4^\circ$  (upward). After the temporary supports had been removed, the weight of the pipe plus water plus spreader beam caused the FR joints to rotate  $\theta_{FR} = 5.8^\circ$  while the SE joint angle was still at  $-0.4^\circ$ .

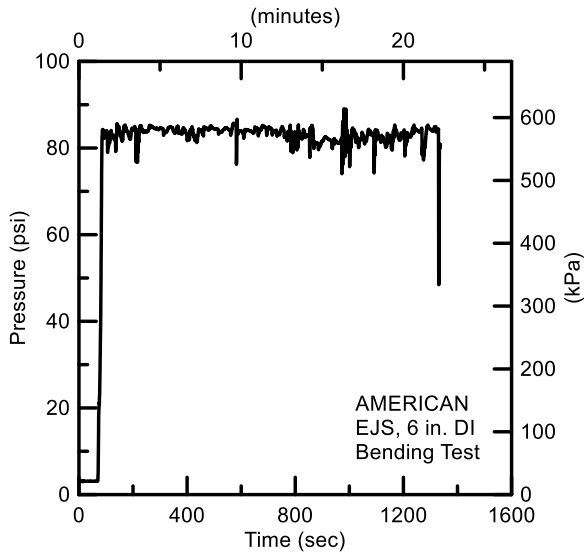


Figure 4.13. Pressure vs. Time for EJS Bending Test

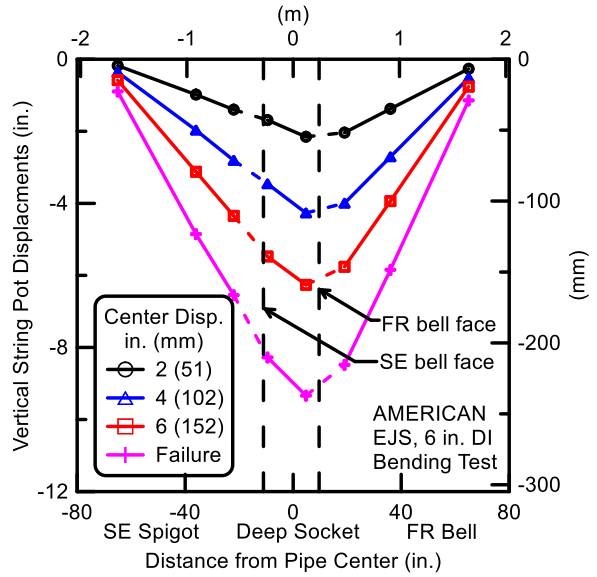
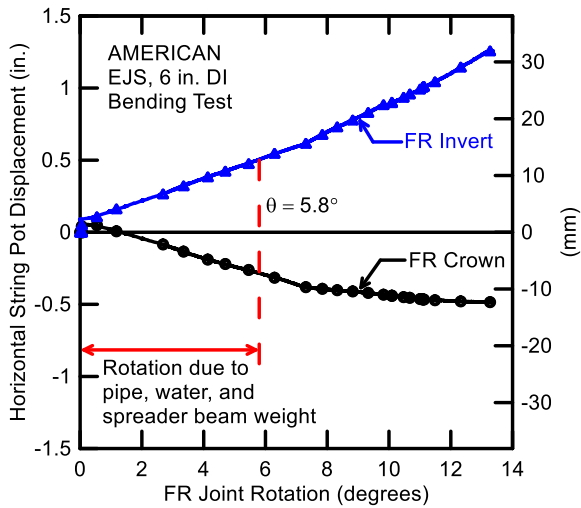
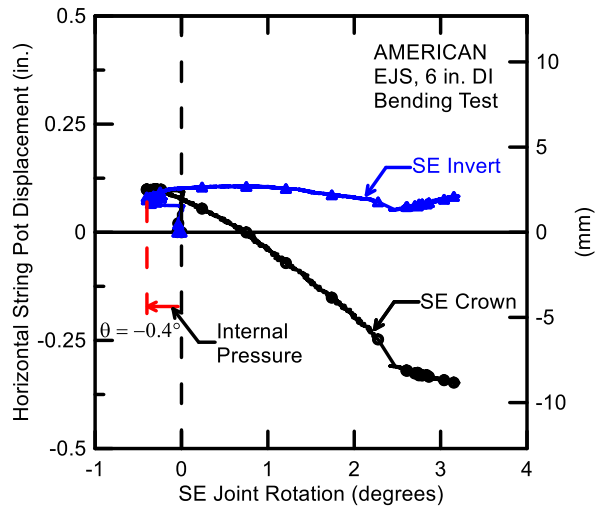


Figure 4.14. VSP Measurements for EJS Bending Test



a) FR Joint



b) SE Joint

Figure 4.15. HSP Measurements vs. VSP Rotation for EJS Bending Test

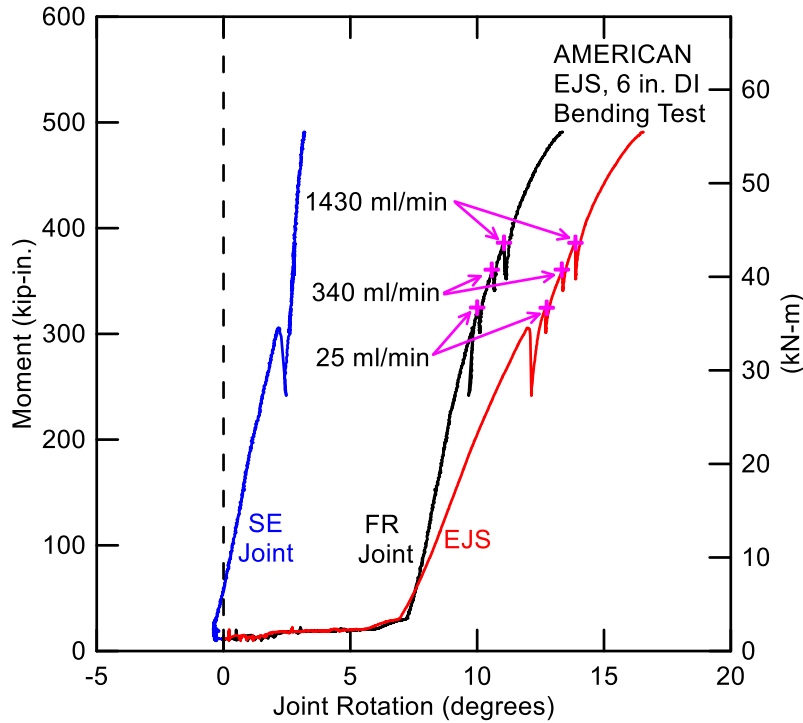
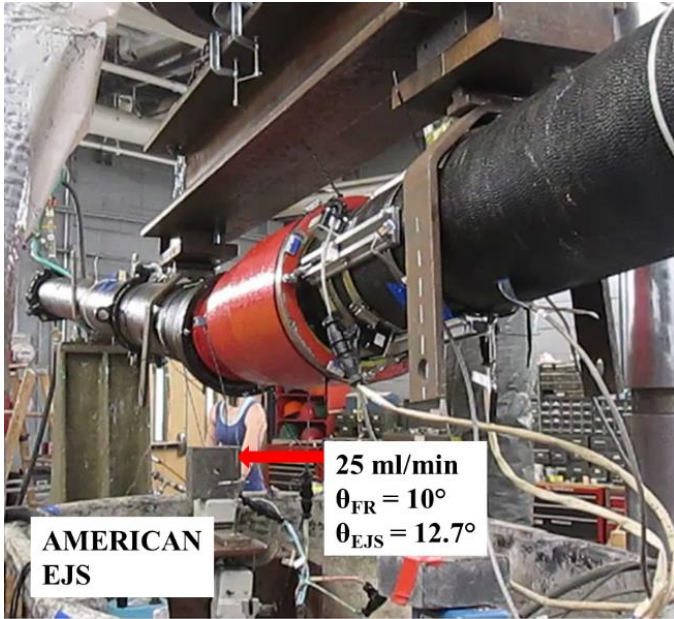


Figure 4.16. Moment vs. Rotation for EJS Bending Test

#### 4.3.7. Moment vs. Rotations

The moment vs. rotation test results are shown in Figure 4.16. The rotation at the SE joint is substantially less than that at the FR joint. There was a moment drop from 305 kip-in. (34.5 kN-m) to 241 kip-in. (27.2 kN-m). This drop was associated by sliding of a rocker support, which stabilized in a new position. A leak first was observed at the FR joint at a rotation of  $\theta_{FR} = 10^\circ$  and an EJS deflection of  $\theta_{EJS} = 12.7^\circ$  at 323 kips-in. (36.5 kN-m) of applied moment. The leak rate was 25 ml/min (Figure 4.17). As the test continued, leakage rate at the FR joint increased. The second leak of 340 ml/min was measured at the FR joint at a rotation of  $\theta_{FR} = 10.6^\circ$  and an EJS deflection of  $\theta_{EJS} = 13.4^\circ$  at 360 kips-in. (40.7 kN-m) of moment. Figure 4.18 shows a leak of 1,430 ml/min developed at the FR joint of at a rotation  $\theta_{FR} = 11^\circ$  and an EJS deflection of  $\theta_{EJS} = 13.9^\circ$  at 386 kips-in. (43.6 kN-m) of moment. The test was stopped when the FR bell cracked causing pipe failure as shown in Figure 4.19. The maximum EJS deflection at failure was  $\theta_{EJS} = 16.6^\circ$  with an associated moment of 491 kips-in. (55.5 kN-m)

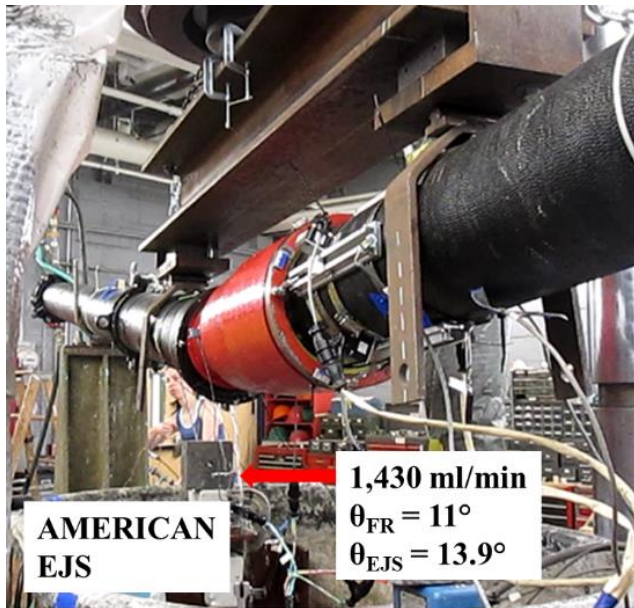


a) Side View

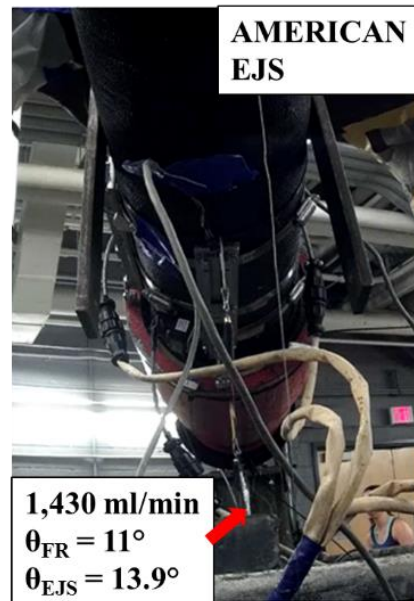


b) Underside View

Figure 4.17. First Leak (25 ml/min) at FR Joint in EJS

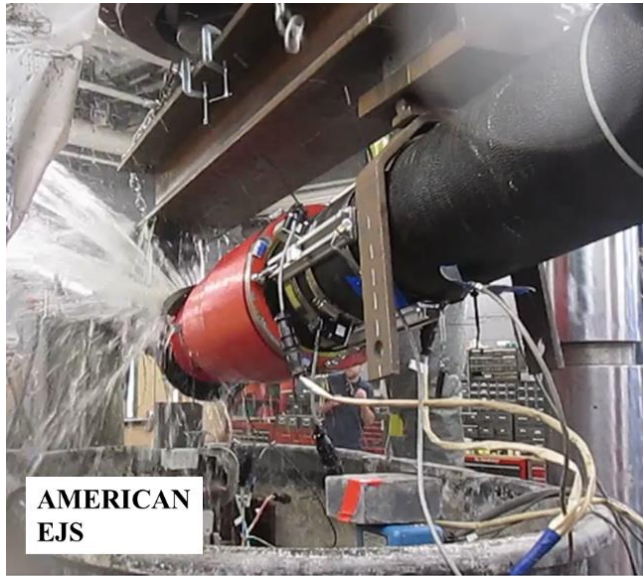


a) Side View



b) Underside View

Figure 4.18. Leak (1,430 ml/min) at FR Joint in EJS



a) Side View



b) Underside View

Figure 4.19. Pipe Failure at FR Bell in EJS

#### 4.4. Summary of Four-Point Bending Tests

Four-point bending tests were performed on sections of 6 in. (150 mm) ductile iron (DI) with an AMERICAN Flex-Ring (FR-FRE) joint and on a nominal 6-in. (150-mm) section with the AMERICAN Earthquake Joint System (EJS.) The purpose of these tests was to develop moment vs. rotation relationships for these types of joints. Instrumentation to measure joint rotations included horizontally and vertically orientated string potentiometers. The specimens were loaded in a 400 kip (1780 kN) Baldwin hydraulic test frame.

One test on the FR-FRE joint and one on the EJS were performed. Table 4.3 summarizes the moment and rotation data when first leakage was observed for each test. The first leak of 3.5 ml/min in the FR-FRE joint occurred at a rotation of  $\theta = 7.8^\circ$  and an applied moment of 155 kip-in. (17.5 kN-m). The test was stopped when the joint reached a rotation of  $\theta = 9.9^\circ$  and a moment of 337 kip-in. (38.1 kN-m) with continuous flow of 100 ml/min. In the EJS bending test, first leakage of 25 ml/min was observed at the FR joint at an FR joint rotation of  $\theta_{FR} = 10^\circ$  and an EJS

deflection of  $\theta_{EJS} = 12.7^\circ$  with an associated moment of 323 kip-in (36.5 kN-m). The test was continued until the FR bell cracked at  $\theta_{EJS} = 16.6^\circ$  with a moment of 491 kips-in. (55.5 kN-m).

Figure 4.3 presents summary moment-rotation relationships for both the 6-in. (150- mm)-diameter FR-FRE jointed pipe sections and those with the EJS. The allowable deflection for the FR-FRE in the AMERICAN Flex-Ring joint pipe is 5 degrees. The combined allowable deflection for the AMERICAN Earthquake Joint System (EJS) is 8 degrees. These limits are shown in Figure 4.20. Both of the pipe joints tested at Cornell exceeded the allowable deflection without any leaks or pipe damage.

Table 4.3. Results of Four-Point Bending Tests

Test	First Leakage Rate	Rotation	Moment
FR-FRE	3.5 ml/min	7.8°	155 kip-in. (17.5 kN-m)
EJS	25 ml/min At FR joint	$\theta_{FR} = 10^\circ$ $\theta_{EJS} = 12.7^\circ$	323 kip-in. (36.5 kN-m)

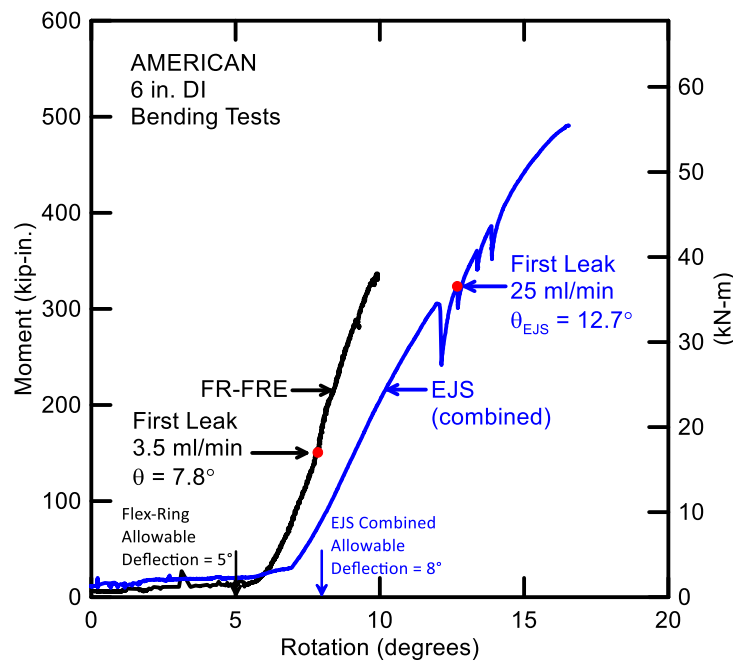


Figure 4.20. Moment-Rotation Results from Four-Point Bending Tests on American DI Pipe Joints

## Section 5

### Large Scale Testing of Fault Rupture Effects

#### 5.1 Introduction

This section presents the results of the large-scale fault rupture test performed with a ductile iron pipeline equipped with AMERICAN Earthquake Joint System (EJS). All testing was performed in the large-scale test basin at the Cornell University Large Scale Lifelines Testing Facility.

#### 5.2 Experimental Setup

Figure 5.1 is a plan view of the test layout which shows the fault rupture plane and approximate locations of the four actuators generating basin movement. The pipeline consisted of five ductile iron pipe segments with four earthquake joint systems positioned at 5 ft (1.5 m) and 15 ft (4.6 m) on either side of the fault. The intersection angle between the pipe and fault was 50°. The objective of the test was to impose abrupt ground deformation on the pipeline, which was representative of left lateral strike slip fault rupture and the most severe ground deformation that occurs along the margins of liquefaction-induced lateral spreads and landslides. The pipeline was constructed to evaluate its capacity to accommodate full-scale fault movement through the simultaneous axial pullout at four different earthquake joint systems. Measuring simultaneous performance of multiple joints allows for confirmation that the pipeline will respond to ground failure as intended, understand the complex interaction among the different joints, and determine the maximum ground deformation and axial pipeline load that can be sustained before joint leakage.

The pipeline was buried in the Cornell large-scale test basin in partially saturated sand that was compacted to have an average friction angle of  $\phi' = 42^\circ$ , equivalent in strength to that of a medium dense to dense granular backfill. The pipeline was assembled so that the FRE and SE spigots at each EJS could pull from the bells approximately 0.5 and 5 in. (12.7 and 127 mm) before the weld rings made contact with the locking ring. During the test, the south part of the basin remained stationary, while the north part was displaced to the north and west by large-stroke actuators to cause soil rupture and slip at the interface between the two parts of the test basin.

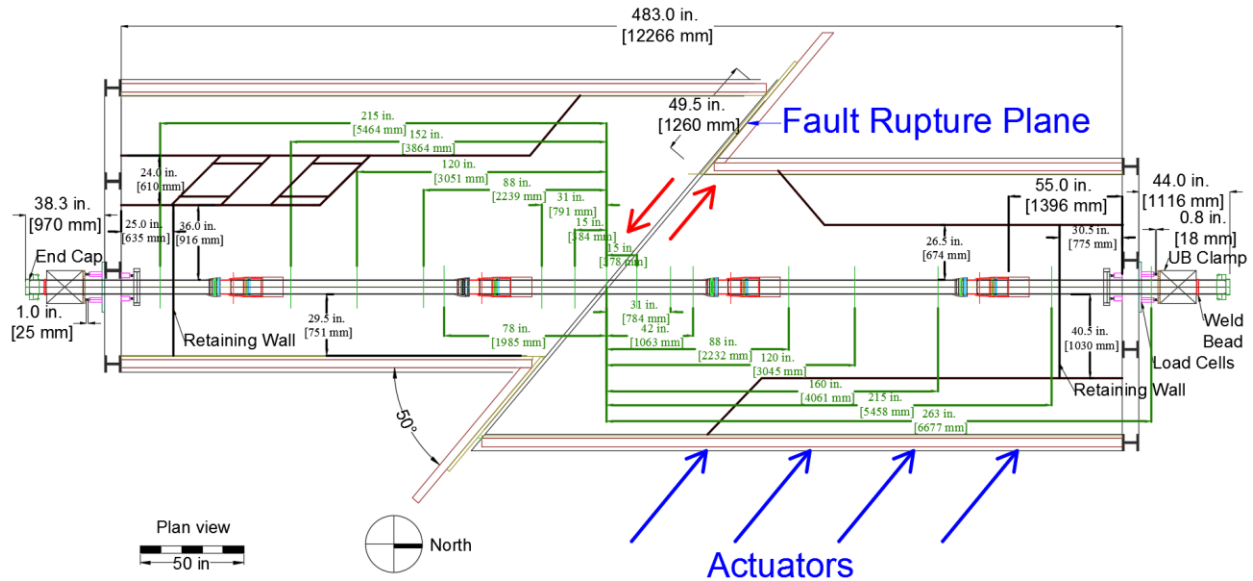


Figure 5.1. Plan View of Pipe Centered EJS Specimen in Test Basin

A 115-in. (2.92-m)-long pipe section was placed directly over the fault, with an intersection angle of  $50^{\circ}$ . Two identical pipes with EJS castings were installed to the north and the south of the center pipe. A 120-in. (3.05-m)-long pipe with an EJS casting was connected at the north end of the pipeline. Lastly, a 95.8-in. (2.43-m)-long pipe with an EJS casting was connected at the south end of the pipeline. The 6.9-in. (175-mm) outer-diameter pipe was placed on a bed of soil 10 in. (254 mm) in depth. The depth of burial to top of pipe was 31 in. (787 mm) resulting in 48 in. (1.22 m) of total soil depth.

The simulated fault rupture caused both tensile and bending strains in the pipeline. The length of the pipeline buried in soil, also described as “test portion,” was approximately 36 ft (11 m) long. The pipe was pressurized with water to approximately 80 psi (552 kPa). The north (movable) portion of the test basin is connected to four MTS hydraulic actuators with load cells controlled by a MTS Flextest GT controller. All actuators were operated in synchronized displacement control.

### 5.2.1 Test Procedure

The general test procedure, after all instruments were installed, soil placed, and pipe filled with water, was:

- a) Begin data acquisition and start the servo-controlled hydraulic system,
- b) Introduce and verify internal water pressure,
- c) Move the test basin at a rate of 1 ft/minute (305 mm/minute) until pipe failure (full pressure loss),
- d) Stop basin movement but maintain hydraulic actuator pressure,
- e) Verify data acquisition, and
- f) Excavate.

At a fault displacement of 36 in. (914 mm), the internal pressure dropped to 25 psi (172 kPa), indicating leakage in the pipeline. Additional 2.5 in. (63.5 mm) of test basin movement was applied resulting in a complete pressure loss in the system. The test was then stopped.

### 5.2.2 Instrumentation

Figure 5.1, a plan view of the test layout, shows the locations of the instruments along the test pipeline. The instrumentation consisted of strain gages at sixteen locations (gage planes) along the pipeline, load cells at the ends of the pipeline and string pots to measure joint displacements and rotations. Sixty-four strain gages were installed in sixteen locations along the pipeline to measure strains and to evaluate axial forces and bending moments. Strain gages were positioned at the crown (C) and invert (I), and at the east (E) and west (W) springlines of the pipe. Table 5.1 provides the number of strain gage station locations with respect to the fault. Strain gage locations were chosen on the basis of the expected deformed shape and axial behavior of the pipeline as determined from direct tension and four-point bending tests performed at Cornell University as well as the results of finite element analyses of the test. Strain gage stations S215 and N263 were installed to provide redundant measurements of the end loads. Strain gage stations close to the joints, S152, S78, S31, N42, N88, N160, and N215, were placed to assess strain concentration near the EJS castings.

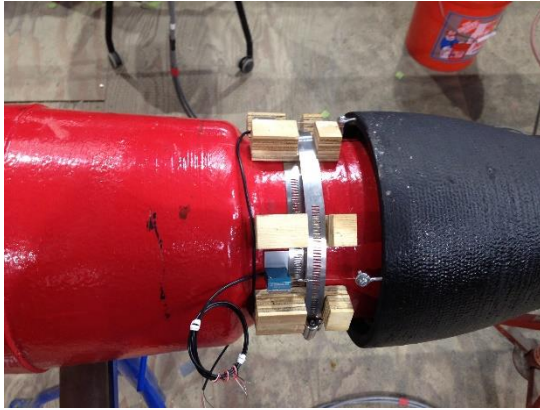
Table 5.1. Strain Gage Locations and Coding System for EJS Split-basin Test

Gage Station	Gages	Distance from Fault
S215	S215E-East Springline, Longitudinal S215C-Crown, Longitudinal S215W-West Springline, Longitudinal S215I-Invert, Longitudinal	215 in. (5.46 m) south
S152	S152E-East Springline, Longitudinal S152C-Crown, Longitudinal S152W-West Springline, Longitudinal S152I-Invert, Longitudinal	152 in. (3.86 m) south
S120	S120E-East Springline, Longitudinal S120C-Crown, Longitudinal S120W-West Springline, Longitudinal S120I-Invert, Longitudinal	120 in. (3.04 m) south
S88	S88E-East Springline, Longitudinal S88C-Crown, Longitudinal S88W-West Springline, Longitudinal S88I-Invert, Longitudinal	88 in. (2.24 m) south
S78	S78E-East Springline, Longitudinal S78C-Crown, Longitudinal S78W-West Springline, Longitudinal S78I-Invert, Longitudinal	78 in. (1.98 m) south
S31	S31EA-East Springline, Longitudinal S31CA-Crown, Longitudinal S31WA-West Springline, Longitudinal S13IA-Invert, Longitudinal	31 in. (0.79 m) south
S15	S15EA-East Springline, Longitudinal S15CA-Crown, Longitudinal S15WA-West Springline, Longitudinal S5IA-Invert, Longitudinal	15 in. (0.38 m) south
0	0E-East Springline, Longitudinal 0C-Crown, Longitudinal 0W-West Springline, Longitudinal 0I-Invert, Longitudinal	0
N15	N15E-East Springline, Longitudinal N15C-Crown, Longitudinal N15W-West Springline, Longitudinal N15I-Invert, Longitudinal	15 in. (0.38 m) north
N31	N31E-East Springline, Longitudinal N31C-Crown, Longitudinal N31W-West Springline, Longitudinal N31I-Invert, Longitudinal	31 in. (0.79 m) north

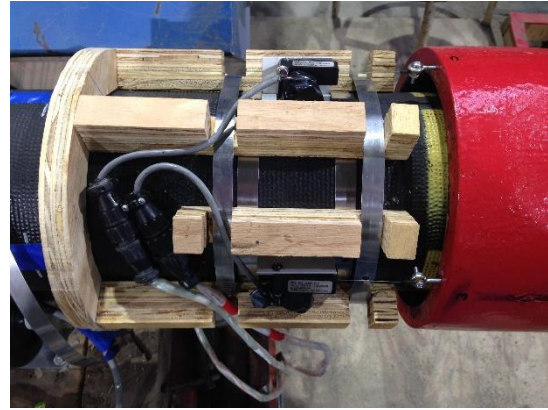
Table 5.1. Strain Gage Locations and Coding System for EJS Split-basin Test (completed)

Gage Station	Gages	Distance from Fault
N42	N42EA-East Springline, Longitudinal N42CA-Crown, Longitudinal N42WA-West Springline, Longitudinal N42IA-Invert, Longitudinal	42 in. (1.07 m) north
N88	N88E-East Springline, Longitudinal N88C-Crown, Longitudinal N88W-West Springline, Longitudinal N88I-Invert, Longitudinal	88 in. (2.24 m) north
N120	N120E-East Springline, Longitudinal N120C-Crown, Longitudinal N120W-West Springline, Longitudinal N120I-Invert, Longitudinal	120 in. (3.04 m) north
N160	N160E-East Springline, Longitudinal N160C-Crown, Longitudinal N160W-West Springline, Longitudinal N160I-Invert, Longitudinal	160 in. (4.06 m) north
N215	N215E-East Springline, Longitudinal N215C-Crown, Longitudinal N215W-West Springline, Longitudinal N215I-Invert, Longitudinal	215 in. (5.46 m) north
N263	N263E-East Springline, Longitudinal N263C-Crown, Longitudinal N263W-West Springline, Longitudinal N263I-Invert, Longitudinal	263 in. (6.68 m) north

Figure 5.2 shows the setup of the string potentiometers (pots). Three string pots were placed at each joint to measure the joint pullout and rotation, as well as spigot to bell face relative movement. Table 5.2 provides the locations and the labeling of the joint string pots to measure joint pullout and rotation. Two string pots were mounted at the east and west springlines of the bell. The other string pot was installed at the crown of the bell. The FRE and SE spigots were inserted into the FR and SE bells at each joint approximately 0.5 and 5 in. (12.7 and 127 mm), respectively. After the instrumentation was installed, protective shielding was wrapped around the joint. Figure 5.3 is an overview of the pipe joint with the protective shielding.

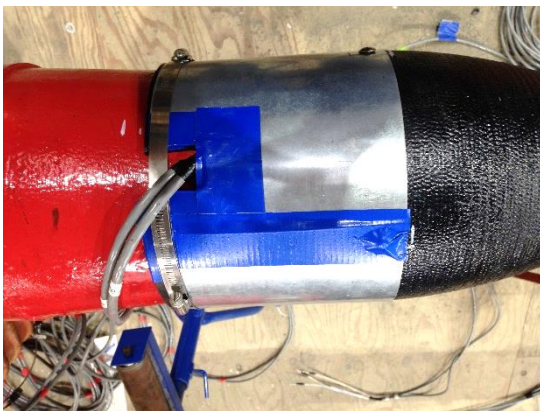


a) FR Joint



b) SE Joint

Figure 5.2 Setup of String Pots



a) FR Joint



b) SE Joint

Figure 5.3 Pipe Joints with Protective Shielding

Four calibrated load cells were positioned at each end of the test basin. Table 5.3 provides the locations and the labeling of the load cells. Twenty-nine survey marks were scribed along the crown of the specimen at approximately 12-in. (300-mm) intervals. The pipe was surveyed with a total station instrument prior to burial to determine its initial position, and again after the test, to provide a measure of global pipeline deformation.

Table 5.2. String Pot Locations and Labeling for EJS Split-basin Test

Location	Displacement Measurement Device	Type and Stroke
S15 FR Joint	S15 FR Disp E – East Springline S15 FR Disp C – Crown S15 FR Disp W – West Springline	String pot ± 1 in. String pot ± 1 in. String pot ± 1 in.
S15 SE Joint	S15 SE Disp E – East Springline S15 SE Disp C – Crown S15 SE Disp W – West Springline	String pot ± 5 in. String pot ± 5 in. String pot ± 5 in.
S5 FR Joint	S5 FR Disp E – East Springline S5 FR Disp C – Crown S5 FR Disp W – West Springline	String pot ± 1 in. String pot ± 1 in. String pot ± 1 in.
S5 SE Joint	S5 SE Disp E – East Springline S5 SE Disp C – Crown S5 SE Disp W – West Springline	String pot ± 5 in. String pot ± 5 in. String pot ± 5 in.
N5 FR Joint	N5 FR Disp E – East Springline N5 FR Disp C – Crown N5 FR Disp W – West Springline	String pot ± 1 in. String pot ± 1 in. String pot ± 1 in.
N5 SE Joint	N5 SE Disp E – East Springline N5 SE Disp C – Crown N5 SE Disp W – West Springline	String pot ± 5 in. String pot ± 5 in. String pot ± 5 in.
N15 FR Joint	N15 FR Disp E – East Springline N15 FR Disp C – Crown N5 FR Disp W – West Springline	String pot ± 1 in. String pot ± 1 in. String pot ± 1 in.
N15 SE Joint	N5 SE Disp E – East Springline N5 SE Disp C – Crown N5 SE Disp W – West Springline	String pot ± 5 in. String pot ± 5 in. String pot ± 5 in.

1 in. = 25.4 mm

Table 5.3. Load Cell Locations and Labeling for EJS Split-basin Test

Location	Load Cell
South End	SW Top Ld – West, Top SE Top Ld – East, Top SW Bot Ld – West, Bottom SE Bot Ld – East, Bottom
North End	NW Top Ld – West, Top NE Top Ld – Outer, East, Top NW Bot Ld – West, Bottom NE Bot Ld – East, Bottom

### 5.2.3 Soil Preparation

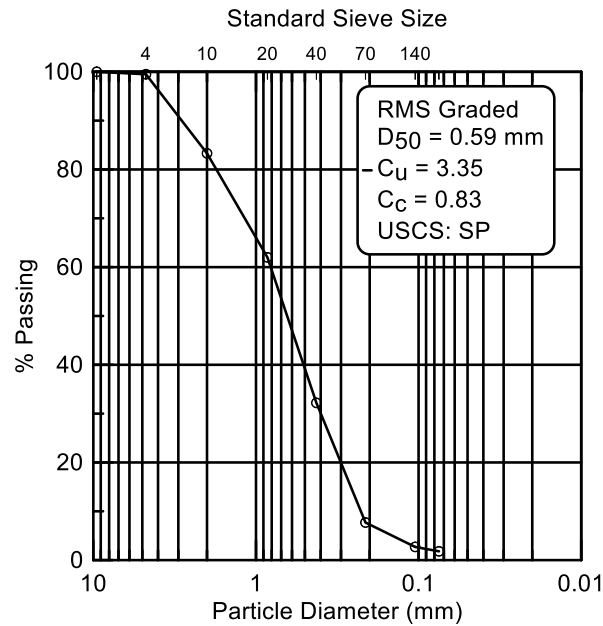
The soil used during the test was crushed, washed, glacio-fluvial sand obtained from RMS Gravel, Dryden, NY, consisting of particles mostly passing the ¼ in. (6.35 mm) sieve. Figure 5.4 is the grain size distribution of the RMS graded sand. Approximately 6-in. (152-mm)-thick lifts of soil were placed and compacted until there was 31 in. (787 mm) cover of compacted sand above the pipe crown. Every layer was compacted to the same extent and moistened with water in a similar way to achieve uniformity. Dry density measurements were taken for each layer using a Troxler Model 3440 densitometer. Moisture content measurements were obtained using both soil samples and the densitometer at the same locations.

The target value of dry density was  $\gamma_{dry} = 106 \text{ lb/ft}^3$  ( $16.7 \text{ kN/m}^3$ ), and the target value of moisture content was  $w = 4.0 \%$ , corresponding to an angle of shearing resistance (friction angle) of the sand of approximately  $42^\circ$ . Eight measurements of dry unit weight and moisture content were made for each soil lift. The average and standard deviation of all dry unit weight measurements were  $108.4 \text{ lb/ft}^3$  ( $17.0 \text{ kN/m}^3$ ) and  $1.1 \text{ lb/ft}^3$  ( $0.17 \text{ kN/m}^3$ ), respectively. Moisture content measurement had an average of 4.4% and standard deviation of 0.6%. The angle of shearing resistance of the soil, based on correlations with soil unit weight established at Cornell, was  $\phi' = 41\text{-}42^\circ$ . The soil strength properties are representative of a well-compacted dense sand.

## 5.3 Experimental Results of Split Basin Test

### 5.3.1 Test Basin Movements

Four actuators are connected between the movable portion of the test basin and the modular reaction wall in the laboratory. From south to north, the actuators are identified as short-stroke actuator 1 (SSA1), short-stroke actuator 2 (SSA2), long-stroke actuator 1 (LSA1), and long-stroke actuator 2 (LSA2). Each SSA actuator has a displacement range of  $\pm 2 \text{ ft}$  ( $\pm 0.61 \text{ m}$ ) for a total stroke of 4 ft (1.22 m) and load capacity of 100 kips (445 kN) tension and 145 kips (645 kN) compression. Each LSA actuator has a displacement range of  $\pm 3 \text{ ft}$  (0.91 m) for a total stroke of 6 ft (1.83 m) and load capacity of 63 kips (280 kN) tension and 110 kips (489 kN) compression.



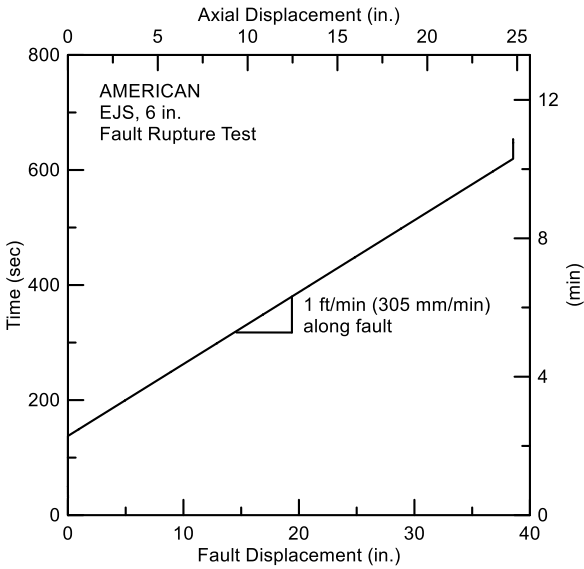


Figure 5.5. Fault Displacement vs. Time

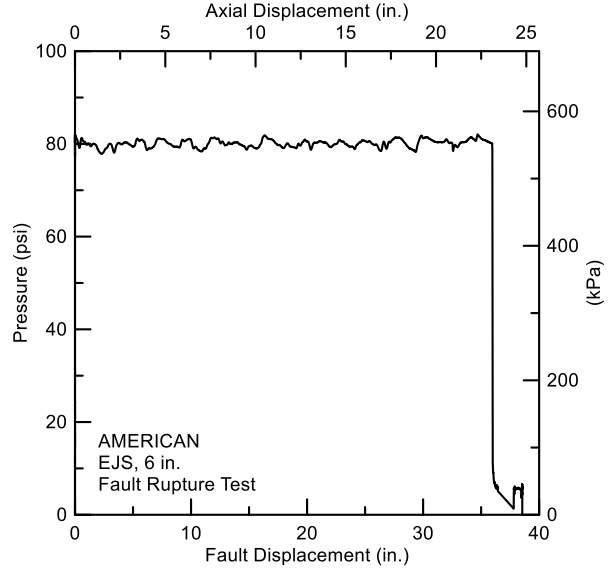


Figure 5.6 Internal Water Pressure vs. Fault Displacement

### 5.3.3 Joint Pullout

The joint pullout movements and rotations were measured using string potentiometers (string pots.) The string pot locations are given in Section 5.2.2 and shown in Table 5.2. Each joint has a total of six string pots. Three at the FR bell and three at the SE bell, for a total of six. The positioning and protection of these pots was difficult and required great attention to detail and anticipated rough treatment during the tests. However, these measurements are critical in evaluating the overall behavior of the EJS system.

The collective average movements of the FR and SE joints are shown in Figures 5.7 to 5.8, respectively. Figure 5.9 shows the total movements of the S15, S5, N5, and N15 earthquake joint systems. FR and SE joint rotations are provided in Figures 5.10 and 5.11, respectively. Figure 5.12 presented the total EJS deflections at S15, S5, N5, and N15. The movements of each portion of the double-jointed EJS at a fault displacement of 36 in. (914 mm) are given in Table 5.4. This fault movement is that at which the S15 FR bell failed. This corresponds to an axial test basin displacement of  $(36 \text{ in.}) \cos 50^\circ = 23.1 \text{ in. (587 mm.)}$  The failure mode for this test was ductile iron breakage at the FR bell of joint S15. A description of the failure and photos are shown in a later section.

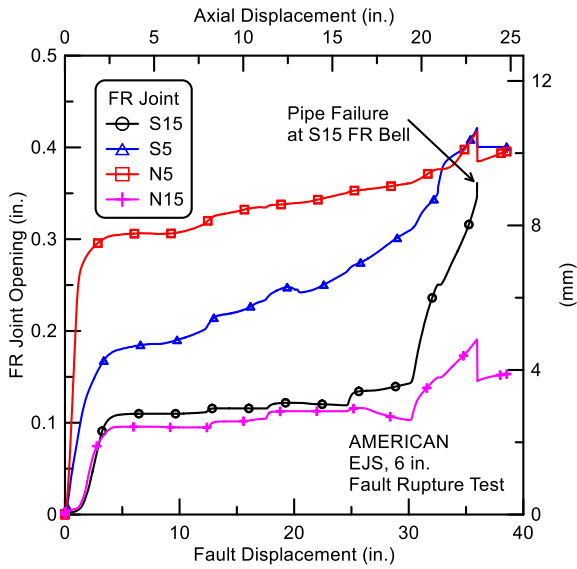


Figure 5.7. Average FR Joint Openings vs. Fault Displacement

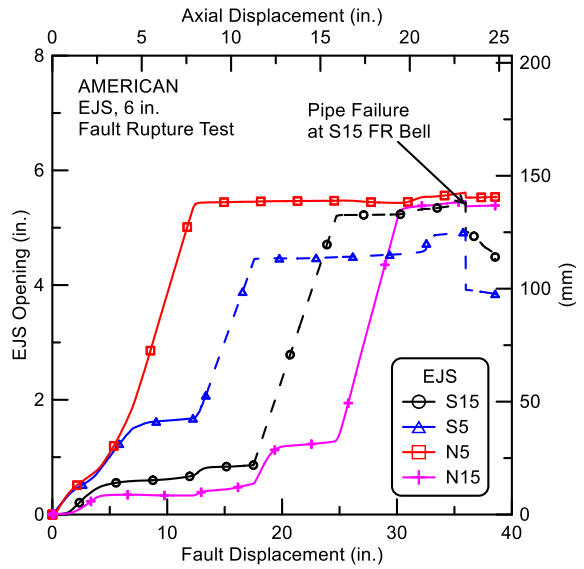


Figure 5.8. Average SE Joint Openings vs. Fault Displacement

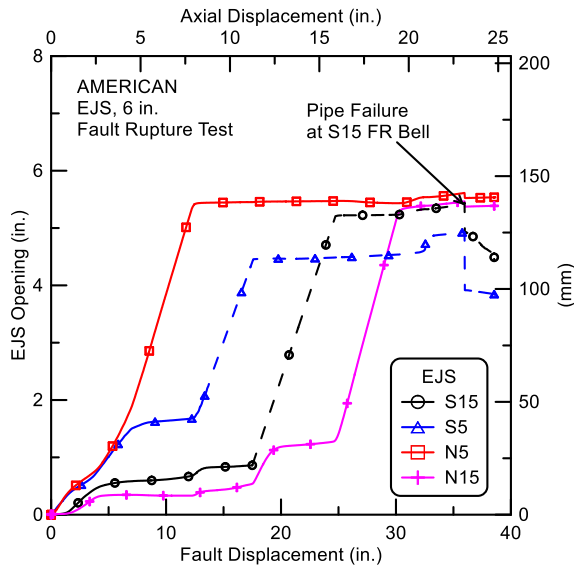


Figure 5.9. Total EJS Openings for All Joints vs. Fault Displacement

Table 5.4. Joint Openings at 36 in. (914 mm) Fault Movement

Test Joint	Joint Extension		
	FR (in.)	SE (in.)	EJS (in.)
S15	0.3	5.1	5.4
S5	0.4	4.5	4.9
N5	0.4	5.2	5.6
N15	0.2	5.3	5.5
Average	0.4	5.0	5.4
All four EJS joints	1.4	20.1	<b>21.5</b>
Axial Basin Extension (in.)			23.1
Cornell Tension Tests	5.5 in. per EJS × 4 joints		22.0
AMERICAN performance criteria	4.8 in. per EJS × 4 joints		19.2

1 in. = 25.4 mm

The S15 SE and S5 SE string pots did not provide consistently accurate measurements after 17.5 and 13.4 in. (445 and 340 mm) of fault displacement, respectively. The survey measurements and basin movement were then used to estimate the S15 SE and S5 SE joint displacements beyond these limits as shown in dashed lines in Figures 5.8, 5.9, 5.11, and 5.12.

In Table 5.4 the openings of each of the joints are given, along with the cumulative opening of all four joints. The average joint opening of all joints at the limit pipe condition was 5.4 in. (137 mm.) The summation of the joint displacements was 21.5 in. (546 mm.) When Cornell performed the direct tension tests on the EJS joint, the extension of the joint system at failure was 5.5 in. (140 mm.). It must be noted that when the FR bell fractured at the S15 joint, none of the other joints had failed. All joints were close to or in exceedance of the anticipated limiting displacement. Also, the performance criteria stated for the AMERICAN EJS is  $\pm 2.4$  in. (61 mm) from the mid-point position. The performance limit for four joints would be 19.2 in. (488 mm). Thus, the AMERICAN test specimen total extension exceeded the performance criteria for longitudinal extension, and each joint moved according to the anticipated total extension.

### 5.3.4 Joint Rotations (Deflections)

Joint rotations (deflections) were determined using the string pots at each joint and using survey measurements. In this report “deflection” is used to describe the angular deflection of the pipe, consistent with industry usage. It is critical to note that the observed failure during this test was due to rupture of the ductile iron in the FR bell at joint S15, most likely due to high moment and joint restraint due to the proximity of the joint to the fixed end of the test basin. None of the interior joints with high deflections (rotations) failed.

Joint rotation is calculated from the string pot measurements at each joint as:

$$\text{Rotation (deg)} = \tan^{-1} \left( \frac{\text{East String Pot Displacement} - \text{West String Pot Displacement}}{\text{Separation Distance between the String Pots}} \frac{180}{\pi} \right) \quad (5.1)$$

The joint deflections are shown in Figures 5.10 to 5.12. Figures 5.10 and 5.11 show deflections at the FR and SE joints, respectively. The total EJS deflection is a sum of FR and SE joint deflections, and is shown in Figure 5.12. As the test basin was displaced, the S5 EJS moved closer to the fault and accommodated most of the fault offset with maximum deflection of nearly 9.4 degrees without failure. The N5 EJS was second closest to the fault and deflected about 6.7 degrees in the opposite direction to the S5 EJS. The other two EJS deflections were approximately 1 degree.

During the beginning part of the test, the N5 and S5 earthquake joint systems accommodated most of the test basin movement. The N5 EJS, however, displaced faster such that the spigot weld ring was in contact with the locking ring at 13 in. (330 mm) of fault displacement, and the S5 EJS was fully extended at 17.5 in. (445 mm) of fault displacement. Subsequently, the S15 EJS opened rapidly and became fully extended when the basin reached 25 in. (635 mm) of movement. Axial displacement was then accommodated by the N15 EJS movement up until 30 in. (762 mm) of fault displacement when all four earthquake joint systems were fully opened. At a fault displacement of approximately 36 in. (914 mm), the S15 FR bell failed and leaked, corresponding to an additional 3.9 in. (99 mm) of axial displacement after all earthquake joint systems were extended to a condition of spigot ring/locking ring contact.

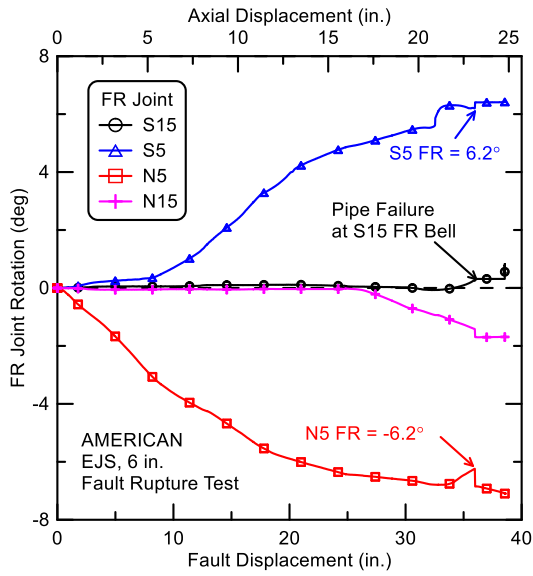


Figure 5.10. FR Rotations vs. Fault Displacement

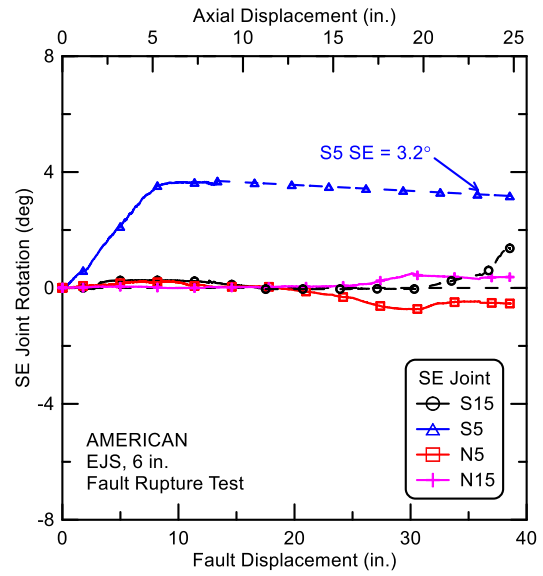


Figure 5.11. SE Rotations vs. Fault Displacement

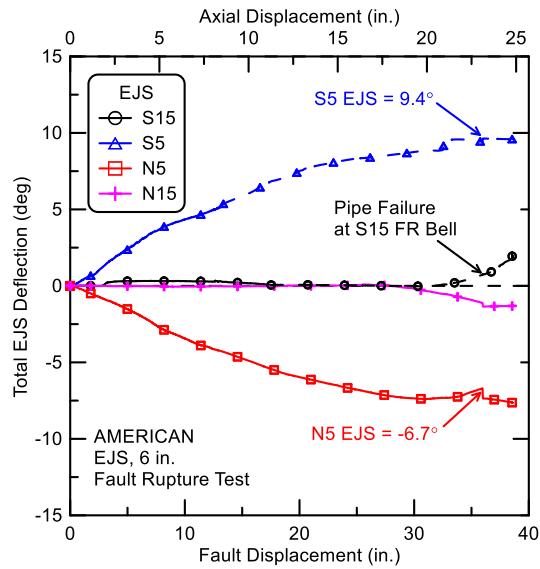
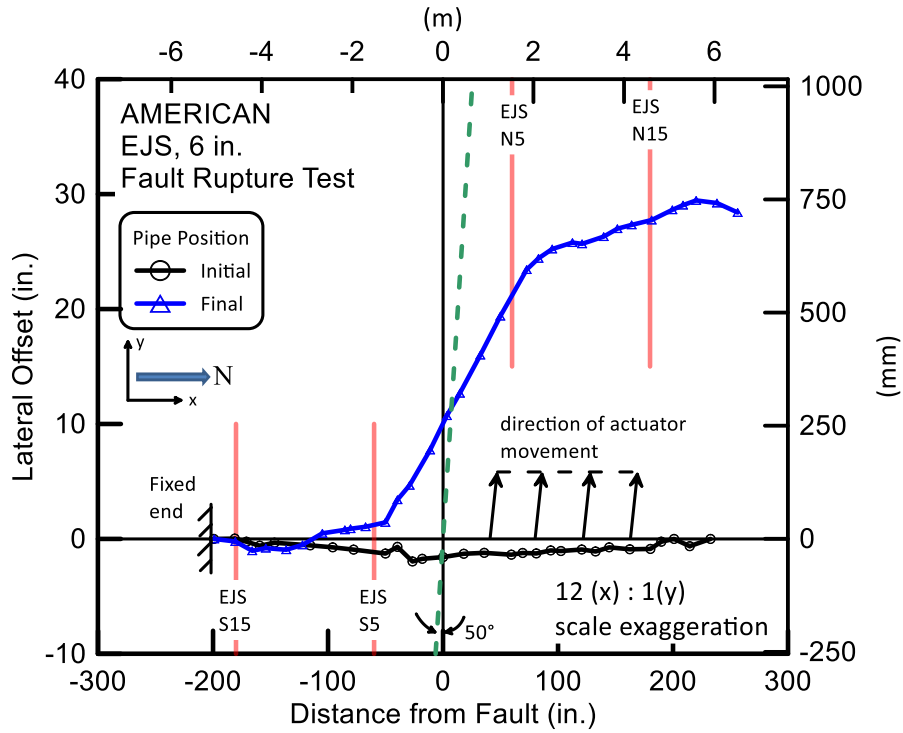


Figure 5.12. Total EJS Deflections vs. Fault Displacement

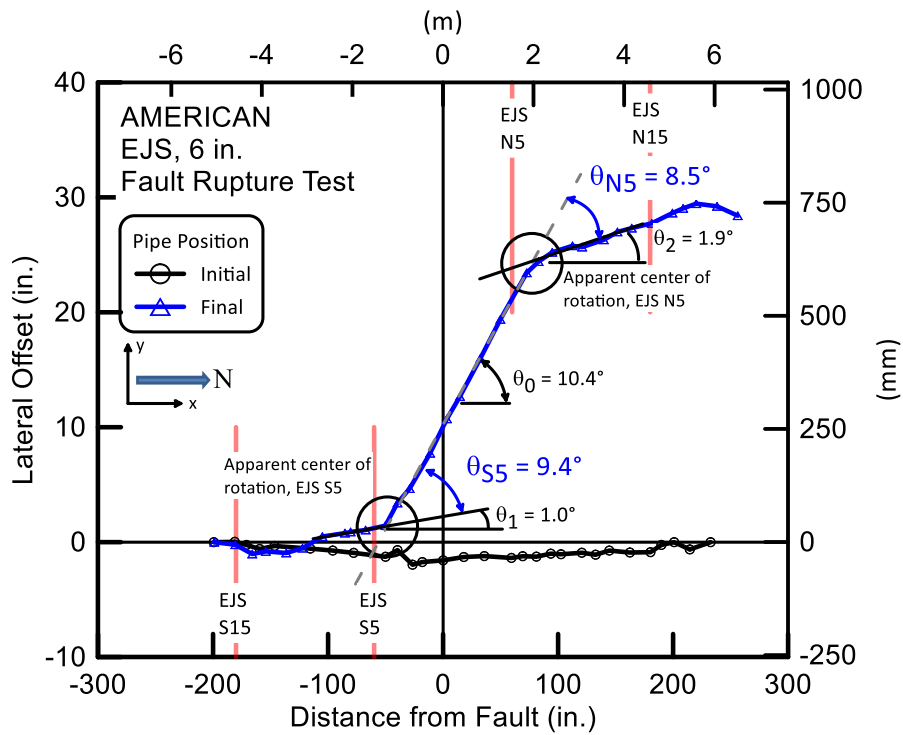
The Bovay Laboratory uses a general coordinate system established in 2012 as part of Cornell's participation in the George E. Brown, Jr. Network for Earthquake Engineering Simulation (NEES). The coordinate system was developed using a Leica Flexline TS02 reflectorless total station to identify baseline positions within the laboratory. When the AMERICAN pipe was placed in the basin and backfilled to approximately the springline depth, survey measurements were taken at marked locations every 12 in. (25 mm) along the pipe crown. These data provide a baseline of the initial pipe position, albeit prior to complete backfill. Following careful pipe excavation with minimal disturbance, these pipe was re-surveyed. These data provide very close locations of the maximum pipe displacement at the maximum basin displacement. The test hydraulics remained on during pipe exposure so as not to allow the entire system to relax.

Figures 5.13 a) shows, on a greatly exaggerated scale, the Leica data for the initial and final pipe positions. The data shown in Figure 5.13 were used to estimate the overall joint deflections at the S5 and N5 EJS. The measurements at the other two joints were too small to provide useful information. The apparent center of rotation of the S5 and N5 joints are shown in the figure. The slope of the mid-portion of the pipeline, which contained no joints, was  $\theta_0 = 10.4^\circ$ . The slope of the pipe beyond the S5 but before the S15 joint was  $\theta_1 = 1.0^\circ$ . The combined deflection of the S5 EJS then was  $\theta_{S5} = 9.4^\circ$ . The slope of the pipe beyond the N5 but before the N15 joint was  $\theta_2 = 1.9^\circ$ . The combined deflection of the N5 EJS then was  $\theta_{N5} = 8.5^\circ$ .

Table 5.5 presents a comparison between the joint deflections determined using the string pot measurements and the survey data. It is believed that the Leica optical survey methods provide a more reasonable overall assessment of the combined joint deflections. Again, it is very important to note that these deflections did not cause any observed leakage or failure at the S5 and N5 joints. These are the joints that accommodated the greatest deflection in response to the large ground displacement. Essentially, these are the two critical joints for the experiment. Both the S5 and N5 AMERICAN EJS experienced joint deflections (rotations) beyond the combined assembly performance limit of  $8^\circ$ .



a) Survey Data



b) Method used for Determining Joint Deflections

Figure 5.13. Joint Deflections from Leica Survey Data

Table 5.5. Joint Deflections

Test Joint	String Potentiometers Data			Survey Data <sup>a</sup>
	FR Rotation (degrees)	SE Rotation (degrees)	EJS Rotation (degrees)	EJS Rotation (degrees)
S15	0.2	0.5	0.7	
S5	6.2	3.2	9.4	9.4
N5	-6.2	-0.5	-6.7	-8.5
N15	-1.4	0.3	-1.1	

a – based on pre- and post-test Leica measurements

Positive refers to rotation in counter-clockwise direction

### 5.3.5 End Loads and Pipe Axial Forces

The axial tensile loads were measured with four load cells at the south end of the test basin and four load cells at the north end. The sum of the four load cells at each end of the test basin gives the total axial end load. Figure 5.14 shows the total load at the south and north ends of the test basin vs. fault displacement. The initial reduction of approximately 1.5 kip (6.7 kN) in the end loads was caused by internal pressurization. The end loads sharply increased at a fault displacement of approximately 30 in. (762 mm), corresponding to an axial basin displacement of 19.2 in. (620 mm), which is close to the sum of the 5.5 in. (114 mm) pullout settings for the four earthquake joint systems.

Also included in Figure 5.14 are axial loads calculated from axial strain gages at planes close to the end of the test specimen. The axial force from average strain gage measurements was calculated as  $F = \epsilon AE$ . The outside diameter of the pipe was  $OD = 6.9$  in. (175 mm) and the average measured wall thickness was  $t_w = 0.3$  in. (7.6 mm). This gives a pipe wall cross-sectional area,  $A = 6.22$  in.<sup>2</sup> (4013 mm<sup>2</sup>). The Young’s modulus of the ductile iron was  $E = 24,200$  ksi (169 GPa), which was determined from tensile coupon tests. The axial forces in the pipe near the load cell locations were consistent with forces measured by the load cells. Loads recorded at the south end of the specimen were slightly greater than those recorded at the north end.

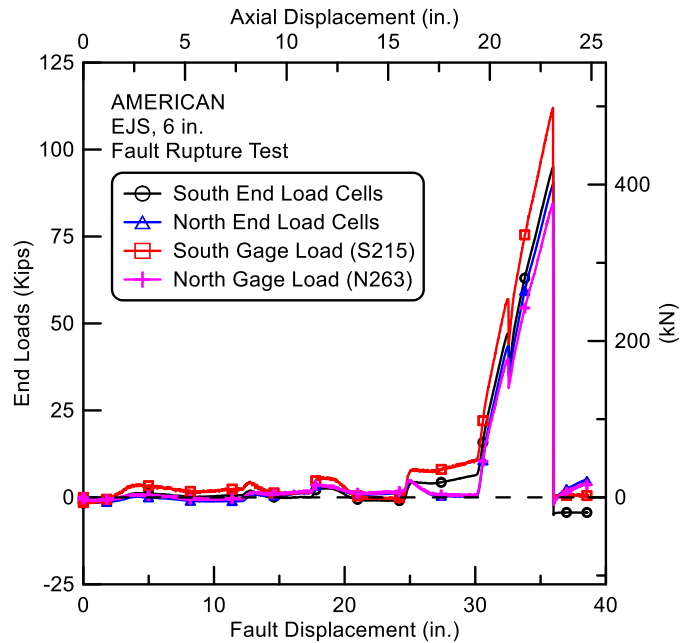


Figure 5.14. Comparison of Average End Force from Load Cells and Strain Gages

The calculated axial loads at each gage plane along the pipeline are presented in Figure 5.15 for various levels of fault displacement. The EJS casting locations are shown in red shaded areas. Figure 5.15 a) shows the tensile forces up to 15 in. (380 mm) of fault movement. Relatively low tensile forces were measured along the pipeline during these initial increments of displacement. The highest axial force was detected near the fault location, and the loads were lower at locations further away from the fault.

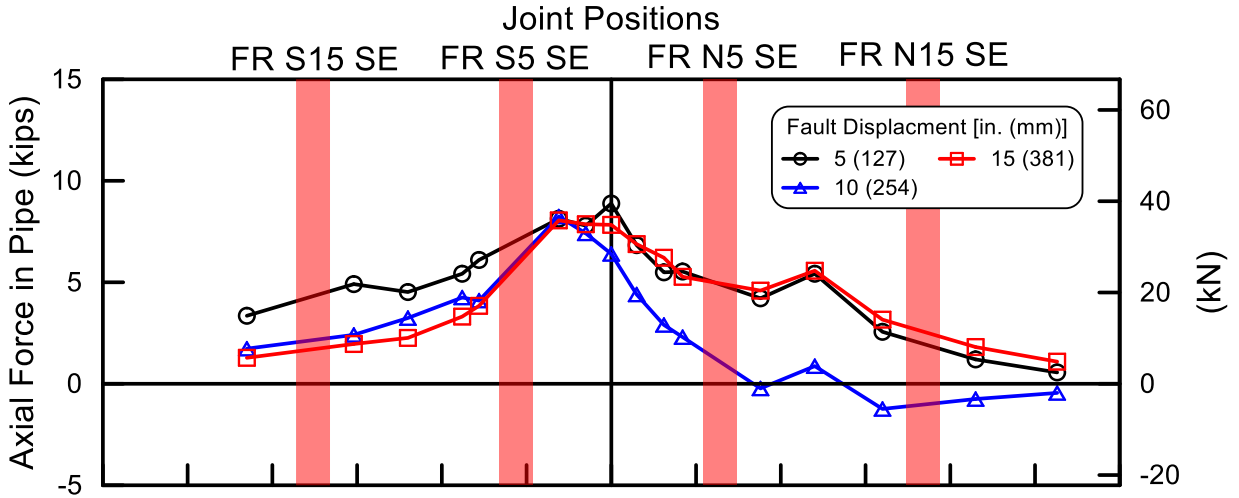
Figure 5.15 b) (note change in scale for load) shows that tensile forces were generally higher with increasing fault displacement. The highest axial force was detected close to the S5 SE joint. However, a rapid increase in tensile force was observed at -152 plane, which was located near the S15 SE joint. Figure 5.15 c) shows that the loads increased rapidly from 30 in. (762 mm) to 36 in. (914 mm) of fault displacement. All joints attained contact between the spigot weld rings and the locking rings at 30 in. (762 mm) of fault displacement. About the same levels of maximum tensile loads were measured along the pipeline during these displacements, with the loads slightly higher towards the south end of the test basin. The peak forces of approximately 112 kips (498 kN) were found near S15 joints at -215 and -152 planes. The peak forces are consistent with the crack at the S15 FR bell, as shown by photos of the pipe failure (Figure 5.18).

### 5.3.6 Bending Moments

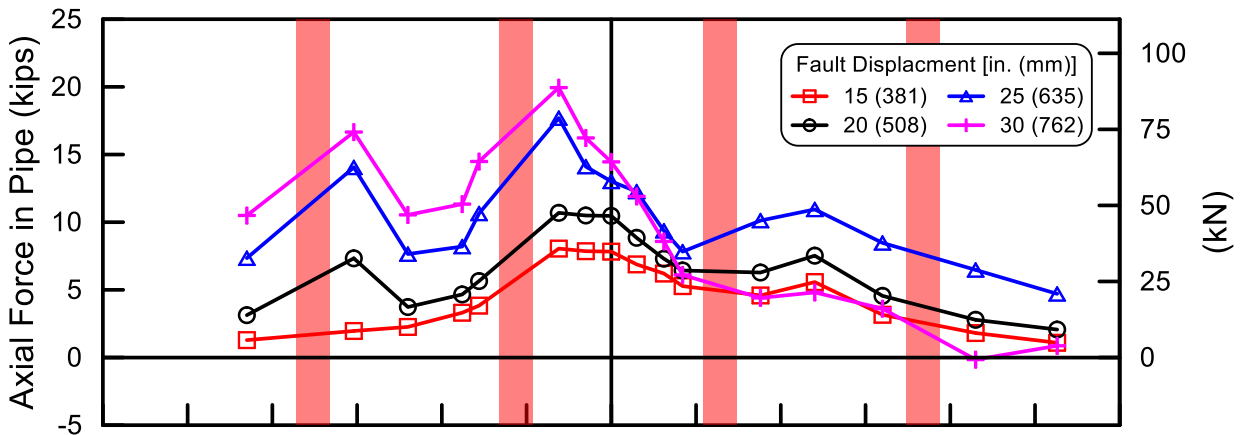
Bending moments,  $M$ , were calculated at each strain gage station along the pipeline as:

$$M = \frac{\varepsilon_{\text{bend}} EI}{c} \quad (5.2)$$

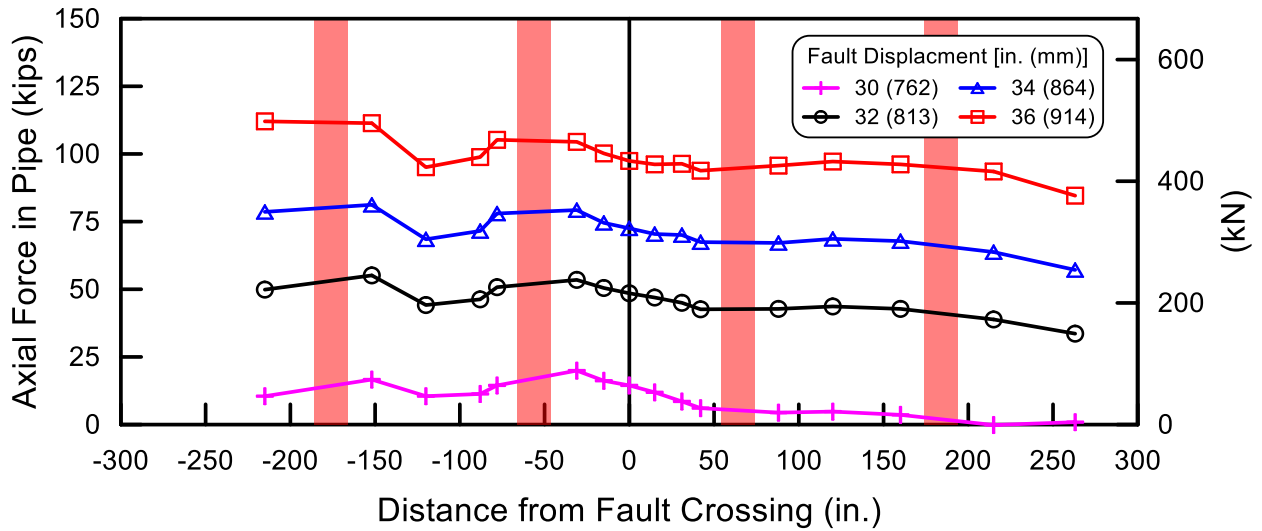
where bending strains,  $\varepsilon_{\text{bend}}$ , is one half the difference between the springline strains;  $E$  is Young's modulus of the ductile iron of 24,200 ksi (169 GPa);  $I$  is moment of inertia of 33.9 in<sup>4</sup> (1410 cm<sup>4</sup>); and  $c$  is distance to outer fiber of 3.45 in (87.6 mm). Figure 5.16 presents the bending moments measured along the pipeline corresponding to various levels of fault displacement. The EJS castings are also shown in red shaded areas. Figure 5.16 a) shows that, during the first 15 in. (381 mm) of fault displacement, bending moments along the pipeline were relatively low. The measurements disclose an anti-symmetric pattern of moment distribution centered on the fault. Figure 5.16 b) (note change in scale for moment) shows that the moments were higher as the fault movement increased. The peak moments were detected near S15 and N15 locations. Figure 5.16 c) shows a consistent bending moment distribution for fault movements of 30 in. (762 mm) to 36 in. (914 mm). At a fault displacement of 30 in. (726 mm) the maximum moments are on the order of 200 kip-in. (22.6 kN-m) in the vicinity of S15 and N15 EJS castings.



(a) 5 to 15 in. (127 to 381 mm) of Fault Displacement

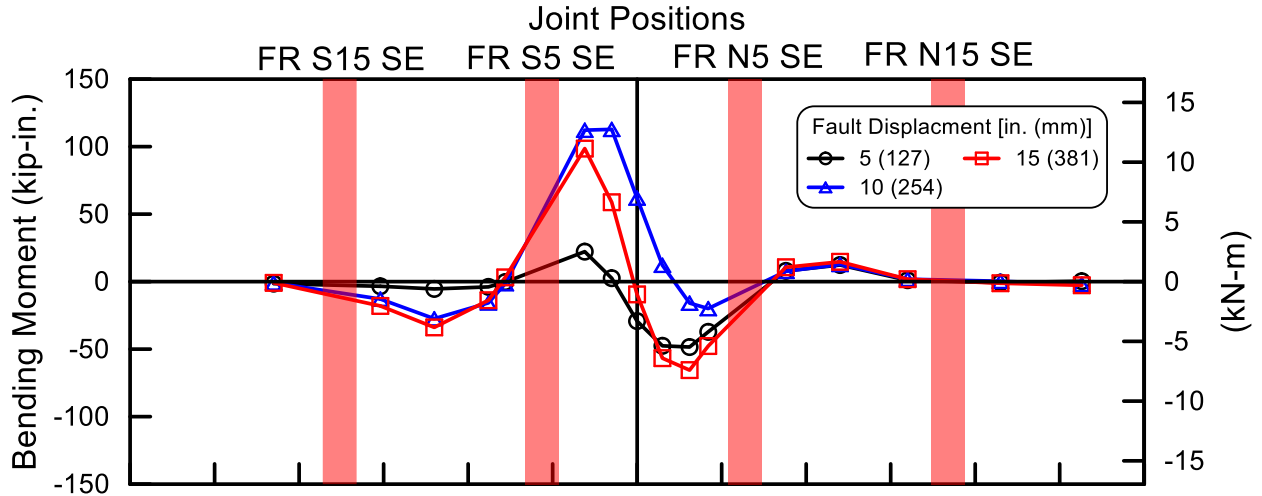


(b) 15 to 30 in. (381 to 762 mm) of Fault Displacement

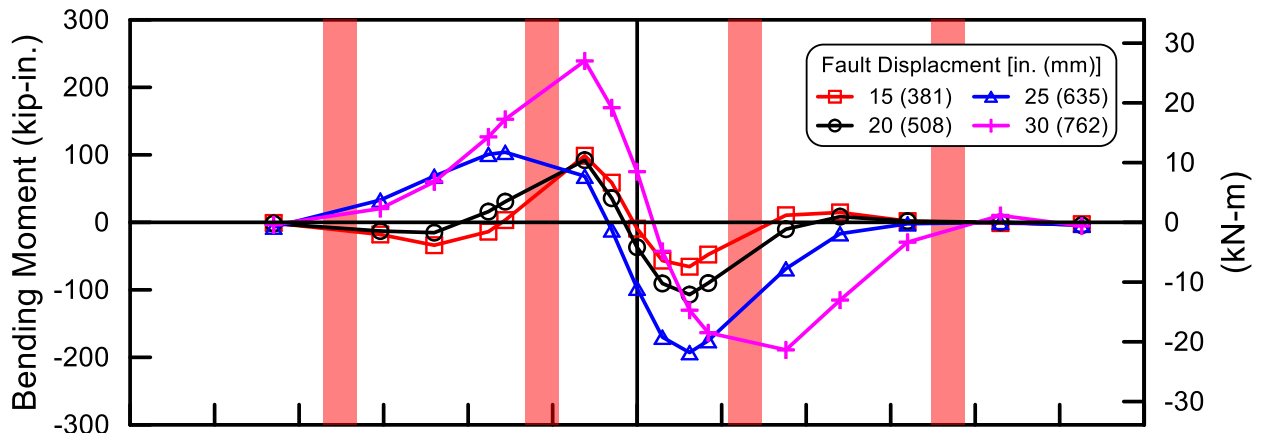


(c) 30 to 36 in. (762 to 914 mm) of Fault Displacement

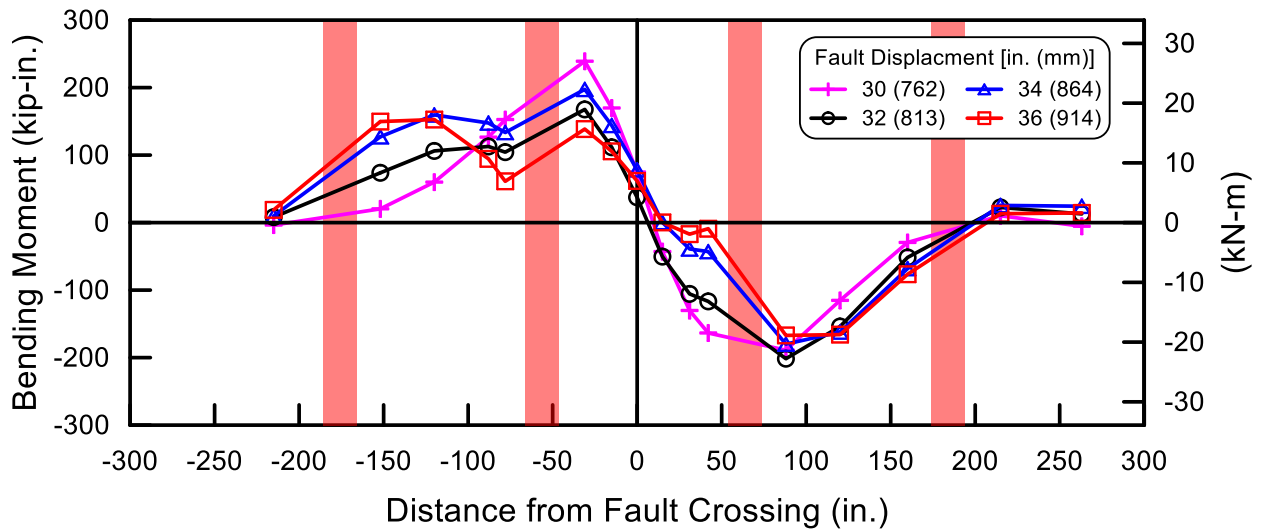
Figure 5.15. Axial Forces in Pipe vs. Distance from Fault



(a) 5 to 15 in. (127 to 381 mm) of Fault Displacement



(b) 15 to 30 in. (381 to 762 mm) of Fault Displacement



(c) 30 to 36 in. (762 to 914 mm) of Fault Displacement

Figure 5.16. Bending Moments in Pipe vs. Distance from Fault

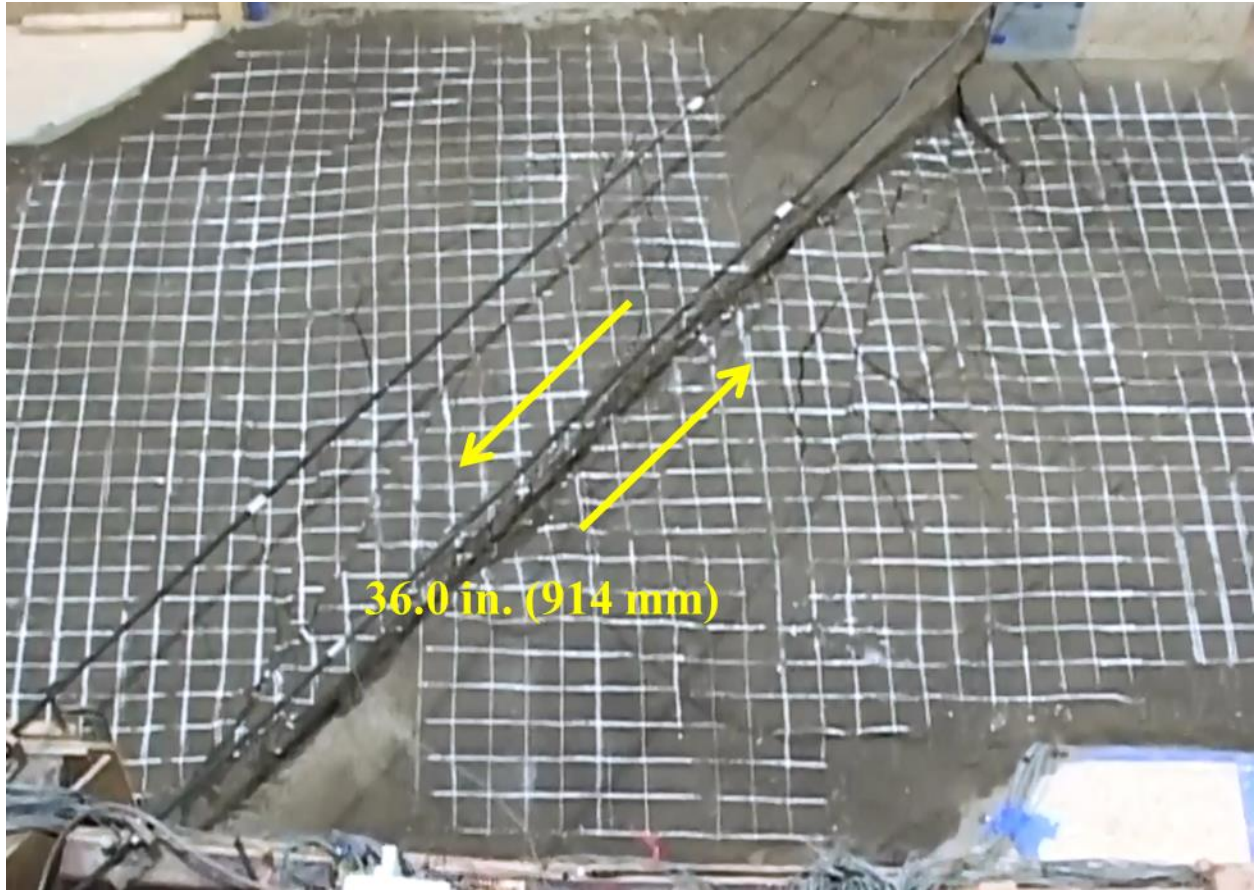


Figure 5.17. Fault Rupture at Pipe Failure

### 5.3.7 Deformed Shape and Pipe Failure

Figure 5.17 shows the fault rupture at pipe failure. Figure 5.18 a) shows a photo of the pipeline before backfilling and burial of the pipe. Failure of the FR bell at EJS S15 was the overall failure mode. After fault rupture, the pipeline was excavated carefully in a manner that preserved its deformed shape as shown in Figure 5.18 b). Angles of S5 and N5 EJS deflection are also illustrated in Figure 5.18 b). These deflection angles were obtained from the Leica data as discussed in Section 5.3.4. Figure 5.19 presents the fractured S15 FR bell without the protective shield. The plan and elevation views of the bell crack are illustrated in Figures 5.19 a) and 5.19 b) respectively.

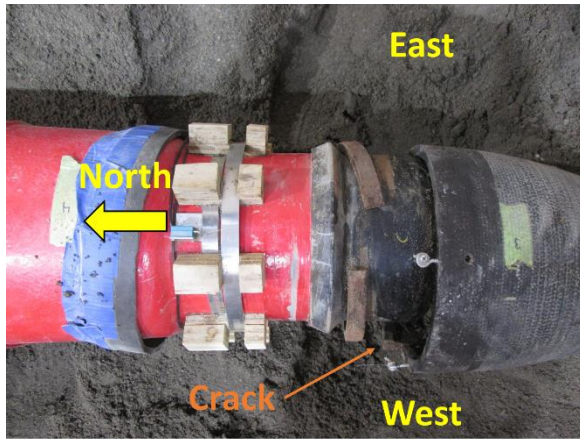


a) Before Burial



b) After Excavation

Figure 5.18. Images of Pipeline (a) before burial and (b) after excavation (angles shown from total station surveying measurements)



a) Plan View of S15 FR Bell



b) Elevation View of S15 FR Bell from West Springline

Figure 5.19. Ruptured Pipe at S15 FR Bell following Test without Protective Shield

#### 5.4 Summary of Large-Scale Testing

A 36-ft (11-m)-long, five-piece section of a ductile pipeline was tested at the Cornell Large-Scale Lifelines Facility. The pipe had a total of four AMERICAN Earthquake Joint Systems. Two EJS castings were located 5 and 15 ft (1.5 and 3.6 m) north of the fault and two EJS castings at the same distances south of the fault. The fault angle was 50°. The pipe was instrumented with sixty-four strain gages installed at sixteen locations along the pipeline to measure strains and to evaluate axial forces and bending moments. Strain gages were positioned at the crown (C), invert (I) east (E) springline, and west (W) springline of the pipe. There were three string pots at each joint to measure joint movements and to evaluate joint rotation. Four load cells were placed outside the test basin at each end, reacting between the test basin structural frame and pipe end restraint to measure axial force. The pipe was pressurized to approximately 80 psi (550 kPa.)

The pipeline was buried in the Cornell large-scale test basin in partially saturated sand that was compacted to have an average friction angle of  $\phi = 42^\circ$ , equivalent in strength to that of a medium dense to dense granular backfill. The depth of burial to top of pipe was 31 in. (781 mm). During the test, the south part of the basin remained stationary, while the north part was displaced to the north and west by large-stroke actuators to cause soil rupture and slip at the interface between the

two parts of the test basin. The north section of the test basin was displaced along a 50° fault at a rate of 12 in. (300 mm) per minute. The basin was displaced until the pipe lost pressure at 36 in. (914 mm) fault displacement, which corresponds to 23.1 in. (587 mm) of axial extension of the test basin and pipe. Following excavation, a fracture was observed near the west springline of the FR Bell of the S15 EJS.

The end forces at the south and north end of the test basin were about 95 and 90 kips (423 and 400 kN), respectively. The axial force in the pipe, as determined from the strain gage readings, was largest at 215 in. (790 mm) south of the fault at 112 kips (498 kN). It is assumed that the axial force in the pipe was at least 112 kips (498 kN).

The test measurements confirm that the pipeline was able to accommodate fault rupture through axial displacements and deflections at all four Earthquake Joint Systems. They also provide a comprehensive and detailed understanding of how the movement was accommodated at each joint, the sequence of movements, and combined axial pullout and rotation at each joint. The total axial movement is 23.1 in. (587 mm), which exceeds the sum of the 5.5 in. (140 mm) joint displacement for all four earthquake joint systems. On average, each EJS displaced on the order of 5.78 in. (147 mm). This displacement was close to movement during previous direct tension testing of the AMERICAN EJS. The maximum deflection measured at the EJS closest to the fault was about 9.6 degrees, thus demonstrating the ability of the joints to sustain significant levels of combined axial pullout and deflection. The maximum stresses sustained by the pipeline, corresponding to the largest pipeline deformation, were well within the elastic range of pipeline behavior.

The ductile iron pipeline equipped with AMERICAN Earthquake Joint System (EJS) was able to accommodate significant fault movement through axial pullout and rotation of the joints. Fault rupture simulated in the large-scale test is also representative of the most severe ground deformation that occurs along the margins of liquefaction-induced lateral spreads and landslides.

The amount of tensile strain that can be accommodated with the ductile iron pipeline will depend on the spacing of the AMERICAN Earthquake Joint Systems and the positioning of the spigot within the bell at the pipeline joints. The pipeline used in the large-scale split-basin test was able to accommodate a minimum of 21.5 in. (546 mm) of axial extension, corresponding to an average tensile strain of 4.4% along the pipeline. Such extension is large enough to accommodate the great

majority (over 99%) of liquefaction-induced lateral ground strains measured by high resolution LiDAR after each of four major earthquakes during the recent Canterbury Earthquake Sequence (CES) in Christchurch, NZ (O'Rourke, et al., 2014). These high resolution LiDAR measurements for the first time provide a comprehensive basis for quantifying the ground strains caused by liquefaction on a regional basis. To put the CES ground strains in perspective, the levels of liquefaction-induced ground deformation measured in Christchurch exceed those documented in San Francisco during the 1989 Loma Prieta earthquake and in the San Fernando Valley during the 1994 Northridge earthquake. They are comparable to the levels of most severe liquefaction-induced ground deformation documented for the 1906 San Francisco earthquake, which caused extensive damage to the San Francisco water distribution system. The test confirms that the ductile iron pipes equipped with the AMERICAN Earthquake Joint Systems are able to sustain large levels of ground deformation through axial displacement and deflection under full-scale conditions of abrupt ground rupture.

## Section 6

### Finite Element Simulations

Two-dimensional (2D) finite element (FE) analyses were performed for 6-in. (150-mm)-diameter DI pipeline using soil and geometric parameters consistent with the large-scale test basin experiment presented in Section 5. The purpose of these analyses is to demonstrate the ability to numerically simulate the performance of the AMERICAN EJS to the same ground deformation imposed on the 6-in. (150-mm) pipeline in the large-scale split-basin test.

#### 6.1 Large-Scale Split Basin Test

Figure 6.1 is a plan view of the large-scale split basin test layout, which was used to generate fault rupture effects of 6-in. (150-mm)-diameter DI pipeline consisting of five pipe segments connected with AMERICAN EJS joints. The figure shows the fault rupture plane and approximate locations of the four actuators driving the ground failure. A detailed description of the test is provided in Section 5, and only the key features of the testing are summarized in this section of the report.

The objective of the test was to impose abrupt ground deformation on the pipeline, which was identical to left lateral strike slip fault rupture and representative of the most severe ground deformation that occurs along the margins of liquefaction-induced lateral spreads and landslides. The pipeline was constructed to evaluate its capacity to accommodate full-scale fault movement through the simultaneous axial pullout at four different joints. Measuring simultaneous performance of multiple joints allows for confirmation that the pipeline will respond to ground failure as intended, understand the complex interaction among the different joints, and determine the maximum ground deformation and axial pipeline load that can be sustained before joint leakage.

The full-scale test pipeline was buried in the Cornell large-scale test basin in partially saturated sand that was compacted to have an average friction angle of  $\phi' = 42^\circ$ , equivalent in strength to that of a medium dense to dense granular backfill. The pipeline was positioned so that the spigot end of the SE section was fully homed in the FR bell, and the FE spigot fully homed in the SE

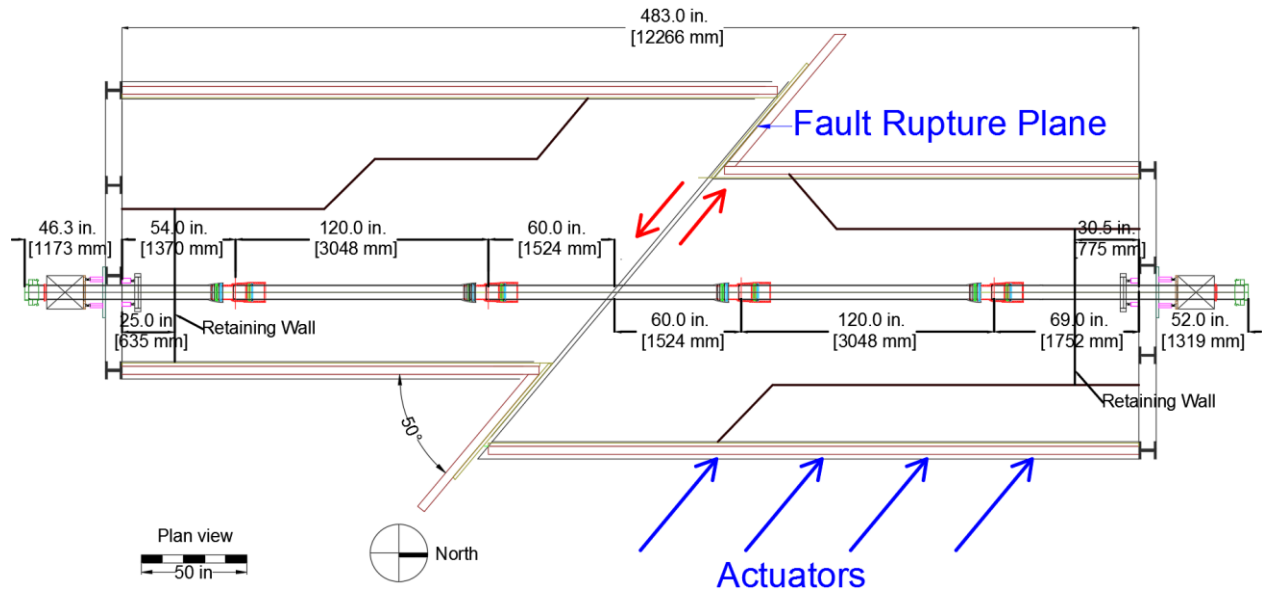


Figure 6.1. Plan View of Large-Scale Split Basin Test for AMERICAN Test

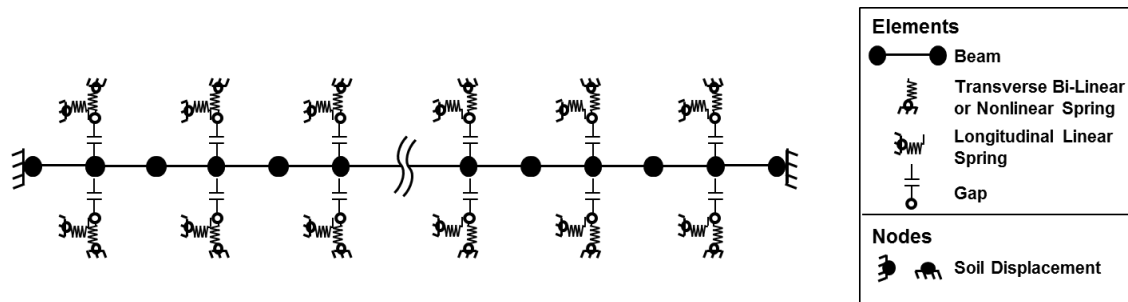


Figure 6.2. 2D FE Model Setup for a Pipeline under Fault Rupture

bell. This allows the maximum extension of the EJS. The dimensions for allowable extension were based on those measured during the Cornell direct tension tests of 0.5 in. (12.7 mm) and 5.0 in., (127 mm) for the FR and SE joint, respectively, so each joint could pull from the bell approximately 5.5 in. (140 mm) before fully extended. The performance criterion for the 6 in. (150 mm) AMERICAN EJS is stated as  $\pm 2.4$  in. (61 mm) from the midpoint position.

The depth of burial to top of pipe was 31 in. (787 mm). During the test, the south part of the basin remained stationary, while the north part was displaced to the north and west by large-stroke actuators to cause soil rupture and slip at the interface between the two parts of the test basin.

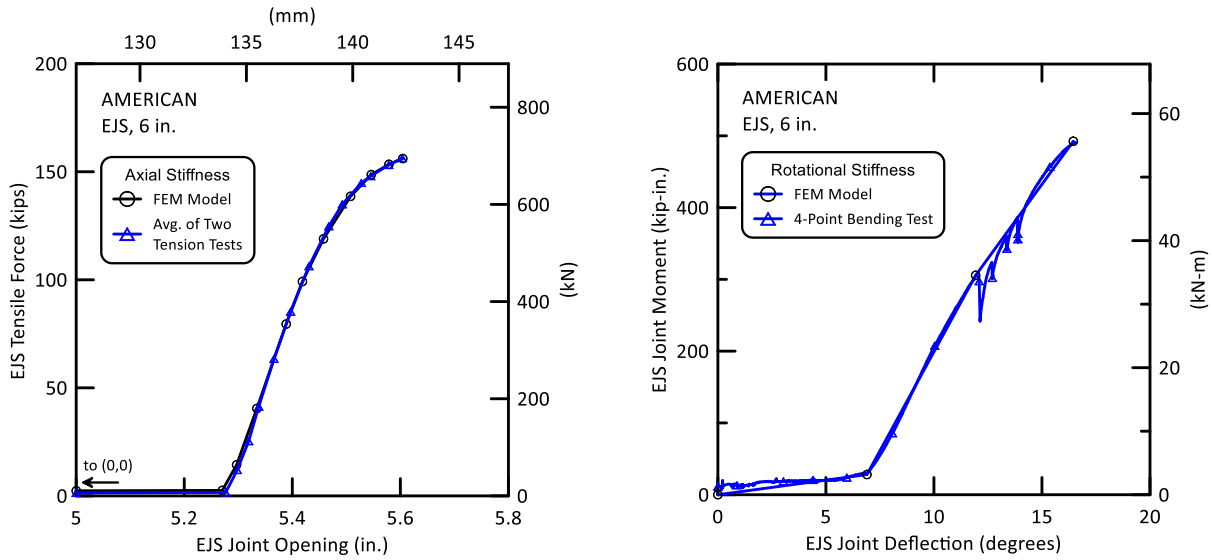
## 6.2. Finite Element Simulations

Figure 6.2 shows a schematic of the 2D FE model of the pipeline response under strike-slip fault conditions, which was developed with the software ABAQUS (2014). The modeling procedure followed is in accordance with the Guidelines for Seismic Design of Oil and Gas Pipelines (ASCE, 1984) and the most recent developments in soil-pipeline interaction modeling (Jung et al., 2016; O'Rourke et al., 2016). Transverse bi-linear springs account for force vs. displacement relationships for lateral and longitudinal pipe movement. The transverse springs were calibrated on the basis of experimental measurements and numerical results for lateral force vs. displacement relationships presented by Jung et al., (2013). The longitudinal springs follow a bi-linear force vs. displacement relationship as recommended in the ASCE Guidelines. The maximum lateral and longitudinal forces per unit pipe distance are a function of soil properties, pipeline diameter and burial depth. The springs are connected to the pipeline with uniaxial gap elements (type gapuni in ABAQUS) that transfer forces parallel and perpendicular to their axes only when the corresponding normal springs carry compressive forces. This transfer is achieved by allowing separation of the gap elements when tensile normal forces are activated in response to load relaxation and separation between soil and pipe. The force per unit distance transferred through the gap element parallel to the pipeline longitudinal axis is controlled by the Coulomb friction law so it is proportional to the normal force acting on the pipeline at each level of deformation. Procedures developed by O'Rourke, et al., (2016) for converting lateral pipe forces to longitudinal frictional forces were used in the finite element simulations.

## 6.3 Finite Element Model Characteristics

The pipeline model was composed of 167 beam elements (type b33) and the soil resistance normal and parallel to the pipeline was simulated with 340 springs (type spring2). The ground displacements are imposed at the nodes of the transverse and longitudinal springs. The beam elements used in the finite element model follow a DI stress-strain relationship with Young's modulus,  $E = 24,200$  ksi (170 GPa) and Poisson's ratio,  $\nu = 0.28$ . The proportional limit and yield stress,  $\sigma_{prop}$  and  $\sigma_y$ , were 34.1 ksi (225 MPa) and 50.6 ksi (349 MPa), respectively. These values based on tensile test data reported in Section 2.

The joints were modeled with two independent nonlinear springs, one for force vs. displacement and one for moment vs. rotation. A third linear spring was used to model the shear force at each



a) EJS Axial Force-Displacement

b) EJS Moment-Deflection

Figure 6.3. Nonlinear Axial Force-Displacement and Moment-Deflection Relationships for EJS Analytical Modeling

joint. The results of the joint tension tests, presented in Section 3, and the four-point bending tests presented in Section 4, and were used to model the axial force vs. displacement and moment vs. deflection (rotation) relationships of the joints. These relationships are given in Figure 6.3. Figure 6.3a) shows the axial force vs. displacement relationship used in the numerical modeling. The tension test data are the average of the two EJS joint tension tests presented in Section 3. In Figure 6.3 a), the force-displacement relationship below 5 in. (127 mm) is not shown, but goes through (0,0). Figure 6.3b) gives the moment-deflection relationship used in modeling the EJS along with the test data used to develop the modeling curve. The moment-deflection model is for the combined EJS rotation, which includes the FR-FRE and SE casting deflections.

The 2D FE analyses were performed for 6-in. (150-mm)-diameter DI pipeline with AMERICAN Earthquake Joint Systems (EJS) joints using the test set-up shown in Figure 6.1, and soil conditions as described above. All pipeline dimensions used in the FE simulations are consistent with those measured at Cornell and also provided by AMERICAN for ANSI/AWWA C150/A21.50 Pressure Class 350 pipe.

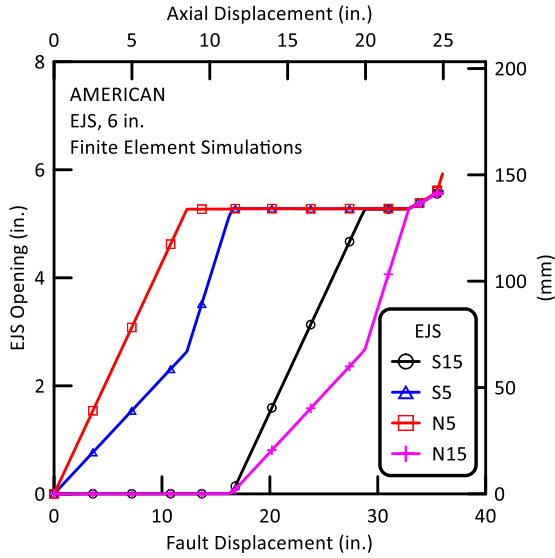
#### 6.4. Finite Element Simulation Results

Figures 6.4a) and 6.4b) present the FE simulation results and test basin measurements for the total (combined FR-FRE and SE casting) EJS joint opening vs. fault displacement for the 6 in. (150 mm) pipeline. The sequence of joint openings is well-identified, as well as the progression of movements. Figures 6.5a) and 6.5b) present the FE simulation results and test basin measurements for the combined EJS joint deflection vs. fault displacement, respectively, for the 6 in. (150 mm) pipeline. Both of these comparisons are in good agreement with the large-scale experimental results.

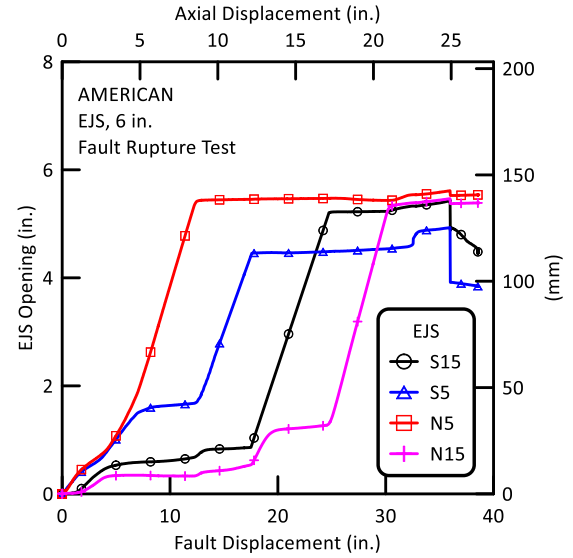
Figure 6.5 presents the axial pipe forces from both the finite element simulations and test basin measurements for the AMERICAN pipe at 20 in. (508 mm) and 34 in. (864 mm) of fault displacement. At 20 in. of fault displacement, the two joints closest to the fault were in full extension. At 34 in. (864 mm) of fault displacement, all four joints were fully extended. The axial loads at 34 in. (864 mm) had increased to a level just before failure of the joint farthest south of the fault, which occurred at 36 in. (914 mm) of fault movement.

As the fault displacement increases, the axial forces in the pipeline increase. This is shown in Figure 6.6, where the pipe forces at the fault crossing (gage plane 0) are shown vs. fault displacement. Forces are relatively small, the order of 10-12 kips (45-55 kN) at 20 in. of fault movement in contrast to approximately 80 kips (235 kN) at 34 in. (864 mm) of fault displacement. The maximum axial force from the simulation compares well with the maximum measured force at 34 in. (864 mm) of fault movement, with less than 10% difference between the maximum analytical and measured axial load.

The FE bending moments are compared with the measured bending moments at various locations along the pipeline for 20 in. (508 mm) and 34 in. (864 mm) in Figure 6.8a) and b), respectively. The measured bending moments were calculated on the basis of measured bending strains and pipe material and geometric properties. The maximum FE bending moment in the pipeline for 20 in. (508 mm) of fault displacement was approximately 110 kip-in. (12.4 kN-m), which compares very well with the measured maximum moment of nearly the same value. The maximum FE bending moment in the pipeline for 34 in. (864 mm) of fault displacement was approximately 250 kip-in. (28.2 kN-m), which exceeds the maximum measured moment by about 25%.

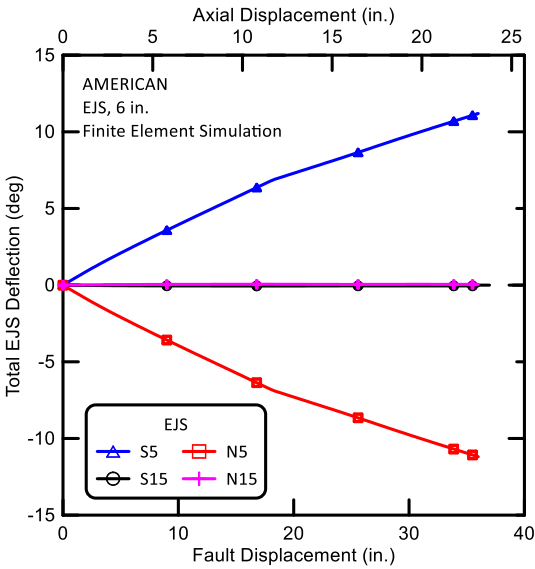


a) Finite Element Simulations

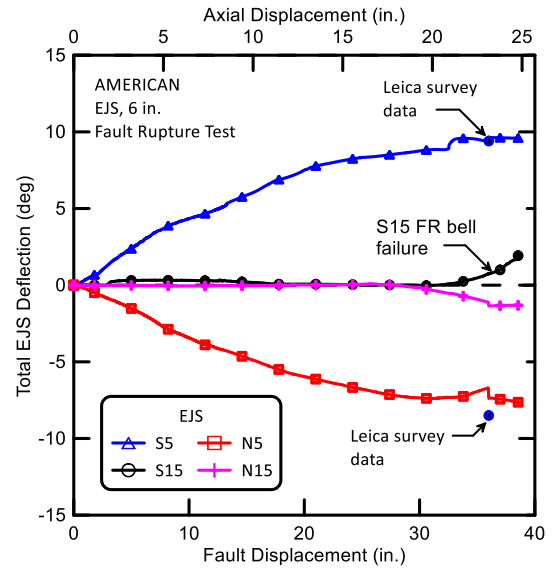


b) Test Basin Measurements

Figure 6.4. Total EJS Joint Opening vs. Fault Displacement for 6 in. (150 mm) Pipes



a) Finite Element Simulations



b) Test Basin Measurements

Figure 6.5. Total EJS Joint Deflections vs. Fault Displacement for 6 in. (150 mm) Pipes

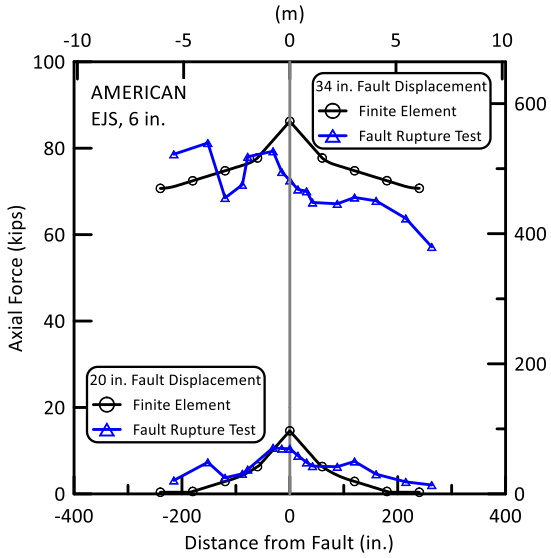


Figure 6.6. Axial Pipe Forces vs. Fault Displacement

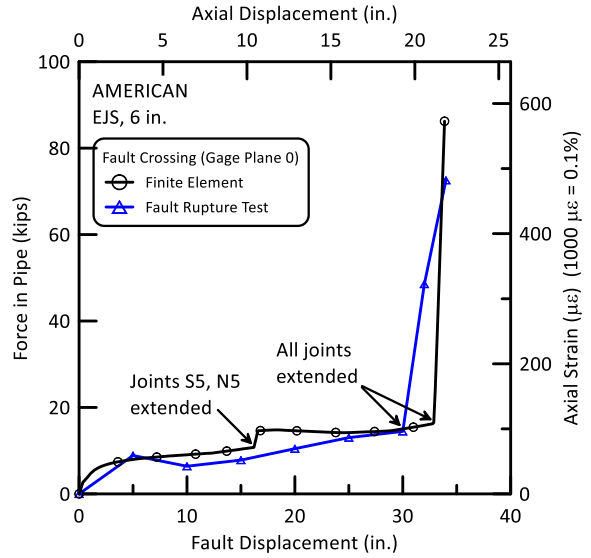
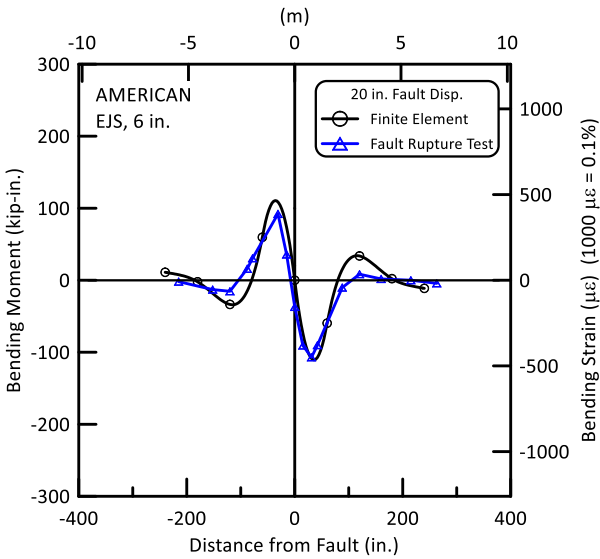
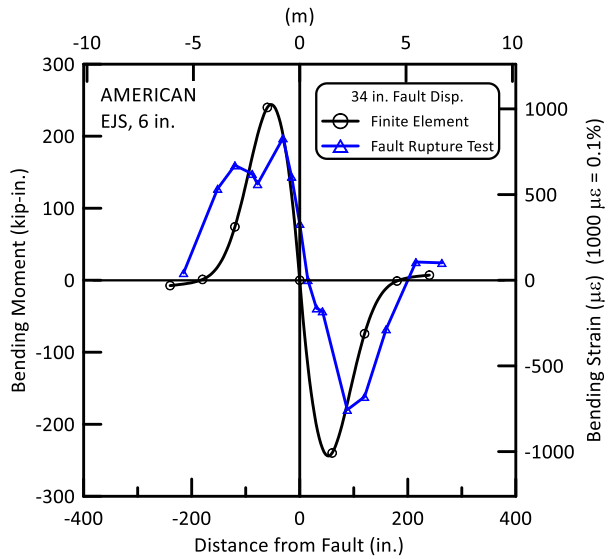


Figure 6.7. Axial Pipe Forces at Fault Crossing vs. Fault Displacement



a) Finite Element Simulations



b) Test Basin Measurements

Figure 6.8. Bending Moment vs. Fault Displacement for 6 in. (150 mm) Pipes

Table 6.1. FEA and Measured Maximum Axial Forces, Moments, and Strains for 6 in. (150 mm) AMERICAN Pipe with EJS

Maximum Axial Tensile Force		Maximum Bending Moment	
FEA	Measured	FEA	Measured
~87 kips	~81 kips	~250 kip-in.	~200 kip-in.
~385 kN	~360 kN	~28 kN-m	~23 kN-m
Maximum Axial Tensile Strain		Maximum Bending Strain	
FEA	Measured	FEA	Measured
~580 $\mu\epsilon$	~ 540 $\mu\epsilon$	~1050 $\mu\epsilon$	~840 $\mu\epsilon$

1000  $\mu\epsilon$  = 0.1 % strain

### 6.5. Summary of Finite Element Simulations

Two-dimensional (2D) finite element (FE) analyses were performed for 6- (150-mm)-diameter DI pipelines with the AMERICAN EJS joints using soil, pipe, and test dimensions consistent with the large-scale split basin test performed at Cornell University for a 6-in. (150-mm)-diameter pipeline. All pipeline dimensions used in the FE simulations are consistent with those for Pressure Class 350 available from AMERICAN and the DI material properties consistent with those of pipe commercially available from AMERICAN and tested as described in previous sections of this report. Test results from direct tension tests and four-point bending tests on EJS specimens were used to determine axial and rotational stiffnesses for the special earthquake resistant joints. A summary of the finite element simulations and the measured values for axial force, bending moment, and pipe strains are given in Table 6.1

The FE simulation results for joint opening vs. fault displacement and joint rotation vs. fault displacement, respectively, are in close agreement with those of the 6 in. (150 mm) pipeline used in the large-scale split basin test. The FE and measured maximum axial force are in close agreement at high levels of fault displacement. The FE bending moments at various locations along the pipelines also compare well with the measured bending moments.

## **Section 7**

### **Summary**

American Cast Iron Pipe Company has developed a hazard resistant ductile iron (DI) pipe joint, called the AMERICAN Earthquake Joint System (EJS). Sections of 6-in. (150-mm) ductile iron pipes with the AMERICAN Earthquake Joint Systems were tested at Cornell University to 1) evaluate the stress-strain-strength characteristics of the DI, 2) determine the capacity of the joint in direct tension and compression, 3) evaluate the bending resistance and moment vs. rotation relationship of an AMERICAN Flex-Ring (FR-FRE) joint and the AMERICAN Earthquake Joint System (EJS), and 4) evaluate the capacity of a 6-in. (150-mm) DI pipeline with AMERICAN Earthquake Joint Systems to accommodate fault rupture using the Cornell full-scale split-basin testing facility.

Test results are summarized for tensile stress-strain-strength characteristics, direct joint tension and compression, bending test results, pipeline response to fault rupture, and significance of test results under the headings that follow.

#### **Tensile Stress-Strain-Strength Characteristics**

The uniaxial tension testing of ductile iron (DI) from AMERICAN specimens was completed in accordance with ASTM – E8 2013 standards (ASTM, 2013). The modulus, yield stress, and ultimate stress were 24,200 ksi, 50.6 ksi, and 65.3 ksi (167 GPa, 348 MPa, and 450 MPa), respectively. The specimens exceeded ANSI/AWWA C151/A21.51-09 60-42-10 specifications (AWWA, 2009). The yield and ultimate stresses are 20.5% and 8.8% greater than the specifications, respectively.

#### **Direct Joint Tension and Compression**

Two tension tests and one compression test were performed on the 6-in. (150-mm)-diameter AMERICAN earthquake joint system (EJS) ductile iron pipes. Tension Test 1 reached a maximum force of 155 kips (689 kN) at 0.45 in. (11 mm) of FR joint opening and 5.1 in. (130 mm) of SE joint displacement. The maximum axial load for Tension Test 2 was 144 kips (641 kN) at 0.41 in. (10 mm) of FR joint opening and 5.1 in. (130 mm) of SE joint displacement. In both tests, the FR bells cracked circumferentially at the peak tensile forces resulting in loss of pressure. This force exceeds Class A of ISO 16134-2006 (ISO, 2006) tensile capacity of 17D, where D is the nominal diameter in inches, and the force is expressed in kips, which is equivalent to 102 kips (450 kN).

The compressive testing showed that the AMERICAN EJS was able to accommodate axial loads to a compressive level at about the DI proportional limit. When pipe reached a compressive load of 256 kips (1,140 kN), which exceeded the proportional limit of 212 kips (943 kN), localized plastic deformation within the joint occurred, resulting in leakage.

### **Bending Test Results**

Four-point bending tests were performed on sections of 6 in. (150 mm) ductile iron (DI) to evaluate the moment vs rotation relationships of the AMERICAN Flex-Ring (FR-FRE) joint and the AMERICAN Earthquake Joint System (EJS). The first leak of 3.5 ml/min in the FR-FRE joint occurred at a deflection  $7.8^\circ$  and an applied moment of 155 kip-in. (17.5 kN-m). In the EJS bending test, first leakage of 25 ml/min was observed at the FR joint at an FR joint rotation of  $10^\circ$  and an EJS deflection of  $\theta_{EJS} = 12.7^\circ$  with an associated moment of 323 kip-in (36.5 kN-m). Both of the AMERICAN Flex-Ring joint pipe and the AMERICAN EJS tested at Cornell exceeded the allowable deflection of  $5^\circ$  and  $8^\circ$ , respectively, without any leaks or pipe damage.

### **Pipeline Response to Fault Rupture**

A 36-ft (11-m)-long, five-piece section of a ductile pipeline was tested at the Cornell Large-Scale Lifelines Facility. The pipe had a total of four AMERICAN Earthquake Joint Systems, equally spaced about a  $50^\circ$  fault. The pipe was pressurized to approximately 80 psi (550 kPa). The pipe was placed on a bed of compacted partially saturated sand, aligned, instruments checked, and then backfilled with compacted sand to a depth of cover of 31 in. (787 mm) above the pipe crown. The north section of the test basin was displaced along a  $50^\circ$  fault at a rate of 12 in. (300 mm) per minute. At a fault displacement of roughly 36.0 in. (914 mm), the pipe lost pressure. An additional 2.5 in. (63.5 mm) of test basin movement was applied, resulting in a complete pressure loss in the system, and the test was then stopped. The 36.0 in. (914 mm) fault displacement corresponds to 23.1 in. (587 mm) of axial extension of the test basin and pipe. Following excavation, a fracture was observed near the west springline of the FR Bell of the S15 EJS.

The test measurements confirm that the pipeline was able to accommodate fault rupture through axial displacements and deflections at all four Earthquake Joint Systems. They also provide a comprehensive and detailed understanding of how the movement was accommodated at each joint, the sequence of movements, and combined axial pullout and rotation at each joint. The total axial movement is 23.1 in. (587 mm), which exceeds the sum of the 5.5 in. (140 mm) joint displacement

for all four earthquake joint systems. On average, each EJS displaced on the order of 5.78 in. (147 mm). This displacement was close to movement during previous direct tension testing of the AMERICAN EJS. The maximum deflection measured at the EJS closest to the fault was about 9.6 degrees, thus demonstrating the ability of the joints to sustain significant levels of combined axial pullout and deflection. The maximum stresses sustained by the pipeline, corresponding to the largest pipeline deformation, were well within the elastic range of pipeline behavior.

The ductile iron pipeline equipped with AMERICAN Earthquake Joint System (EJS) was able to accommodate significant fault movement through axial pullout and rotation of the joints. Fault rupture simulated in the large-scale test is also representative of the most severe ground deformation that occurs along the margins of liquefaction-induced lateral spreads and landslides.

### **Finite Element Simulations**

Two-dimensional (2D) finite element (FE) analyses were performed for a 6-in. (150-mm)-diameter pipeline with AMERICAN EJS joints. The geometry and material characteristics used for the soil, pipe, and test dimensions were consistent with the large-scale split basin test performed at Cornell University. All pipeline dimensions used in the FE simulations are consistent with those for thickness Pressure Class 350 ductile iron available from AMERICAN.

The FE simulation results for joint opening vs. fault displacement and joint rotation vs. fault displacement, respectively, are in close agreement with the experimental measurements from the 6 in. (150 mm) pipeline used in the large-scale split basin test. The cumulative openings for all four joints showed a continuous increase until all joints were fully extended, then increased rapidly.

The FE simulations show that the maximum axial forces in the pipe were approximately 87 kips, and those measured were approximately 81 kips (385 and 360 kN, respectively.) The maximum bending moments from the analytical simulations were approximately 250 kip-in. and those measured were 200 kip-in. (28 and 23 kN-m, respectively.) The maximum axial strain predicted for the 6-in. (150-mm)-diameter pipelines is approximately 580  $\mu\epsilon$  (vs. 540 measured), and the maximum predicted bending strains were 1050  $\mu\epsilon$  (vs. 840 measured). The FE simulations for 6-in. (150-mm)-diameter pipe compare well with the measurements of maximum axial and bending responses measured in the large-scale split basin test at Cornell, thus providing confidence in the FE results.

## **Significance of Test Results**

The amount of tensile strain that can be accommodated with ductile iron pipelines will depend on the spacing of the AMERICAN Earthquake Joint Systems and the positioning of the spigot within the bell at the pipeline joints. The pipeline used in the large-scale split-basin test was able to accommodate 23.1 in. (581 mm) of axial extension, corresponding to an average tensile strain of 4.4% along the pipeline. Such extension is large enough to accommodate the great majority (over 99%) of liquefaction-induced lateral ground strains measured by high resolution LiDAR after each of four major earthquakes during the recent Canterbury Earthquake Sequence (CES) in Christchurch, NZ (O'Rourke, et al., 2014). These high resolution LiDAR measurements for the first time provide a comprehensive basis for quantifying the ground strains caused by liquefaction on a regional basis. To put the CES ground strains in perspective, the levels of liquefaction-induced ground deformation measured in Christchurch exceed those documented in San Francisco during the 1989 Loma Prieta earthquake (e.g., O'Rourke and Pease, 1997; Pease and O'Rourke, 1997) and in the San Fernando Valley during the 1994 Northridge earthquake (e.g., O'Rourke, 1998). They are comparable to the levels of most severe liquefaction-induced ground deformation documented for the 1906 San Francisco earthquake, which caused extensive damage to the San Francisco water distribution system (e.g. O'Rourke and Pease, 1997; O'Rourke, et al., 2006). The tests confirm that the ductile iron pipes equipped with the AMERICAN Earthquake Joint Systems are able to sustain large levels of ground deformation through axial displacement and deflection.

## References

- ABAQUS, (2014) “Theory Manual of ABAQUS,” ABAQUS, Inc., Providence, RI.
- ASCE. (1984) “Guidelines for the Seismic Design of Oil and Gas Pipeline Systems”, Committee on Gas and Liquid Fuel Lifelines, ASCE, Reston, VA.
- ASTM International (2013). “Standard Test Methods for Tension Testing of Metallic Materials”, *ASTM Standards*. E8/E8M - 13a, 1 – 28.
- AWWA (2009). “Ductile Iron Pipe, Centrifugally Cast for Water”, *AWWA Standard*. ANSI/AWWA C151/A21.51-09.
- International Organization of Standardization [ISO] (2006), “Earthquake- and Subsidence-Resistant Design of Ductile Iron Pipelines,” ISO 16134.
- Jung, J., O’Rourke, T.D., and Olson, N. A. (2013) “Lateral Soil-Pipe Interaction in Dry and Partially Saturated Sand” Journal of Geotechnical and GeoEnvironmental Engineering, ASCE, Vol. 139, No. 12, pp. 2028-2036.
- Jung, J.K., T. D. O’Rourke, and C. Argyrou (2016) ‘Multi-Directional Force-Displacement Response of Underground Pipe in Sand’ Canadian Geotechnical Journal, Vol. 53, pp. 1763 – 1781.
- O’Rourke, T.D. (1998). “An Overview of Geotechnical and Lifeline Earthquake Engineering”, Geotechnical Special Publication No. 75, ASCE, Reston, VA, Proceedings of Geotechnical Earthquake Engineering and Soil Dynamics Conference, Seattle, WA, Aug. 1998, Vol. 2, pp.1392-1426.
- O’Rourke, T.D. and J.W. Pease (1997). “Mapping Liquefiable Layer Thickness for Seismic Hazard Assessment”, Journal of Geotechnical Engineering, ASCE, New York, NY, Vol. 123, No.1, January, pp. 46-56.
- O’Rourke, T.D., A. Bonneau, J. Pease, P. Shi, and Y. Wang (2006). “Liquefaction Ground Failures in San Francisco” Earthquake Spectra, EERI, Oakland, CA, Special 1906 San Francisco Earthquake Vol. 22, No. 52, Apr., pp. 691-6112.
- O’Rourke, T.D., Jeon, S-S., Toprak, S., Cubrinovski, M., Hughes, M., van Ballegooy, S., and Bouziou, D. (2014) “Earthquake Response of Underground Pipeline Networks in Christchurch, NZ”, Earthquake Spectra, EERI, Vol. 30, No.1, pp. 183-204.
- O’Rourke, T.D., J.K. Jung, and C. Argyrou (2017) “Underground Infrastructure Response to Earthquake Induced Ground Deformation”, Soil Dynamics and Earthquake Engineering, in press.
- Pease, J.W. and T.D. O’Rourke (1997), “Seismic Response of Liquefaction Sites”, Journal of Geotechnical Engineering, ASCE, New York, NY, Vol. 123, No. 1, January, pp. 37-45.